



The fabrication process of microfluidic devices integrating microcoils for trapping magnetic nano particles for biological applications

Hong Ha Cao

► To cite this version:

Hong Ha Cao. The fabrication process of microfluidic devices integrating microcoils for trapping magnetic nano particles for biological applications. Other [cond-mat.other]. Université Paris Sud - Paris XI, 2015. English. NNT: 2015PA112150 . tel-01350864

HAL Id: tel-01350864

<https://theses.hal.science/tel-01350864>

Submitted on 2 Aug 2016

HAL is a multi-disciplinary open access archive for the deposit and dissemination of scientific research documents, whether they are published or not. The documents may come from teaching and research institutions in France or abroad, or from public or private research centers.

L'archive ouverte pluridisciplinaire **HAL**, est destinée au dépôt et à la diffusion de documents scientifiques de niveau recherche, publiés ou non, émanant des établissements d'enseignement et de recherche français ou étrangers, des laboratoires publics ou privés.

UNIVERSITÉ PARIS SUD

L'Institut d'Électronique Fondamentale

Ecole doctorale: Sciences et Technologies de l'Information des Télécommunications et des Systèmes (STITS – ED 422)

Discipline: physique

Microsystèmes pour Biomédical

Thèse de doctorat

Présentée par : **CAO Hong Ha**

Sujet: Procédé de fabrication de dispositifs microfluidiques intégrant des microbobines – Piégeage de nanoparticules magnétiques pour des applications en biologie

Composition du jury:

Mme Isabelle MABILLE	MCF, HDR	Rapporteur	Université Pierre et Marie Curie Institut de Recherche de Chimie
Mr Benoit PIRO	PR	Rapporteur	Université Paris Diderot Laboratoire ITODYS
Mr Bruno LEPIOUFLE	PR	Examineur	Ecole Normale Supérieure de Cachan SATIE
Mme Claire SMADJA	PR	Examineur	Université Paris Sud Institut Galien paris-Sud
Mme Marion WOYTASIK	MCF	Examineur	Université Paris-Sud Institut d'Electronique Fondamentale
Mme Elisabeth DUFOUR-GERGAM	PR	Directeur de thèse	Université Paris-Sud Institut d'Electronique Fondamentale
Mr Emile MARTINCIC	MCF	Invité	Université Paris-Sud Institut d'Electronique Fondamentale
Mr Mehdi AMMAR	MCF	Invité	Université Paris-Sud Institut d'Electronique Fondamentale

July 21st, 2015

For my family,

With the deep gratitude for the encouragement to overcome the hard time when I studied in France and had to live far from you for over three years from March 2012



Hải Anh (Tinny), Vân Anh, Hồng Hà, Phương Linh (Tommy)



Acknowledgment

Foremost, I would like to express much appreciation to my supervisor Prof. Elisabeth DUFOUR-GERGAM, who gave me a chance to be a PhD. student at her group (MicroSystèmes pour le Biomédical, L'Institut d'Électronique Fondamentale (IEF), l'Université Paris Sud) in the first time I met her in Hanoi, Vietnam over past three years. She helped me a lot to make plan and scientific ideal for my research in the topic of microfluidic devices and application, and she created best condition for me to approach environment working with modern machines in clean room of laboratory. I also sincerely thank her financial support for my experiment and life during the time I studied at IEF. In addition, she also wholeheartedly helped me a lot in administrative formalities of university and laboratory, specially in documents to the Ministry of Education and Training – Vietnam. One more time, I would like thank for her help in facilitating a good relationship with other colleagues in past recent time.

I would like to give a precious thanks to Dr. Marion WOYTASIK, who helped directly me a lot as a supervisor. Although she was very busy, she had carefully guided me from first technics of basic and simple experiments when I began to approach the topic of my research. In addition, she also helped thoroughly me to overcome difficulties in writing, correcting papers and manuscripts, as well as in matters of documents in French.

I also would like to give a sincere thanks to Dr. Emile MARTINCIC and Dr. Mehdi AMMAR, who spent much time to help me in the theory, simulation and practice of the magnetic field in chapter 3 and papers, the theory and applications of biology in chapter 4. They gave me guidance in detail in designing microcoils, performing experiments with trapping magnetic beads and bead-based immunoassays. They also carefully helped me to write and correct my thesis. All the assessments, comments and correction in my writing improved my skill in writing and specialist knowledge of research objectives.

I would like to thank Assc. Prof. TRAN Dai Lam in Institute of Materials Science, Vietnam Academy of Science and Technology, who introduced me to Prof. Elisabeth DUFOUR-GERGAM and then I had opportunity to be a PhD. student in IEF, University Paris Sud. He also gave me useful discussion in my topic research.

I would like to sincerely thank Prof. Alain BOSSEBOEUF, who supported me to get an opportunity to participate the Namis School September, 2013 in Korea. He also supported me documents and procedures involving in the administration of laboratory. With supports of him and Prof. Elie LEFEUVRE about the equipment helped me to obtain results in this thesis. Kindly thanks gives to Dr. Johan MOULIN, who helped me in the beginning of the magnetic calculation and equipment setup for the first experiment of trapping magnetic beads. I would like to give a special thanks to Dr. Philippe COSTE, who helped me a lot in problems involving to information technology and computers, and also to Prof. Pierre-Yves JOUBERT, who helped me to apply all documents to Laboratory IEF, thus, I had a chance to have financial support from Laboratory. I also sincerely thank Ms. Magdalène COUTY, who enthusiastically helped me to carry out first experiments in a clean room of IEF in fabricating PDMS microfluidics, she also helped me about documents in French during the time I worked with her office No. 102 Building 220, IEF. I would like to thank Ms. Meritxell CORTES, who helped me a lot in the fabrication of microcoils and English writing, we had friendly time when she worked at IEF.

I sincerely thank Prof. Niko HILDEBRANDT, who gave me the best working conditions when I worked with the fluorescence microscopy for experiments. I also thank colleagues as Shashi, Stina... in Bio Nano Photonics team, who guided me using the fluorescence microscopy. A sincere thank give to Dr. Claire SMADJA, who helped and supported me to take first ELISA experiments in the laboratory of Paris-Sud Institut Galien, Faculté de Pharmacie, Université Paris-Sud. In this ELISA experiments, I also would like to thank Kiarach Mesbah, GIANG Phuong Ly, Mohamed MIRAOU, who helped me to obtain first experiences about working in biology.

I would like to give my sincere thanks to my colleagues DINH Thi Hong Nhung, Magdalena COUTY, Feriel HAMDI, who worked with me in project of reversible packaging of PDMS microfluidic chip. I would like to thank Monica ARAYA-FARIAS, who worked with me on PDMS microchip fabrication, and LE VAN Quynh, who helped me in the SEM measurement.

I would like to sincerely thank all my Vietnamese friends, who have friendly shared in works and life during the time I worked and stayed in France. Those of my friends helped me a lot in the administrative procedure in French: ĐINH Thị Hồng

Nhung, Vũ Thị Nhung, MAI Văn Huy, LÊ Thanh Nghị. Other friends (Hung, Trường, Cẩm, Chung, Lâm, Vân Anh, Hoàng, Quỳnh, Mai, Trang, Huy, Tuấn, Phương, Khuyển, Tiệp+Nuong...) sincerely shared with me many things in works and life. I am also happy to have French friends (Aida, Sarah, Vincent, Alexandre, Guillaume, Iman, Pierre,...).

Most importantly and above all, I would like to give my love and thank to my family, specially to my wife, NGUYỄN Vân Anh, who spent much time to take care with love my two daughters, CAO Hải Anh and CAO Phương Linh, although she was very busy and her health was not good. They are always a great motivation to encourage me during the time I worked in France and I had to live away from home.

I would like to express my great gratitude to my parents, my parents-in-law, who encouraged and helped me and my wife and children in over three years ago. I also express my most sincere thanks to all big family members, who encouraged me in finishing this thesis.

I would like to thank the French RENATECH network and the Vietnamese Overseas Scholarship Program (Project - 322) of the Vietnamese government for the financial support during the study period at IEF, Univ. Paris-Sud, France. I also thank colleagues at Department of Physical chemistry, School of Chemical Engineering, Hanoi University of Science and Technology, Vietnam, who facilitated my study in France.

CONTENTS

Acknowledgments	i
Résumé/Summary	ix
Nomenclature	x
CHAPTER 1. CONTEXT	1
CHAPTER 2. REVIEW OF MICROFLUIDICS FOR BIOLOGICAL APPLICATIONS	5
2.1 Short overview of the historical development of microfluidics	6
2.2 Introduction to microfluidic system	7
2.2.1 Microfluidics concepts	7
a. Generalities	7
b. Advantages of microfluidics in chemical and biological applications:.....	9
2.2.2 Microfluidics' theoretical aspects.....	10
a. Reynolds number.....	10
b. The profile of velocity flow in a rectangle channel.....	11
2.3 Magnetic bead-based immunoassay	11
2.3.1 Magnetic micro/nano beads in immunoassay.....	12
a. Introduction of functionalized magnetic beads	12
b. Magnetic properties of the materials of bead's core.....	14
2.3.2 Immunoassay principles.....	15
2.3.2.1 Introduction of immunoassay.....	15
2.3.2.2 Bio-components in immunoassay	16
a. Capture antibody and immuno-sorbent/solid phase.....	17
b. Detection antibodies (antibodies conjugated enzyme).....	19
c. Enzyme and antigens	20
2.3.3 General protocol of magnetic bead-based immunoassay.....	20
2.4 Microfluidics in magnetic bead-based immunoassay	22
2.4.1 Magnetism and trapping/transporting magnetic beads in microfluidics	22
2.4.1.1 Permanent magnet for manipulating magnetic beads in microfluidics	22
2.4.1.2 Electromagnet for manipulating magnetic beads in microfluidics.....	24
2.4.2 Bead-based immunoassay inside microfluidics	28
2.4.3 Microfluidics fabrication.....	30
2.4.3.1 Microchannel fabrication.....	30
a. Materials for microchannel network.....	30
b. PDMS as a popular materials for microfluidics.....	32
2.4.3.2 Packaging PDMS microfluidic chip	33
a. Irreversible bonding	33
b. Reversible bonding.....	34
2.5 Conclusions.....	36
References	37

CHAPTER 3. MICROCOILS DESIGN AND FABRICATION	41
3.1. Introduction	42
3.2. Magnetic field/force theory.....	43
3.2.1. Magnetic field of straight and finite wire.....	43
3.2.2. Magnetic force: theory.....	47
3.3. Magnetic field simulation and calculation	48
3.3.1. FE simulation of microcoils	48
3.3.2. Simulation results.....	50
a. General considerations on the magnitude and shape of the magnetic field.....	50
b. Coil geometry effect on the power loss and heating.....	53
c. Power consumption and merit factors	55
d. Conclusions:	57
3.4. Planar coils fabrication and characterization	57
3.4.1. Mask design.....	58
3.4.2. Fabrication process of coils	59
3.5. Conclusions	62
References	63
CHAPTER 4. FABRICATION OF MICROFLUIDIC CHIPS AND APPLICATIONS.....	65
4.1. Introduction	66
4.2. Microfluidic chips fabrication	67
4.2.1. PDMS channel.....	67
a. Design of PDMS channel network	67
b. Channel fabrication.	68
4.2.2. Valves switch.....	70
a. Design of multi-valves switch	71
b. Multi-valve switch fabrication.....	72
4.2.3. Microfluidic chip packaging.....	73
4.2.3.1. PDMS / PDMS reversible packaging based on stamping technique	74
4.2.3.2. Reversible packaging based on anti-adhesive under-layer	75
4.2.4. General conclusions in microfluidic chip fabrication:.....	77
4.3. First trapping experiments with microfluidic chip	79
4.3.1. Study on the temperature of the microchip	79
a. Experiment description.....	79
b. Results and discussion.....	80
4.3.2. Magnetic nanobeads trapping experiments.....	81
a. Magnetic beads	81
b. Microfluidic chip.....	82
c. Experiment description.....	83
4.3.3. Results and discussion	85
a. Trapping magnetic beads in a narrow channel.....	85

b. Trapping magnetic beads in a wide channel: current value effect.....	86
c. Trapping magnetic beads in a wide channel: time cumulative experiment	88
4.3.4. Conclusion of trapping experiment	90
4.4. Microfluidic chip for on-chip magnetic beads-based immunoassay	91
4.4.1. Modification of PDMS surface.....	91
4.4.1.1. Materials and surface modification protocol	92
a. Materials:	92
b. Protocol of surface modification and bonding process	93
4.4.1.2. Results and discussions	95
a. The effect of PEO treatment on PDMS surface.....	95
b. The effect of BSA and PEO treatment on PDMS surface	96
c. Roughness study by AFM	97
d. Adsorption of fluorescent dye on modified PDMS surface.....	98
4.4.2. First steps in bead-based immunoassay inside microfluidic chip.....	100
4.4.2.1. General IgG grafting protocol.....	101
a. The preparation of materials.....	101
b. IgG grafting protocol.....	103
4.4.2.2. Experiment and results in micro test tube (control experiment)	104
a. Protocol description	104
b. Results and discussion	105
4.4.2.3. Experiments in microfluidic chip.....	108
a. Setup of microfluidic chip for grafting IgGs:.....	109
b. IgG grafting protocol.....	110
c. Results and discussion.....	113
4.4.3. Conclusions from applying microfluidic chip with embedded microcoil in immunoassay	118
4.5. General conclusion of chapter 4	119
References.....	120
5. Conclusion and prospects	123
APPENDICES	127
Publications:	128
APPENDIX 1. Chapter 3 – Microcoils design and fabrication	129
APPENDIX 2. Paper	
“Reversible bonding by dimethyl-methylphenylmethoxy siloxane – based stamping	
technique for reusable poly(dimethylsiloxane) microfluidic chip”	134
APPENDIX 3. Chapter 4 - Leakage test and peeling off channel.....	139
APPENDIX 4. Chapter 4.....	140

Résumé

Le but de cette étude est de concevoir, fabriquer et caractériser une puce microfluidique afin de mettre en oeuvre la capture de nanoparticules magnétiques fonctionnalisées en vue de la reconnaissance d'anticorps spécifiques (couplage d'une très grande spécificité et sensibilité). Après avoir modélisé et simulé les performances de la microbobine intégrée dans le canal de la puce microfluidique en prenant soin de limiter la température du fluide à 37°C, la capture devant être effective, le microsystème est fabriqué en salle blanche en utilisant des procédés de fabrication collective. La fabrication du microdispositif en PDMS a aussi donné lieu à l'optimisation de procédés de modification de surface afin d'assurer la ré-utilisation du microdispositif (packaging réversible) et la limitation de l'adsorption non spécifique.

L'immobilisation des anticorps sur les billes (300 nm) a été menée à l'intérieur du canal en utilisant un protocole de type ELISA éprouvé. Le procédé a montré qu'il était également efficace pour cet environnement puisque nous avons pu mettre en évidence la capture de nanoparticules.

Summary

In this study, a concept of microfluidic chip with embedded planar coils is designed and fabricated for the aim of trapping effectively functionalized magnetic nanobeads and immobilizing antibody (IgG type). The planar coils as a heart of microfluidic chip is designed with criterion parameters which are optimized from simulation parameters of the maximum magnetic field, low power consumption and high power efficiency by FE method. The characterization of microcoils such as effectively nanobeads (300 nm) at low temperature ($<37^{\circ}\text{C}$) is performed and confirmed. The channel network in PDMS material is designed for matching with entire process (including mixing and trapping beads) in microfluidic chip. A process of PDMS's surface modification is also carried out in the assemble step of chip in order to limit the non-specific adsorption of many bio substances on PDMS surface. The microfluidic chip assemble is performed by using some developed techniques of reversible packaging PDMS microfluidic chip (such as stamping technique, using non-adhesive layer, oxygen plasma combining with solvent treatment). These packaging methods are important to reused microchip (specially the bottom substrate) in many times.

The immobilization of antibody IgG-type is performed inside microfluidic chip following the standard protocol of bead-based ELISA in micro test tube. The result showed that IgG antibodies are well grafted on the surface of carboxyl-beads (comparing to result of standard protocol); these grafted antibodies are confirmed by coupling them with labeled second antibody (Fab-FITC conjugation).

Nomenclature

Abbreviation	Acronyms
Ab, Abs	Antibody, antibodies
Ag, Ags	Antigen, antigens
BSA	Bovine serum albumin
CMOS	Complementary metal–oxide–semiconductor
DMPMS	Dimethyl methylphenylmethoxy siloxane
ELISA	Enzyme-Linked ImmunoSorbent Assay
FEM	Finite element method/modelling
FITC	Fluorescein isothiocyanate
HRP	horseradish peroxidase
IBE	Ion beam etching
IgG	Immunoglobulin G
Igs	Immunoglobulins
LoC	lab-on-a-chip
MB/MBs	Magnetic nano bead/beads
MEMS/NEMS	Micro/Nano electronic mechanic systems
mNP/mNPs	Magnetic nano particle/particles
NP/NPs	Nano particle/particles
PBS	Phosphate buffered saline
PDMS	Poly(dimethyl siloxane)
PECVD	Plasma-enhanced chemical vapor deposition
PEO	Poly(ethylene oxide)
RIE	<i>Reactive-ion etching</i>
SU-8	Epoxy based negative photoresist
TAS/ μ -TAS	Total analysis system / micro total analysis system
TMB	3,3',5,5'-Tetramethylbenzidine

CHAPTER 1. CONTEXT

Microfluidics: in search of a killer application

“Companies and academic researchers are developing more and more microfluidic devices. But what the technology stakeholders really want is an application that will trigger widespread adoption of microfluidics by biologists”. *Nathan Blow reported in [1]*.

In analytic biochemistry assay, to specifically detect the presence of a target/substance (an antigen) in analyte, the Enzyme-Linked Immune-Sorbent Assay (ELISA) has been used widely as a diagnostic tool in medicine, biology, and plant pathology. This nowadays well known method was developed based on the radioimmunoassay, which is a technique using radioactively labeled antigens or antibodies and was first published in 1960 by Rosalyn Sussman Yalow and Solomon Berson [2]. Until the 70s of the 20th century, the ELISA method was developed and became one of the most specific method in immunoassay (i.e. HIV virus, Alzheimer or cancerous biomarker [3-6]), a keyword in literature [7-10]. Basically, ELISA is typically based on the “sandwich” structure of primary antibody (Ab) – antigen (Ag) – second antibody (with labeled conjugation). The detection of Ab or Ag, is performed easily in two ways: direct ELISA and indirect ELISA (including supported surface or capture antibody as basic platform), by using fluorogenic, electrochemiluminescent, this method presents various advantages like high sensitivities/ultrasensitive and the possibility to multiplex the detection [11].

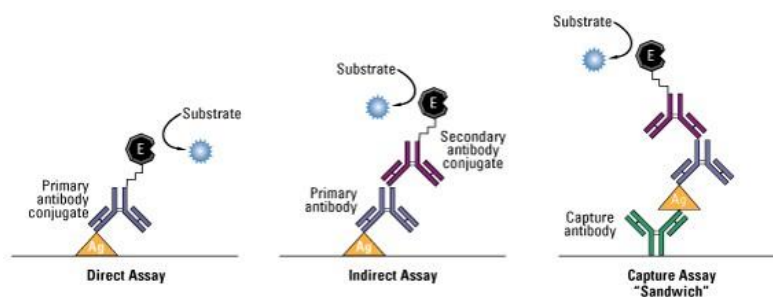


Figure 1.1. An example of Common ELISA formats. In the assay, the antigen of interest is immobilized by direct adsorption to the assay plate or by first attaching a capture antibody to the plate surface. Detection of the antigen can then be performed using an enzyme-conjugated (E) primary antibody (direct detection) or a matched set of unlabeled primary and conjugated secondary antibodies (indirect detection)⁽¹⁾.

Figure 1.1 shows the three common ELISA formats. In the direct detection format, the capture antibody that reacts directly with the antigen is a labeled primary antibody. Direct detection can be performed with antigen that is directly immobilized on the assay plate or with the capture assay format. Direct detection is not widely used in ELISA but is quite common for immuno-histochemical staining of tissues and cells. Secondly, the indirect detection method uses a labeled secondary antibody for detection. The secondary antibody has specificity for only the primary antibody (*i.e.* capture antibody) or the assay will not be specific for the antigen. Generally, this is achieved by using capture and primary antibodies from different host species (*e.g.*,

⁽¹⁾ <https://www.lifetechnologies.com>

mouse IgG and rabbit IgG, respectively). For sandwich assays, it is beneficial to use secondary antibodies that have been cross-adsorbed to remove any antibodies that have affinity for the capture antibody.

Traditional ELISA tests are performed in wells, which are passively bind antibodies and proteins. Recent evolutions of the technic involving nanobeads present a lot of advantages for future analysis applications. The use of functionalized magnetic nano/micro beads allows the detection of ultralow concentration (few zepto-grams) of targets (proteins, cells) in extremely small volume (few μL) of analyte [6, 12-15]. Currently, the on-chip bead-based ELISA system (“snapshot” ELISA techniques) has higher sensitivity than standard ELISA techniques, using magnetic micro/nano beads to increase surface-to-volume ratio combined with microfluidic devices using major bead magnetic trapping methods (by permanent magnet [16, 17] or electromagnet [13]).

Let us recall that many typical microfluidic devices are currently under development, ranging from single components such as flow sensors and valves for gas pressure regulation, to complex micro-fluid handling systems for chemical and biological analyses. Many function modules (such as sensors) can be integrated on a single substrate or complex modules of microfluidics. Specially, researchers had an ambition to make these devices portably, or to integrate many components into hand-held format for variety of point-of-care application.

In this study, we propose to develop a new type on-chip bead-based immunoassay platform with embedded planar coils, designed and fabricated for the aim of trapping effectively functionalized magnetic nano/micro beads, and the immobilization of capture antibodies inside microchannel.

In immunoassay procedure, the planar coils will play an important role of separating/sorting magnetic beads.

The study will be presented in four chapters describing first some items about microfluidics and immunoassays bottlenecks, the simulation of the microcoils to optimize the device, the fabrication and the process development used for the chip fabrication, the first biological experiments and, at last the conclusion and emerging ideas.

We will see in the chapter 3 the microcoils designed with criterion parameters optimized from simulation parameters to obtain maximum magnetic field, low power consumption and high power efficiency. These values are calculated by Finite Element (FE) method thanks to ANSYS® software. Simulation results will also predict the affection of coil's geometries (including the size, number of turn, parameters of conductors, etc.) on power loss and heating of coils while they are working. We will also study the surface temperature during operation which is so important to take into account for biological medium. This chapter will finish with the microcoils fabrication process. In the chapter 4, we will present some original processes to assemble the bottom substrate (holding the microcoils) with PDMS cap holding the microchannel network. Three techniques of reversible bonding are developed: (i). Coating layer of non-adhesive material; (ii). Stamping technique using dimethyl-methylphenylmethoxy siloxane (DMPMS) conformal coating as adhesive layer; (iii). Oxygen plasma treatment for bonding PDMS to PDMS. We also studied the process to functionalize the beads outside and inside the chip and the trapping of the specific elements.

CHAPTER 2. REVIEW OF MICROFLUIDICS FOR BIOLOGICAL APPLICATIONS

- *Introduction of microfluidic systems*
 - *Review of historical development*
 - *Introduction of processes and components in microfluidic chip*
-

“Microfluidics, a technology characterized by the engineered manipulation of fluids at the submillimeter scale, has shown considerable promise for improving diagnostics and biology research. Certain properties of microfluidic technologies, such as rapid sample processing and the precise control of fluids in an assay, have made them attractive candidates to replace traditional experimental approaches.” *Eric K. Sackmann et al. reported in [18].*

2.1 Short overview of the historical development of microfluidics

Microfluidics attracts the attention of scientists since the 1950s who desire to manipulate small volume (micro/nano liter) of liquids in micro channels/capillaries. It is marked by revolution in exploiting molecular distributions between mobile and stationary phase in a small column [19] and capillary electrophoresis. It was known that, processes in very small and long capillary had some advance performances thanks to the large surface-to-volume ratio. Until 1970s, some first microfluidic devices were used in the research of gas chromatograph at Stanford University [20] and ink jet printer nozzles on silicon wafer at IBM [21, 22]. In the early 1990s, Manz et al. [23] reported a microfluidic potential for addressing issues facing analytical methods, now it is called micro Total Analysis System (μ TAS), and hence the term of “Lab-on-a-chip” – LoC was introduced. It can be said that microfluidics has been become “hot” research topic in chemical and biological analysis since then [18]. From the 2000s, microfluidics has the potential to significantly change the way modern biology is performed, [24]. In many conventional assays, it's possible to integrate many analytical steps (such as sample loading, rinsing, reaction, separation, mixing, detection, etc.) into single or fully-automated platform. By these advantages, the Lab-on-a-chip system can greatly reduce the cost and time in each analysis and multiplexed analysis can be developed.

Nowadays, many different microfluidic devices ranging from single components such as flow sensors and valves for gas pressure regulation, to complex micro-fluid handling systems for chemical and biological analyses can be integrated on a single substrate. The dream of the scientists of the 1970s researchers seems very near because it is now possible to make portably devices integrating many components into hand-held format for variety of point-of-care (PoC) application. It can take fast or mobility analysis.

In chemical, medical and biological analysis, microfluidics can be used in some major applications: measuring molecular diffusion coefficients [25]; pH [26], chemical binding coefficients [27], and enzyme reaction kinetics [28]. Other applications for microfluidic devices include capillary electrophoresis [29], immunoassays [30], flow cytometry [31], sample injection of proteins for analysis via mass spectrometry [32], PCR amplification [33], DNA analysis [34], cell analysis [15] and chemical gradient

formation [35], clinical diagnostics [30, 36]. We will see very shortly some of them in the next sections.

2.2 Introduction to microfluidic system

2.2.1 Microfluidics concepts

a. Generalities

Microfluidic chip can be identified as a micro device that deals with the flow of liquid inside one or more tiny channels with at least one dimension of nano/micrometers size. Concerning the terms of microfluidics, it can be considered to both science and technology (including: research on theoretical of flows, transport phenomena, interaction in tiny space with the high surface area to volume ratio; microfabrication technology of microfluidic chip for application in chemical/biological analysis – such as Lab-on-a-chip). An example of microfluidic devices is shown in Figure 2.1 (a) ⁽¹⁾. This microfluidic chip is used as a micro-reactor and micro-mixture device of two substances injected in inlet 1 and 2. The reaction's product is released through outlet.

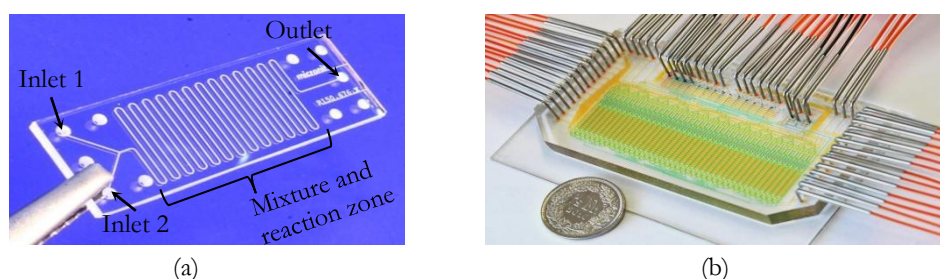


Figure 2.1. (a) Microfluidic chip using as micro-reactor and micro-mixture device ⁽¹⁾; (b) A high-throughput automated cell culture system with integrated multiplexer, peristaltic pump, cell inlet and waste output, [37].

Another example is shown in Figure 2.1 (b), a complicated microfluidic chip with multi-inlet and outlet is used as a high-throughput automated cell culture system with integrated multiplexer, peristaltic pump, cell inlet and waste output [37, 38].

Regarding the miniaturization of the fluidic devices, many researchers realized the benefits of working in small scale of microfluidic devices, because the process inside microchannel has advantages of new effects and better performance. Commonly, the scale of microfluidics corresponds to the scale of study's objectives. The relationship between the volume scale of analyte and length scale of size's devices is shown in

⁽¹⁾ A product of Micronit Microfluidics, <http://www.micronit.com/>

Figure 2.2. It also shows the size characteristics of typical microfluidic devices compared to other common objects.

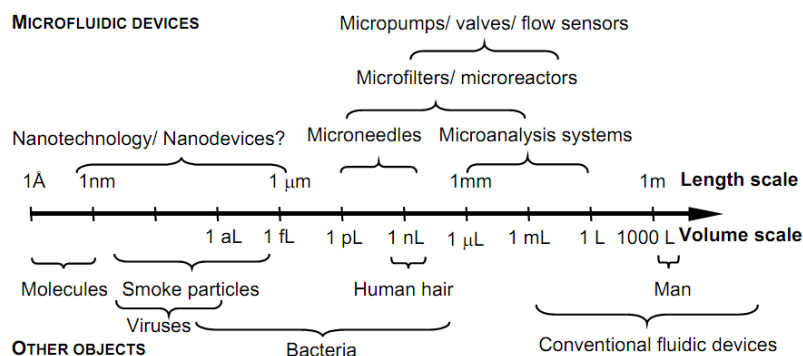


Figure 2.2. Size characteristics of microfluidic devices [39].

- **Microfluidics chip is commonly structured from basic modules:**
 - *Channel network* (including parts of driving flows, function parts for mixing, separating flow, creating droplets or trapping, etc.). Figure 2.3 shows an example of microfluidic chemotaxis device [40]. The device consists of a gradient-mixing module and a chemotaxis observation module. This device is developed for generating precise and stable gradients of signaling molecules to investigate the effects of individual and combined chemo-effector gradients on *Escherichia coli* chemotaxis.

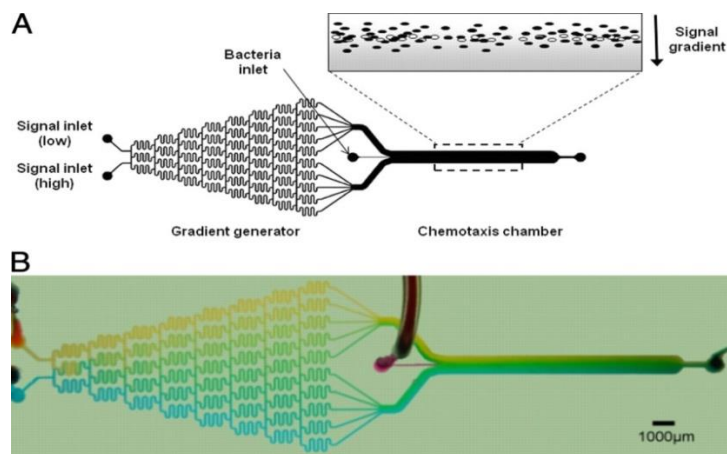


Figure 2.3. Microfluidic chemotaxis device. (A) Schematic representation of the microfluidic device. (B) Food dye representation of gradient formation in the microfluidic device, showing the formation of a range of greens from blue and yellow inputs.

- *Bottom substrate* contains integrated analyzing components (i.e. electrochemical sensors, trapping particles (including magnetic or non-magnetic particles, biomolecules or cluster of molecules, etc.), temperature sensors, heater, optical analyzing components, etc. Some integrated circuits could be also coupled with

microfluidic parts like it is shown Figure 2.4 , an integrated circuit (IC)/microfluidic hybrid system for magnetic manipulation of biological cells [41]. This hybrid system consists of an IC and a microfluidic system fabricated on top. Biological cells attached to magnetic beads are suspended inside the microfluidic system that maintains biocompatibility. The IC contains a microcoil array circuit that produces spatially-patterned microscopic magnetic fields.

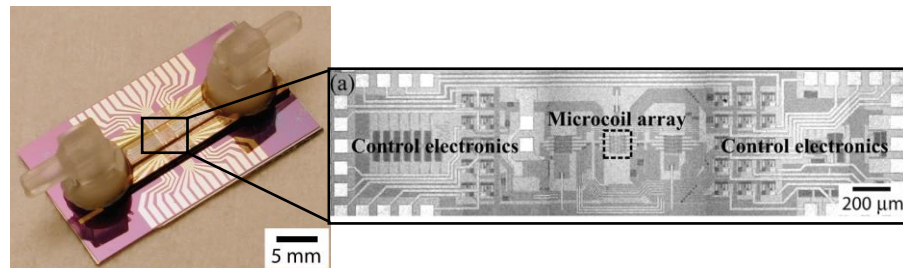


Figure 2.4. SiGe/Microfluidic Hybrid Prototype and Micrograph of the SiGe IC for controlling a microcoil array, [41]

- Tubing connection (for connecting supplier pump of chemical/biological substances and valve switch (internal or exterior valves))
- Motherboard: for connecting bottom substrate to control circuit

b. Advantages of microfluidics in chemical and biological applications:

In literature, a primary goal for much of the microfluidics community is to develop technologies that enhance the capabilities of investigations in biology and medical research. Many microfluidic studies describe methods that aim to replace traditional macro scale assays, and usually perform proof-of-concept experiments that attempt to demonstrate the efficiency of the new approach. A summary of the advantages are listed in Table 2-1.

Table 2-1. Some main advantages attained with microfluidic systems, [42] p-5

Microfluidic Advantage	Description
Less sample and reagent consumption	Microfluidic devices typically require $10^2 - 10^3$ less sample volume than conventional assays.
Enhanced heat transfer	Higher surface area-to-volume ratio of microfluidic channels increases effective thermal dissipation.
Faster separations	Higher E-fields results in faster sample migration.
Laminar flow Electro-kinetic manipulation	Low Reynolds number flows reduce sample dispersion. Electroosmotic flow enables fluid pumping with flat "plug-like" velocity profiles solely via applied E-fields.
Lower power consumption	Fewer components and enhanced thermal dissipation require less power input.

Parallelization	Several assays can be “multiplexed”, or run in parallel on a single chip.
Portability	System integration and reduced power allows for assays to be conducted using portable, hand-held device.
Improved separation efficiency	Efficiency in electrophoretic and chromatographic separations (i.e. number of theoretical plates) proportional to L/d

2.2.2 Microfluidics’ theoretical aspects

In microfluidics, some problems appear with several factor: the size of the section of the channels, the nature of the surface (wettability), capillary force, high electric field, non-ideal fluid (blood, serum, etc.) and emergence of bubbles.

a. Reynolds number

Microfluidic devices almost always boast smooth laminar flow, as opposed to turbulent flow which is of a stochastic nature and marked by the presence of “eddies” that disrupt parallel streamlines. The Reynolds number (Re) compares the magnitudes of inertial force to viscous forces in a flow. It is a dimensionless parameter used to determine the transition from laminar to turbulent regimes ($Re < 2100$ - 2400 : laminar flow, no turbulence, $Re > 4000$: turbulences).

The Reynolds number is defined as, [42]:

$$Re = \frac{D \cdot u}{\nu} \quad (2_1)$$

where u is the flow velocity, ν is the kinematic viscosity (fluid dynamic viscosity on fluid density ratio), and D is the cylindrical channel diameter.

For a diameter of 10 to 100 μm in common conditions, Re is inferior to 1. The fluid is in laminar condition and we can see that the fluid behavior in microchannel can considerably deviate from those in macroscopic devices.

We can note that the surface forces, which originate due to intermolecular forces, could be important in microchannel flows. These forces are generally ignored at macro scale. Surface effects also alter the value of viscosity. It is found that the apparent viscosity is lower in the narrower channel, which is contrary to the expected trend [43, 44].

b. The profile of velocity flow in a rectangle channel

The processes of the fabrication of the channels induce that the channel are never cylindrical. Figure 2.5 shows some plots of the contours of the velocity field and of the velocity field along the symmetry axes, [42]. The fact that, no analytical solution is known to the Poiseuille-flow problem with a rectangular cross-section, it always contains the side-wall effects.

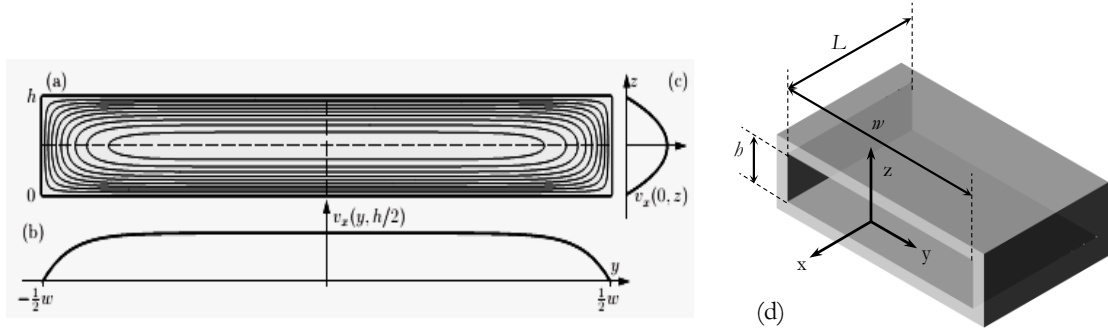


Figure 2.5. (a) Contour lines for the velocity field $v_x(y, z)$ for the Poiseuille-flow problem in a rectangular channel. The contour lines are shown in steps of 10% of the maximal value $v_x(0, h/2)$. (b) A plot of $v_x(y, h/2)$ along the long centerline parallel to e_y (unit vector on y -axis). (c) A plot of $v_x(0, z)$ along the short centerline parallel to e_z (unit vector on z -axis). (d) Geometry and shape of rectangle channel, [42].

In this case, the constant Reynolds number calculus, based on hydraulic diameter needs to introduce a quantity named “laminar equivalent” diameter [45] D_h defined by:

$$D_h = 2 \frac{hw}{h+w} \quad (2_2)$$

$$Re_h = \frac{D_h \cdot u_x}{\nu} \quad (2_3)$$

where u_x is the average velocity along x axis

Based on the Re value and velocity profile of the liquid in channel, the mixing and cleaning process inside channel need to be controlled by controlling the flow rate of liquids in experiments in order to limit the side-wall effect. Designed specific mixing three zones are added in channel networks to improve the mixing of substances in experiments.

2.3 Magnetic bead-based immunoassay

This part of chapter will discuss about the state of the art of objectives in bead-based microfluidic systems applied for immunoassay.

Nano/micro beads are frequently used as an immobilization/carrier surface to capture target analytes of interest in immunoassay, such as proteins and nucleic acids, from a biological sample. Nano/micro magnetic beads offer several advantages over planar surfaces (in standard ELISA protocol in wells) such as large specific surface to support biological interactions (increasing sensitivity or decreasing the limitation of analyte concentration). In the ELISA test, the typical sandwich structure is created as shown Figure 2.6. With the availability of the serial of commercial beads and multi-functionalization of microfluidic system, multiple targets in samples can be detected simultaneously.

The integration of microcoils as electromagnet into microfluidic systems for magnetic beads-based biosensing is interesting to replace the permanent magnet in ELISA test in micro test tube because in this case, the external magnetic field can be controlled automatically by an electric circuit to attract the beads, stop the trapping or maintain the magnetic field.

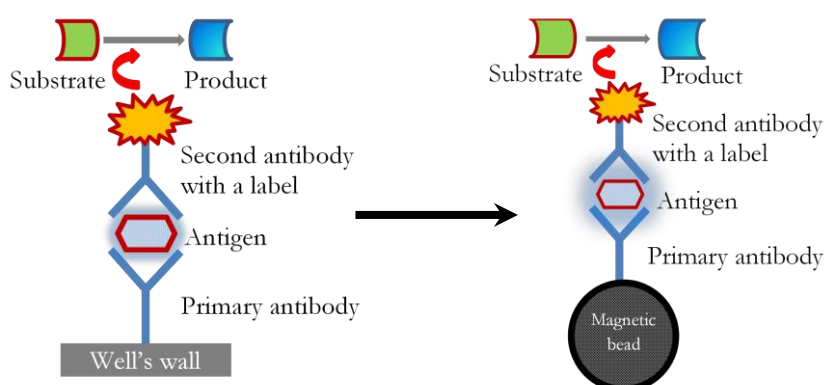


Figure 2.6. Sandwich structure of ELISA test on well's platform and on beads' surface

2.3.1 Magnetic micro/nano beads in immunoassay

In the development of building the bead-based immunoassay inside microfluidic chip, all materials such as: nano/micro magnetic beads with functional groups, primary antibody (or capture antibody) targets, second antibody with fluorescent label (or detection antibody), which concern to the immobilization antibody (IgG-type) in chapter of the application of microfluidic chip, are presented in the next section.

a. Introduction of functionalized magnetic beads

Specific antibodies are immobilized on beads' surface and are enable to couple the specific target cells/proteins or viruses. Then, these beads are separated in the

solution by using a magnetic force (generally a magnet). Currently, commercial micro/nano magnetic beads are available and they are used in research, pilot research or analytical devices [46, 47].

In current applications, beads can be classified into two main types: non-magnetic (silica and polymer beads) and magnetic/super-paramagnetic beads (iron oxide – Fe_2O_3 or Fe_3O_4 , alloy or rare earth materials – NbFeB or SmCo), but the majority of these particles are super-paramagnetic, i.e. they have no magnetic memory. The size of these beads, which can play an important role, is in range of few nanometers to few micrometers and selects exactly the diameter.

The surface's beads could be also functionalized/immobilized by specific functional groups corresponding to the aims of analyzing processes. There are some common types of functionalization, Figure 2.7:

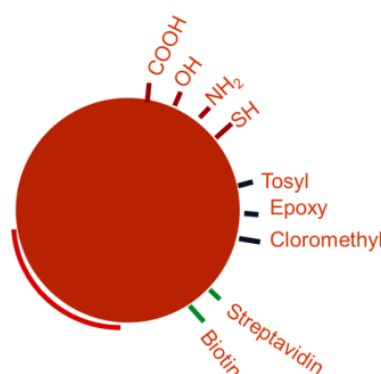


Figure 2.7. Description of functional groups on beads' surface

Many types of commercial super-paramagnetic nanoparticles (fabrication, physical and chemical properties, bio-compatible characterization, etc.) for many applications are introduced in [47]. In our study, we use commercial carboxyl magnetic beads of 300 nm diameter (Carboxyl-Adembeads, purchased from Ademtech).

These beads are uniform Super-Paramagnetic Iron Oxide Nanoparticles (SPIONs), Figure 2.8 shows the core shell structure of carboxyl-Adembeads.

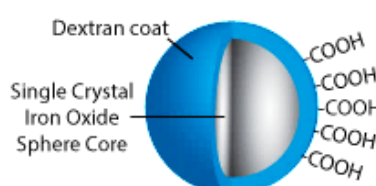


Figure 2.8. The description of the core and shell structure of Carboxyl-Adembeads

Physical characteristics ⁽¹⁾:

- Diameter: 300 nm (CV max 20%)
- Density: approx. 2.0 g/cm³
- Magnetization at saturation: approx. 40 emu/g
- Specific surface area: 15 m²/g
- Iron oxide content: approx. 70%
- COOH density: > 350 μ mol/g
- Solid content: 30 mg/ml (3%)

b. Magnetic properties of the materials of bead's core

Generally, super-paramagnetic materials are preferred to fabricate cores of magnetic beads. The most important behavior of this material shares with para-magnetism the absence of magnetization when the external magnetic field is removed and with ferromagnetism the high levels of magnetization reached under the influence of a low magnetic field.

Other interesting properties these beads are their short relaxation time in which magnetization goes to zero after the effect of an external magnetic field (typical values are around 10⁻⁹-10⁻¹⁰s). Under an alternating external magnetic field, their magnetic moment is quickly reoriented.

A comparison of magnetic properties between ferromagnetic and super-paramagnetic materials is shown in Figure 2.9, we can see that the super-paramagnetic nanoparticles show no remanent magnetization (M_r).

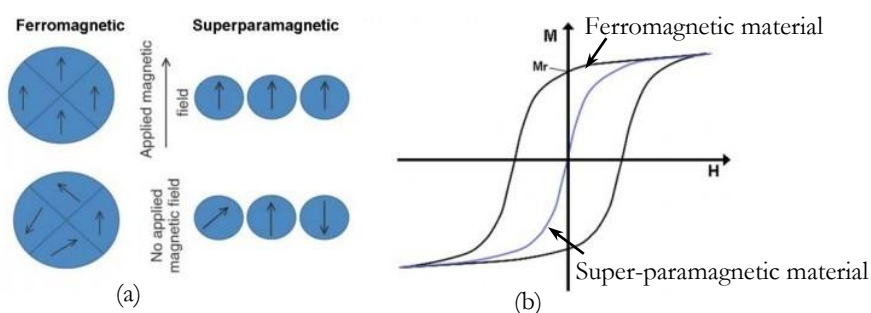


Figure 2.9. (a) The magnetic moments of both ferromagnetic and superparamagnetic nanoparticles under an external magnetic field/ no magnetic field; (b) Typical magnetization curves of ferromagnetic (black line) and super-paramagnetic (blue line) particles. [46, 48].

⁽¹⁾ <http://www.ademtech.com/>

2.3.2 Immunoassay principles

2.3.2.1 Introduction of immunoassay

It is known that, an immunoassay is a test that relies on biochemistry to measure the presence and/or concentration of an analyte. There are two strategies using this method: qualitative (yes or no) or quantitative results.

Analytes can be normally large proteins, antibodies produced in human bodies as a result of an infection. These assays are highly adaptable and can be applied to many formats depending on the needs of the end user. Principle components of an immunoassay designed to detect a specific analyte, (such as influenza nucleoprotein, Alzheimer or cancerous markers) are the antibodies carefully selected to ensure the detection of the analyte **at low concentration with high specificity**, meaning will not react with similar antigens. The second feature of an immunoassay is the system that is designed to detect the binding of the specific antibody to the target analyte. Originally the signal from an immunoassay resulted from an enzyme acting on a substrate to yield a colored solution with the amount of color in the solution being equivalent to the amount of antigen in the test solution (ELISA).

ELISAs can be developed with a number of modifications to the basic procedure. The key step of ELISA format, immobilization of the antigen of interest, can be accomplished by direct adsorption to the assay plate/special surface (bead's surface or channel's surface) or indirectly via a capture antibody that has been attached to the surface. The antigen is then detected either directly (labeled primary antibody) or indirectly (labeled secondary antibody). The most powerful ELISA assay format is the sandwich assay. This type of capture assay is called a "sandwich" assay because the analyte to be measured is bound between two primary antibodies – the capture antibody and the detection antibody. The sandwich format is used because it is sensitive and robust, and we have already talked about this in the previous section.

Generally, the immunoassay can be classified into some approach methods:

- *Competitive vs. non-competitive*: In a competitive immunoassay there is a competition between labeled and unlabeled antigen for a limited number of binding sites on the antibody. All reactants are mixed together either simultaneously or sequentially. In a typical non-competitive assay (immunometric assay) an excess amount of an antibody is used to capture the analyte from the sample. A labeled second antibody

is added and binds to the first antibody-antigen complex to form a sandwich. The complex formed is then measured. Non-competitive techniques are more sensitive and reproducible than competitive ones.

- *Homogenous vs. Heterogeneous*: Heterogeneous assays involve the binding of antigen to antibody followed by physical separation of the bound antigen from the unbound antigen prior to measurement. If the immunoassay does not require any physical separation step after mixing antigen and antibody and measurement of bound label occurs in the presence of unbound label, the assay is homogenous. Heterogeneous assays tend to be more versatile and sensitive.
- *Isotopic vs. non-isotopic*: Isotopic immunoassays use radioactive labels on the antigen or antibody. Non-isotopic methods use enzyme reactions, chromophores, fluorescent labels, or luminescent labels in order to detect the antigen-antibody complex.
- *Limited reagent vs. excess reagent*: In limited reagent assays, the number of available binding sites on the antibody is limited compared to the concentration of labeled and unlabeled antigen (a competitive immunoassay). Non-competitive assays are reagent excess assays.

In the study on the application of microfluidic chip for immobilizing antibody IgG-type on surface of the carboxyl-beads in next chapter, the process of immobilization is based on the method of competitive vs. non-competitive. This method is popularly used in most of ELISA test inside channel or in micro test tube. This method has also some advantages compares to other methods: ***high specificity***, since two antibodies are used the antigen/analyte is specifically captured and detected; ***suitable for complex samples***, since the antigen does not require purification prior to measurement; ***flexibility and sensitivity***, since both direct and indirect detection methods can be used.

2.3.2.2 Bio-components in immunoassay

As described in previous part, the sandwich ELISA format is preferred in many protocol of immunoassay (i.e. detection Alzheimer marker, cancerous marker, etc.) [49, 50]. In each ELISA assay, there are some basic components that are used in procedure. Three necessary ELISA reagents include: immune-sorbents (solid phase); conjugates (antibodies, antigens and enzyme); and substrates (substrates of enzyme).

a. Capture antibody and immuno-sorbent/solid phase

All ELISAs rely on the specific interaction between an epitope, a small linear or three dimensional sequence of amino acids found on an antigen, and a matching antibody binding site. The antibodies used can be either monoclonal (derived from unique antibody producing cells called hybridomas and capable of specific binding to a single unique epitope) or polyclonal (a pool of antibodies purified from animal sera that are capable of binding to multiple epitopes). However, polyclonal antibodies are more typically used for the secondary detection layer in indirect ELISAs, while monoclonal antibodies are more typically used for capture or primary detection of the antigen.

In sandwich ELISA structure, primary antibodies (conjugate antibodies) supplied as commercial products are immobilized on solid surface. In some cases, the immune-sorbent is only coated by functional groups (amine or carboxyl groups), antibodies will be immobilized on activated solid surface in separating step:

The *Immuno-sorbent* (Solid support which has been coated antibodies or antigens) is commonly provided as commercial product (i.e. wells array or particles with nano or micro size of diameter). For particles, they were introduced in previous part. For wells array, they are usually made in polystyrene, cheap material which can present large kind of shapes. This material is strong in adsorbing protein. Antibody or protein antigen remains activity after adsorbed on it.

The *Primary antibodies* (or conjugated antibodies) are immobilized on solid supports. These antibodies are the specific ones which able to conjugate with a specific targets in sample. Thus, proteins G, A, D, E or M type are usually used. In many application, IgGs (main antibody in blood Figure 2.10) are commonly used as a primary antibodies, because of the simple manipulation, population and cost. It is the only isotype that can pass through the placenta, and transferred from the mother's body protects a newborn until a week after birth.

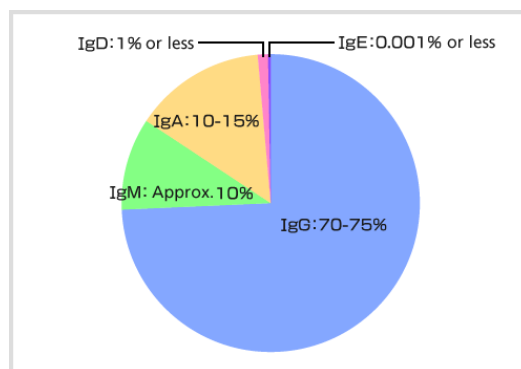


Figure 2.10. Population of 5 types of antibodies in blood (%) ⁽¹⁾

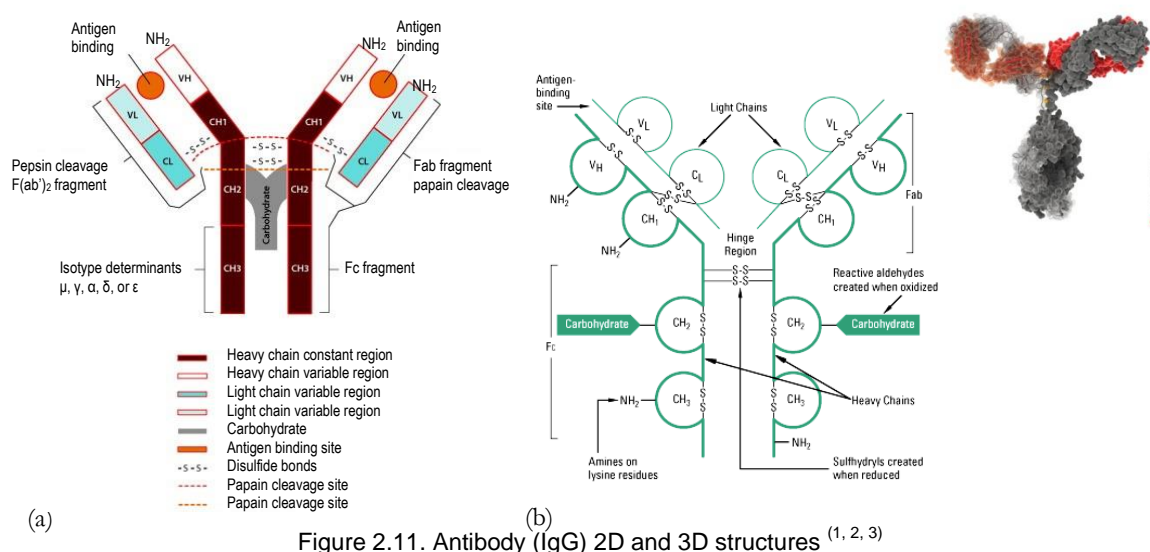
▪ Chemical and biological characterization of antibody IgG-type:

In the chapter 4, this antibody will be used for all experiment of immobilization antibody on carboxyl magnetic beads. All properties as shown below are important to understand the interaction of this antibody to other substances in reaction solution.

It is known that, immunoglobulins (Igs) are produced by B lymphocytes and secreted into plasma. The Ig molecule in monomeric form is a glycoprotein with a molecular weight of approximately 150 kDa that is shaped more or less like a Y [51]. Basic structure of the Ig monomer (Figure 2.11) consists of two identical halves connected by two disulfide bonds. Each half is made up of a heavy chain of approximately 50 kDa and a light chain of approximately 25 kDa, joined together by a disulfide bond near the carboxyl terminus of the light chain. The heavy chain is divided into an Fc portion, which is at the carboxyl terminal (the base of the Y), and a Fab portion, which is at the amino terminal (the arm of the Y). Carbohydrate chains are attached to the Fc portion of the molecule. The Fc portion of the Ig molecule is composed only of heavy chains. Fc regions of IgG and IgM can bind to receptors on the surface of immune-modulatory cells such as macrophages and stimulate the release of cytokines that regulate the immune response. The Fc region contains protein sequences common to all Igs as well as determinants unique to the individual classes. These regions are referred to as the constant regions because they do not vary significantly among different Ig molecules within the same class.

Each IgG monomer is capable of binding two antigen molecules at each amino terminal of the left and right Y's arm. However, amine groups at these positions are different properties and have different behavior in solution during reaction time [52].

⁽¹⁾ <http://www.kyowa-kirin.com>

Figure 2.11. Antibody (IgG) 2D and 3D structures ^(1, 2, 3)

In generally, the immobilization of IgG does not discriminate between possible attachment points near or removed from the specific binding site, which results in spatial orientation of antibodies on the supports that might prohibit formation of an antibody-antigen complex. For instance, if multiple lysine groups, Figure 2.11.b, are present on the surface of an antibody molecule, multiple attachments might occur. This may result in different orientations of the antibody on the support surface depending on which lysine group binds to the support. When immobilization occurs through the antigen binding sites on the Fab' portions, the ability of that antibody to bind antigen may be severely impaired or eliminated entirely [53].

b. Detection antibodies (antibodies conjugated enzyme)

Detection antibodies, as commonly called secondary antibodies, are specific anti-Fabs of antibodies. A secondary antibody aids in the detection, sorting or purification of target antigens by binding to a primary antibody, which directly binds to the target antigen. Secondary antibodies offer increased sensitivity through the signal amplification that occurs at two labeled secondary antibodies binding to the two Fab fragments of primary antibodies. In addition, a given secondary antibody can be used with any primary antibody of the same isotype and target species, making it a more versatile reagent than individually labeled primary antibodies.

⁽¹⁾ <http://www.sigmaaldrich.com>

⁽²⁾ <http://visual-science.com>

⁽³⁾ <http://www.piercenet.com/method/antibody-labeling-immobilization-sites>

Second antibodies are commonly conjugated with enzyme, or some time with only fluorescence/dye. They may be provided in several formats: whole IgG, divalent F(ab')₂ fragments and monovalent Fab fragments. Figure 2.12 shows the structure of FITC-conjugated antibody ⁽¹⁾ (type G) that is commonly used in immunoassay. This substance is also used to detect the grafted antibody IgGs on carboxyl beads in the study of [chapter 4](#).

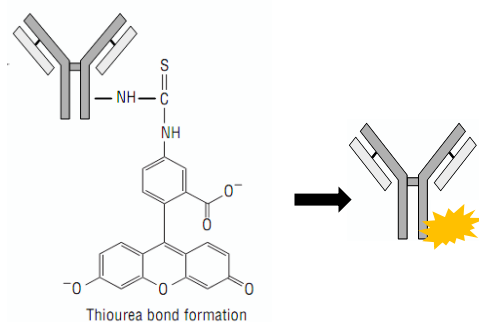


Figure 2.12. FITC-conjugated antibody (IgG)

c. Enzyme and antigens

- Enzymes used in ELISA should meet requirements such as high purity, high conversion rate, favorable specificity, stable properties, rich resources, cheap price and remaining active component and catalytic capacity after becoming conjugate.. In addition, corresponding substrate is easy to be made and stored. Non-ferrous products are easy to be detected. In ELISA, horseradish peroxidase (HRP) and alkaline phosphatases (AP) are usually used.
- Antigen: Antigens (targets in analytes) are components which are interested in analyzing propose. Antigens are any substance that stimulates the immune system to produce antibodies. Antigens can be bacteria, viruses, or fungi that cause infection and disease. They can also be substances, called allergens, which bring on an allergic reaction. Blood transfusions containing antigens incompatible with those in the body's own blood will stimulate the production of antibodies, which can cause serious, potentially life-threatening reactions.

2.3.3 General protocol of magnetic bead-based immunoassay

We have already mentioned that, the bead-based immunoassay present a very high sensitivity and selectivity [6, 54-56].

⁽¹⁾ Fluorescein isothiocyanate – conjugated antibody

In bead-based immunoassay, the reacted or immobilized magnetic beads can be easily separated from the reaction mixtures with a magnet and re-dispersed immediately following removal of the magnet. Therefore, this protocol has been used in a variety of research fields, such as food safety [57], environment monitoring [58], and clinical diagnosis [59].

Figure 2.13 shows a general protocol of bead-based immunoassay that is performed in micro test tube based on immune-magnetic capture and bacterial intrinsic peroxidase activity for a quick detection of *Shewanella oneidensis* ⁽¹⁾, [60]. This protocol includes two processes: (a) The preparation of functionalized magnetic beads (MBs) and immobilizing primary antibodies on beads' surface; (b) The procedure of the colorimetric immune-magnetic assay.

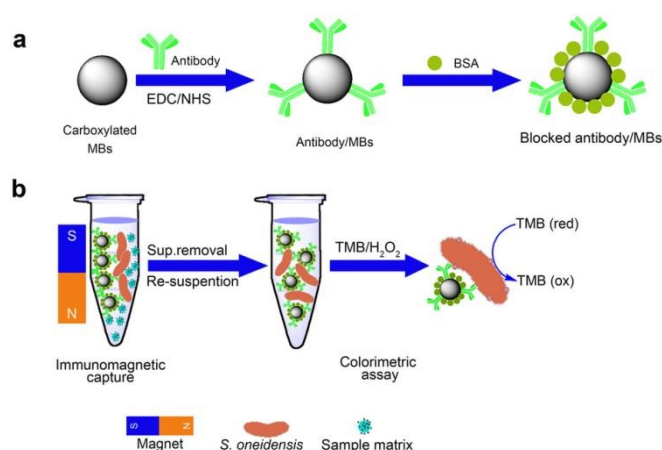


Figure 2.13. Schematic for the antibody/MBs preparation and colorimetric immune-magnetic assay. (a) Preparation procedure of antibody/MBs. (b) The procedure of the colorimetric immune-magnetic assay [60].

In general, the protocol of basic bead-based immunoassay includes following step:

- Activating the functionalized nano/micro magnetic beads by activation chemicals – chemical process (e.g. for carboxyl magnetic beads, EDC and Sulfo-NHS ⁽²⁾ are used to activate the carboxyl groups).
- Immobilizing primary/capture antibody (e.g. IgG-type) on activated beads' surface and blocking immobilized antibodies by bovine serum albumin (BSA) – blocking agent.
- Capturing antigens or biomarker in sample solution, as called immuno-magnetic capture. In this step, antigens/biomarkers are captured by primary antibodies

⁽¹⁾ A bacterium which can reduce poisonous heavy metal and can live in both environments with or without oxygen

⁽²⁾ EDC: 1-ethyl-3-(3-dimethylaminopropyl) carbodiimide; Sulfo-NHS: N-hydroxysulfosuccinimide

- Detecting antigens by fluorescent detection or other methods (e.g. electrochemical detection, time-resolved fluorescence, enzyme-based photometric etc.)

In the study of chapter 4, the immobilization of antibody type-G will be based on this protocol.

2.4 Microfluidics in magnetic bead-based immunoassay

Like the method in standard immunoassay, the microfluidic immunoassay is mainly performed basing on bead-based immunoassay. It means that, the antibodies and antigens can be immobilized on the surface of the microchannels or beads. Immobilization on surfaces of microchannels requires additional steps during the microfabrication process and may suffer from poor reproducibility and reliability. In addition, bead-based immobilization can be performed outside the microchip [61, 62].

2.4.1 Magnetism and trapping/transporting magnetic beads in microfluidics

Manipulating magnetic micro/nano beads in microfluidic chips can be done efficiently with permanent/electro magnets [13, 63-65]. The permanent magnet is known to generate a strong magnetic flux density, *i.e.* from few hundreds mT to 1 T [16, 66, 67]. However, the permanent magnet only generates a permanent field. Consequently, removing or diminishing the magnetic field requires mechanically moving the magnet. Therefore, the magnetic field cannot be turned off immediately.

2.4.1.1 Permanent magnet for manipulating magnetic beads in microfluidics

The best magnetic material using to fabricate permanent magnet is neodymium iron boron (NdFeB). It can generate very strong and stable magnetic field event in small dimensions.

Figure 2.14 shows the magnetic field simulation of different shapes of NdFeB magnets, which generate complex magnetic field patterns event on the small size of magnets. The Figure 2.14 (a) shows the homogenous magnetic field generating by a magnet bar, this field is required for NMR spectroscopy and magnetohydro-dynamic pumping. But it is also suitable for trapping stably magnetic beads in bead-based immunoassay. Figure 2.14 (b) and (c) show inhomogeneous magnetic field generating by needle magnet in NdFeB material or layered structures magnet in iron with the aim is to trap particles or transport materials within a fluid volume.

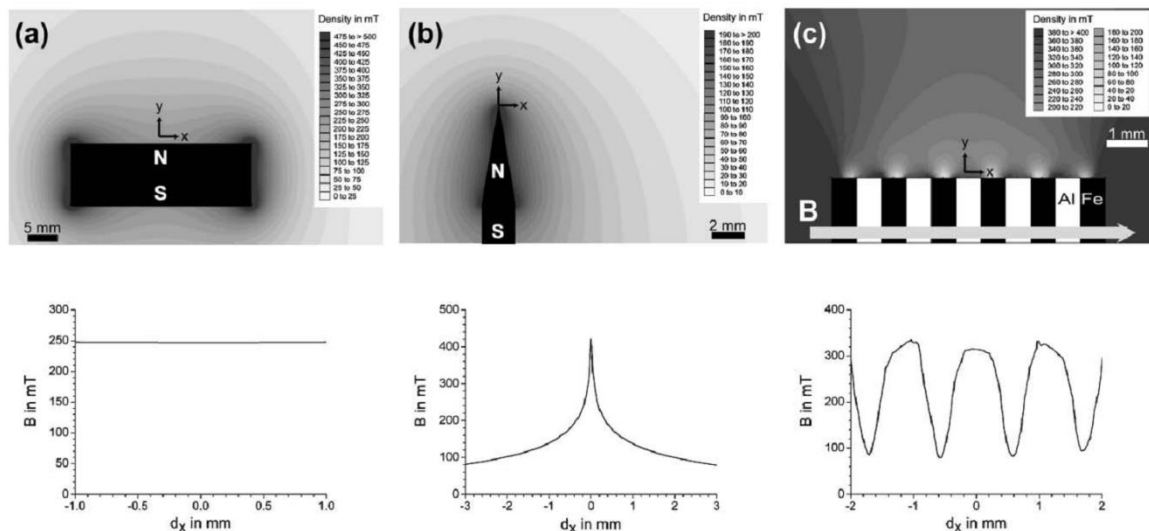


Figure 2.14. Magnetic fields from permanent NdFeB magnets modelled with FEMM-software [68]: (a) A homogeneous field at a distance of 1 mm along the surface of a large magnet. (b) An inhomogeneous field 100mm above the surface of a tapered magnet. (c) A magnetic field with local minima and maxima at 100mm distance above a stack of alternating iron and aluminum blocks.

As an example of use of external magnet, B.A. Otieno et al., 2014 [30], describe the incorporation of a novel on-line chamber to capture cancer biomarker proteins on magnetic beads, which are derivatized with 300,000 enzyme labels and 40,000 antibodies into a modular microfluidic immunoarray (Figure 2.15).

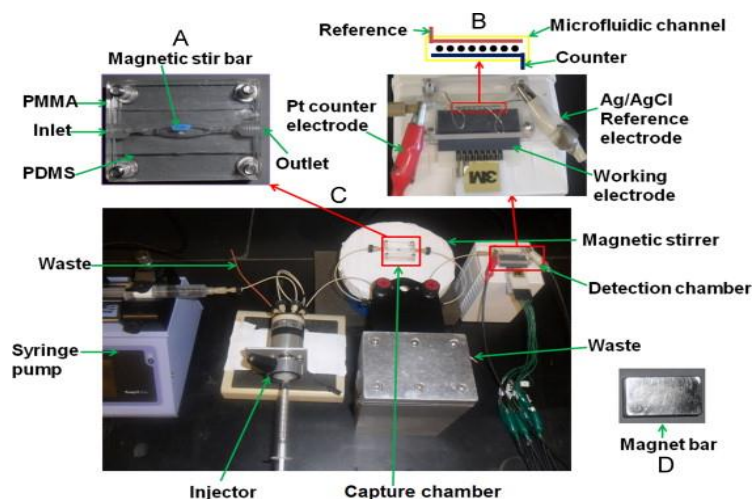


Figure 2.15. Photographs of microfluidic system for on-line protein capture and detection using magnetic beads: (A) Capture chamber in which target proteins are captured on-line from the sample by heavily labeled HRP-antibody-magnetic beads to form protein-bead bio-conjugates. These are washed, and then flowed into the detection chamber (B) in the modular microfluidic system (C). The magnet (D) traps bio-conjugate beads in the channel during injection of sample and washing, and is removed for transfer of beads to the detection chamber, [30].

The capture chamber features an internal layer of flexible PDMS prepared on a machined template to have an oval hole sandwiched in between two flat, machined PMMA plates (Figure 2.15. A). When bolted tightly together, this assembly forms an

oval cylindrical channel 1.5 mm wide, 1.8 mm thick and $100 \pm 2 \mu\text{L}$ in volume housing a tiny magnetic stir bar. In the capture chamber, the magnetic beads are mixed and trapped by the magnetic stir bar. This magnetic bead position is controlled magnetically in the on-line capture chamber for rapid binding of proteins, washing, and delivery to the detection chamber.

2.4.1.2 Electromagnet for manipulating magnetic beads in microfluidics

The use of electromagnets can be a very attractive alternative solution because these magnetic field sources can be controlled and have a fast response. Electromagnets are coils with or without an associated magnetic circuit (e.g., magnetic core). However, electromagnets generate a weaker magnetic field than the one generated from permanent magnets for equivalent dimensions. To enhance the magnetic field strength, high current or special design with extra parts is required [69]. In general, the design of electromagnet is based on some types of geometries such as planar/spiral coils, 3D coils or magnetic tweezers, coil with encapsulated magnetic material cores (e.g. ferromagnetic oxide, Permalloy) [69-72]. Single coil or coils array have been already integrated in microfluidic chip for trapping, mixing or moving magnetic beads [70, 73, 74].

In the case of planar coils (fabricated in single layer coil or multi-layer coil in order to improve the magnetic flux density [41, 70, 75]), the most popular shapes of electromagnet, the magnetic flux density is usually low, from few mT to few hundreds mT depending on the parameters of the coils [76, 77].

Of course, the magnetic field depends on the geometry of coils, and it also depends on the current density applied to coils. When designing coils, in addition to generating the maximum magnetic flux density or magnetic force, the power consumption/power efficiency and heat generation of coils are careful trade off as well.

To design microcoils for application of trapping/mixing magnetic beads and integration into microfluidic chip, the simulation and calculation of magnetic field or magnetic force are required. The results of the calculation based on a simulation model will definite the geometry of coils or other parameters such as: number of turns, dimensions of conductor, etc. The optimal geometries of coils are based commonly on general requirement of the maximum value of magnetic field/force, the

minimum value of power consumption or homogeneous magnetic field, etc. The magnetic field of planar coil is usually calculated basing on the Finite Element Modelling/Method (FEM), and the simulation/calculation software is commonly used as a useful tool for the big simulation (i.e. MatLab®, ANSYS®, COMSOL Multiphysics®).

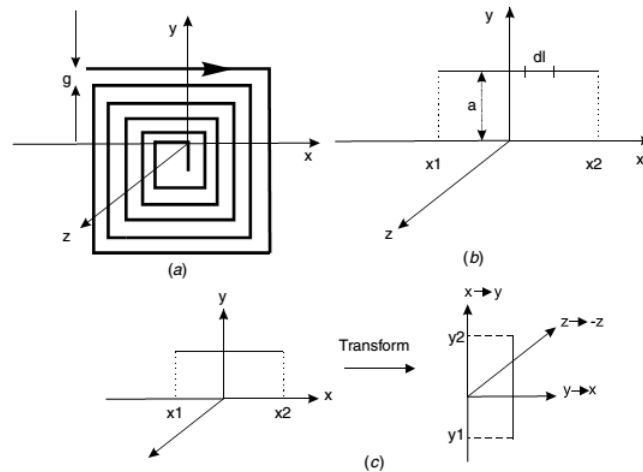


Figure 2.16. Wire arrangement for modeling a planar coil. (a) Wire arrangement of a planar rectangular coil. (b) Arrangement of a horizontal wire segment with finite length. (c) Coordinate transformation to formulate the magnetic field of a vertical segment of wire [76].

Beyzavi et al. [76] used the simple analytical model for the magnetic field of a single straight wire to a spiral shaped rectangular planar coil. This model can then be used for the calculation of the strength, the flux and the resultant force of the magnetic field generated by the microcoil. It also helps to find maximize the field strength and the force. In Figure 2.16, a model of planar coil is used to calculate magnetic field and force. The planar coil is composed of a series of current-carrying wires with finite length, and the magnetic field is calculated from each magnetic field element created by each wire of a finite length should be obtained in the calculation domain. Figure 2.16.a shows the wire arrangement of a planar rectangular coil. Each straight segment of the coil is termed here as a wire segment. Four consecutive wire segments form a turn. Thus, if the number of segments is n , the number of turns is approximately $n/4$. The superposition of the magnetic fields of all these segments results in the total magnetic field of the coil.

Figure 2.17 shows the typical results of the model for a rectangular coil. The field strength was calculated for a line running along the x-axis and through the center of the coil. The modeling results show that the total magnetic field (H_{total}) of a planar

coil has almost the same trend and magnitude as the z-component of its magnetic field strength (H_z).

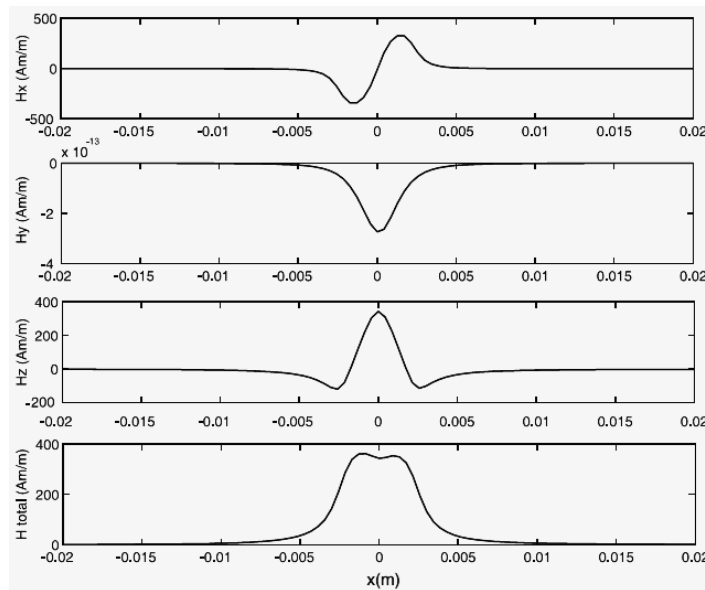


Figure 2.17. Modeling results for magnetic field distribution of a single planar coil on the central line of the coil ($n=47$, $g=200 \mu\text{m}$, $l=0.3\text{A}$, $y=0 \text{ mm}$, $z=1 \text{ mm}$) [76]

R. Fulcrand et al. [70] designed an integrated complex magneto-fluidic lab-on-chip, which is composed of multiple inlets and multiple microcoils within one single device. This simulation model is more complicated than model shown above. A serial of microcoils designs are proposed, and the magnetic field and magnetic force for the trapping and driving beads in microfluidic chip are calculated. The simulation models and results are shown in Table 2-2 and Table 2-3.

Table 2-2. Micro-coils designs and dimensions [70]

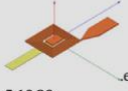
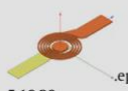
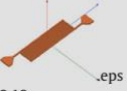
Microcoil design	Square	Circular	Serpentine
3D overview			
Number of turns	5,10,20	5,10,20	9,19
Wire section ($\mu\text{m} \times \mu\text{m}$)	5×5	5×5	5×5
Wire space (μm)	5	5	5

Table 2-3. Maximum magnetic flux density, field gradient and magnetic force, $5 \mu\text{m}$ and $50 \mu\text{m}$ into the microfluidic channel for each design. $I = 100 \text{ mA}$ [70].

	Square	Circular	Serpentine
$B_{Z\text{max}}$ (mT) ($z = 5 \mu\text{m}; 50 \mu\text{m}$)	6.48; 2.34	5.46; 1.78	2.21; 0.3
dB_z/dz (T/m)	180	175	475
$F_{Z\text{max}}$ (pN) ($z = 5 \mu\text{m}; 50 \mu\text{m}$)	2.38; 0.13	2.01; 0.1	0.25; ≈ 0

As shown in Table 2-3, the magnetic flux density along the z and x axes B_x vanishes rapidly with the distance of the particle to the microcoil. Additionally, the

values $B_{z,\max}$ obtained with square and circular for $z = 5 \mu\text{m}$, *i.e.* at the bottom of the channel, are approximatively 3 times higher than those obtained with serpentine structures. Figure 2.18 shows the results of trapping and driving magnetic beads inside microfluidic chip with the arrangement of microcoils in channel.

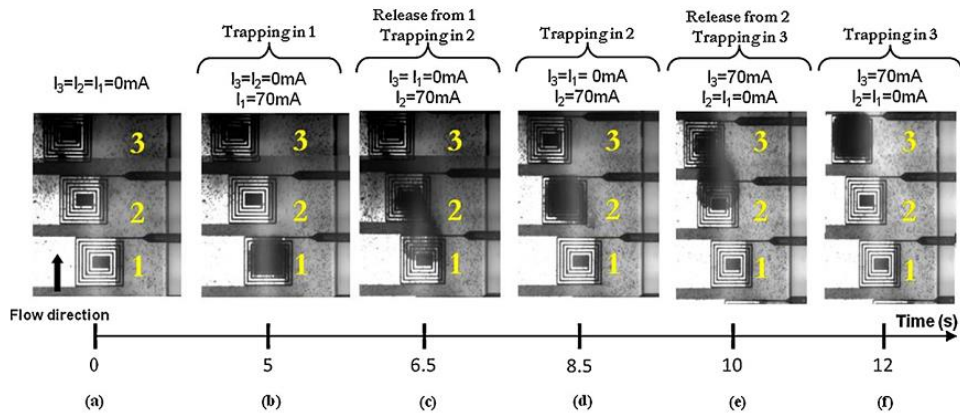


Figure 2.18. Video sequence showing the manipulation of microbeads batch by successive trapping and release. (a) Flow is established and microbeads are injected in the main channel, all micro-coils are switched off. (b) Micro-coil No. 1 is supplied with a current $I = 70 \text{ mA}$, microbeads are trapped. (c) Micro-coil No. 1 is switched off while micro-coil No. 2 is simultaneously powered at $I = 70 \text{ mA}$, the beads batch is shifted from micro-coil 1 to micro-coil 2. (d) The bead batch is immobilized on micro-coil 2 as long as necessary and released in the same way than previously (e) and (f), [70].

A 0.75 nL/s laminar flow was established and microbeads were injected. The first micro-coil was then supplied with 70 mA during 5 s in order to trap a batch of microbeads (Figure 2.18 (b)), which is subsequently displaced by the sequential actuation of two other micro-coils (Figure 2.18 (c–f)). Microbeads' batches can eventually be deflected into a desired outlet taking advantage of the uni-directionality of laminar flows.

One important disadvantage of the use of electromagnets is heat generation induced by the Joule effect [74, 78]. Evaluating the temperature raise is of crucial importance for chips using biological species: an operating temperature range is often required for biological binding reactions or temperature needs to be kept below certain limits in order not to destroy the biological species. In the literature, temperature raise originated from the coils is compensated by several means. In [79], a cooling channel network is integrated in the multi-layered thermal chip to extract heat from coils. In [41], the IC/microfluidic hybrid chip with microcoil array is assembled with a Peltier module (thermoelectric cooler) in order to keep the system temperature at 37°C . A good strategy to limit the need of cooling devices consists in limiting the thermal emission of the coil. Obtaining magnetic field with low energy

could even make unnecessary active cooling. In [74], control strategies of the current flowing through trapping microcoils (by current variation) are used to limit the chip heating to reasonable values. Despite the crucial importance of thermal considerations, very few literatures exist on the thermal design of microcoils.

2.4.2 Bead-based immunoassay inside microfluidics

In this part, some typical studies on applying microfluidic chip with magnet or microcoils in immunoassay are presented.

Lin et al. [80] reported a magnetic bead-based immunoassay using a secondary antibody to label negatively charged DNA fragments for signal amplification. They used an externally magnetic force attaching the analyte tightly to the sensor surface, thereby effectively solving the problem of the analyte protein's distance to the sensor surface surpassing the Debye lengths. The experiment protocol is shown in Figure 2.19.

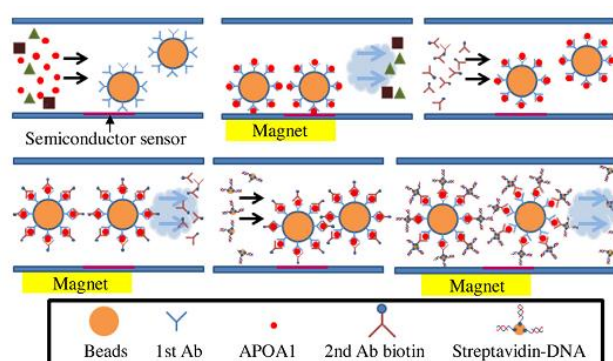


Figure 2.19. Bead-based immunoassay in integrated semiconductor sensor microfluidic chip for detecting apolipoprotein A1 (APOA1) by building sandwich ELISA structure Bead-1st Ab-APOA1-2nd Ab-Streptavidin DNA. The streptavidin-DNA is detected by the semiconductor sensor, [80]

In this study, using a 120 nm magnetic bead, the minimum detection limit of 12.5 ng/mL apolipoprotein A1 can be measured by an integrated semiconductor sensor with a microfluidic chip. Magnetic beads, which are used as a pre-concentrating APOA1 surface, are trapped by a permanent magnet. This magnet is manually manipulated under the bottom of chip.

Choi et al. [72] presented a full on-microfluidic chip immunoassay, including full performing steps of sandwich ELISA inside microchannel and electrochemical detection, as shown in Figure 2.20 using microcoils.

This experiment was performed in a microfluidic chip, which combined two components: capturing beads part with embedded serpentine conductor with semi-

encapsulated Permalloy (electromagnet) for preparing the sandwich ELISA on beads' surface; and detection part with integrated electrochemical electrodes, as shown in Figure 2.21.

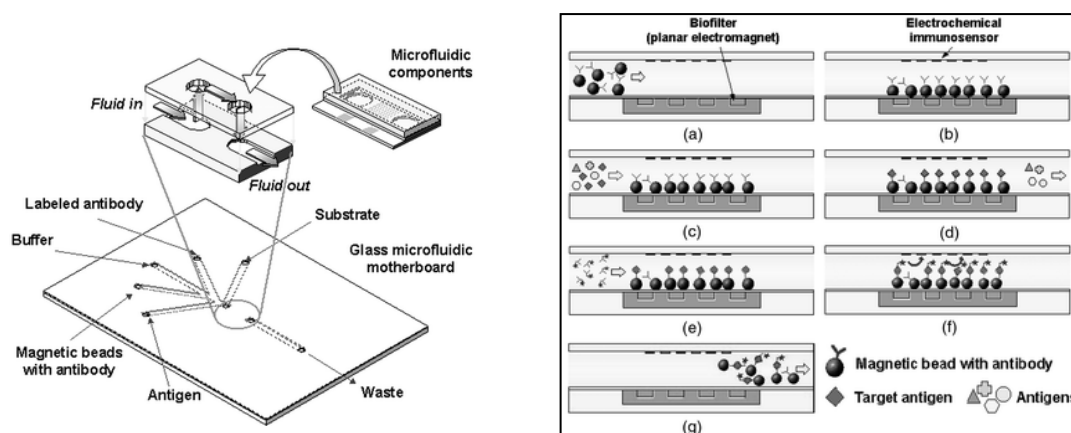


Figure 2.20. Illustration of microfluidic interconnection and surface-mounting technique; Conceptual illustration (on the right) of bio-sampling and immunoassay procedure using magnetic bead approach: (a) injection of magnetic beads; (b) separation and holding of beads; (c) flowing sample; (d) immobilization of target antigen; (e) flowing labeled antibody; (f) electrochemical detection after adding enzyme substrate; and (g) washing out magnetic beads and ready for another immunoassay, [72]

The result showed that, total time required for an immunoassay was less than 20 min including sample incubation time, and sample volume wasted was less than 50 ml during five repeated assays. Fast and low-volume biochemical analysis has been successfully achieved with the developed bio-filter and immune-sensor, which is integrated to the microfluidic system.

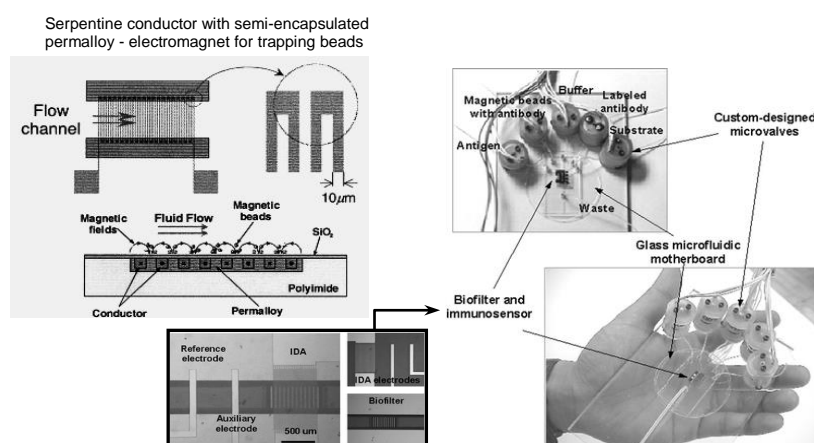


Figure 2.21. Photograph of the fabricated microfluidic biochemical detection system for magnetic bead-based immunoassay; Microphotograph of the integrated bio-filter and biosensor [72]; Serpentine conductor with semi-encapsulated permalloy – electromagnets/bio-filter [81].

It is concluded that, the microfluidic chip with embedded electromagnet and integrated electrochemical electrode is designed and developed to apply effectively to immunoassay.

Finally, the development of microfluidic systems is opened new approach methods in immunoassay with the aim of minimizing and automatizing the devices. In addition, the sensitivity and consumption time/power of analyst methods are interesting. In case of the manipulation magnetic nano/micro beads in microfluidic chips for the bead-based immunoassay, the external magnetic field is generated effectively by electromagnet or permanent magnet. The results of immunoassay prove that each type of magnet (permanent or electro magnet) has specific advantages. Although the electromagnet need a complicate fabrication process, the generated magnetic field is easy to control in the experiment. In contrast, the permanent magnet does not need a fabrication process, the control of the magnetic field is done by manually moved the magnet.

2.4.3 Microfluidics fabrication

Microfluidic device is constituted from two main components: microchannel networks and bottom substrates. The channel network commonly contains the main channel (where most of processes are manipulated in this part) and other support components (such as valve system, connect part, which support the control of procedure). The bottom substrate contains function components (such as electrodes for electrochemical detection; electromagnet for magnetic generation; heating pads; temperature sensor; etc.) or simple flat substrates (silicon, glass, hard plastic). In this part, the most popular techniques and materials are pointed in microfluidics fabrication.

2.4.3.1 Microchannel fabrication

a. Materials for microchannel network

As reported in [82], there are some materials used mainly in fabricating microfluidics (Figure 2.22):

- Glass and silicon/silica/quartz, the first generation of microfluidic device materials, are perfect for capillary electrophoresis and solvent-involved applications but expensive for microfabrication. The microchannel is usually obtained by using deep-etching technique.
- Elastomers, which consist of cross-linked polymer chains (one of the most popular elastomer is PDMS, [83, 84]), enable low-cost rapid prototyping and high density

integration of valves on chip, allowing complicated and parallel fluid manipulation and in-channel cell culture. Even if PDMS is commonly used, it suffers of several drawbacks like non-specific adsorption.

- Thermosets (such as SU-8 photoresist or polyamide), these materials are stable even at high temperatures, resistant to most solvents, and optically transparent. They are also easy to fabricate by using optical lithography or thermos molding with high-aspect ratio and free-standing structure [85, 86].
- Thermoplastics, there some typical materials for microchips such as PMMA, PC, polystyrene (PS), polyethylene terephthalate (PET), and polyvinylchloride (PVC) [87]. But these materials are incompatible with most of organic solvents. However, these materials are widely used in industry and they are convenience in molding and bonding process by using thermos treatment. Two other extremely organic compatible perfluorinated polymers (Teflon PFA and Teflon FEP) are used to improve some disadvantage properties of other thermoplastics above listed.
- Paper, the paper-based microfluidic devices are not required a bonding step as most of devices made from above materials [88]. Paper has highly porous matrix made of cellulose, excellent in wicking liquids. The paper-based microfluidic device is simple and low-cost. In addition, this device is interested in portable analysis device for bioassay-based personalized medical care [88, 89].

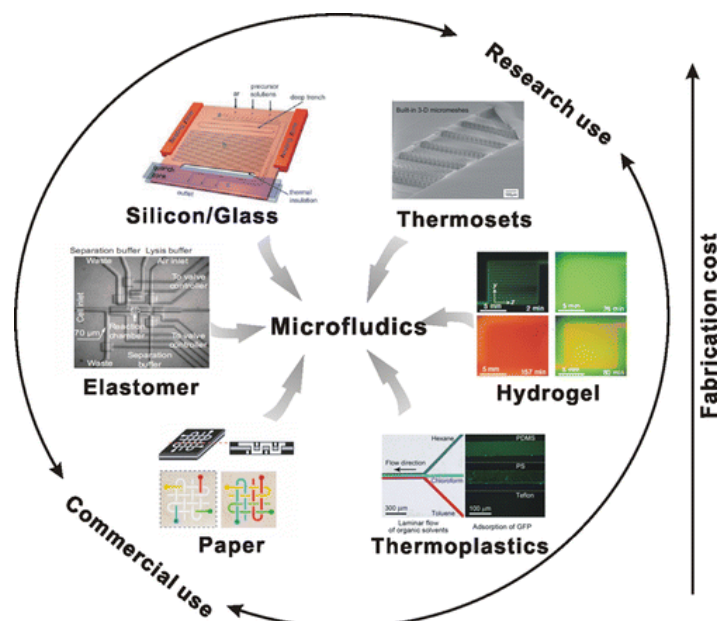


Figure 2.22. The distribution of materials in microfluidics fabrication for research and commercial use, [82].

b. PDMS as a popular materials for microfluidics

From 1990s to now, PDMS has interested many researchers for developing microfluidic devices. This material has many advantages in fabricating and applying for research. This material is also known as the most commonly used silicone polymer for fabricating microfluidic systems [84, 90, 91], and it has been applied in many biological analysis processes: protein, DNA analysis [92, 93]; cells analysis and immunoassays [94, 95] etc. This is due to its physical and chemical properties: (e.g. transparency, flexibility, and bio-compatibility) which also allows the fabrication process of microfluidic chip to be easy, flexible, low cost and low consumption time [96]. Moreover the replica molding process on SU-8 masters by using soft-lithography makes the channel networks design simple [90]. Figure 2.23 shows the flow process in fabricating a simple PDMS microfluidic chip (the bottom substrate is glass slide).

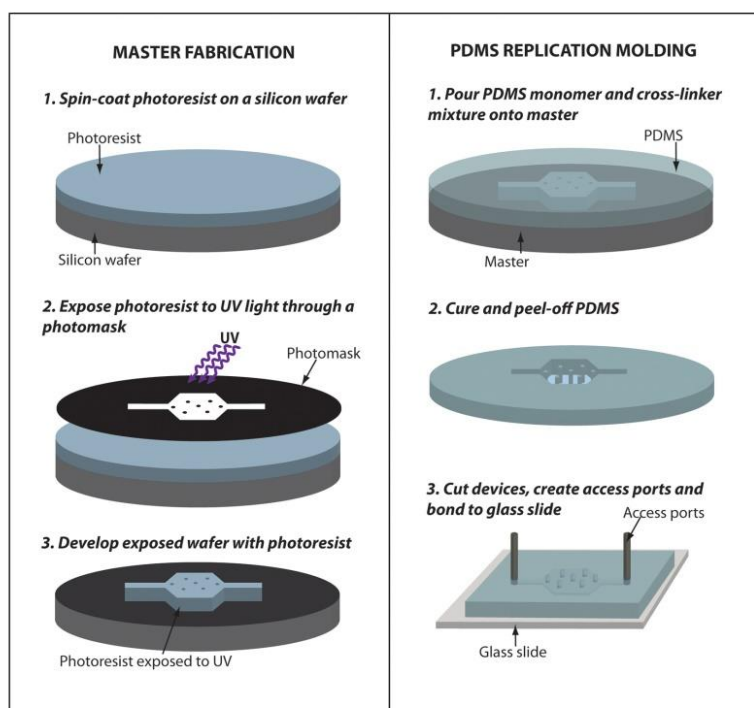


Figure 2.23. The schema of microfluidic fabrication with PDMS replica molding: The master fabrication steps and PDMS replication molding ⁽¹⁾.

Thus, the fabrication of microchannel network in PDMS material is performed in 2 basic processes: Master fabrication, typically a SU-8 photoresist mold obtained by lithography on silicon substrates of in cleanroom environment; and PDMS replication molding.

⁽¹⁾ http://www.wormbook.org/chapters/www_microfluidics/microfluidics.html

2.4.3.2 Packaging PDMS microfluidic chip

In microfluidic fabrication based on PDMS material, the bonding PDMS channel to bottom substrates is an important step in the process of assembling devices. A number of factors influence the quality of the bond, including the type of technique used, the cleanliness of the bonding surfaces, the ratio of PDMS base to cross-linking agent and the curing/baking process. In most cases, the application and complexity of the design will dictate which bonding technique is required to fulfil the design criteria. Some techniques may not be suitable for all applications. Several bonding techniques alter the surface chemistry within the microchannels, which in the case of biomedical applications may be helpful or problematic. Methods in bonding two main units of microfluidics (channel network and bottom substrate) can be classified into two main approaches: irreversible and reversible bonding.

a. Irreversible bonding

PDMS is able to bond on various materials (e.g. PDMS, glass, silicon, etc.). Concerning the irreversible bonding, one of the most common techniques is oxygen plasma treatment, which induces oxidized surfaces of two bonding contact surfaces. By plasma activation, the bond between PDMS channel cap to glass, silicon or surface with cured layers of PDMS is very strong [82, 84]. This approach makes the channels more hydrophilic, allowing for easier fluid filling for a period of time after the oxygen plasma treatment. However, the surfaces can quickly revert to their hydrophobic tendency if exposed to atmosphere. Oxygen plasma treatments are also advantageous because they enable the bonding of PDMS to other materials such as glass. Drawbacks associated with oxygen plasma include: placing the exposed bonding surfaces in a low-vacuum environment in the presence of oxygen gas and the operation of the equipment within a cleanroom facility. The oxygen plasma adds a significant cost to the fabrication process while limiting flexibility with the substrates due to cleanliness requirements and the size restriction of the chamber. Unger et al reported a bonding technique that relied on using a sticky layer with less cross-linking agent (using very high ratio of base:curing agent in preparing step) that would be combined with a hard cross-linked layer of silicone polymer [97].

In plasma condition, surface oxidation exposes silanol groups (Si-OH) at the surface of the PDMS layers that when brought together form covalent siloxane bonds (Si-O-Si), as shown in figure below:

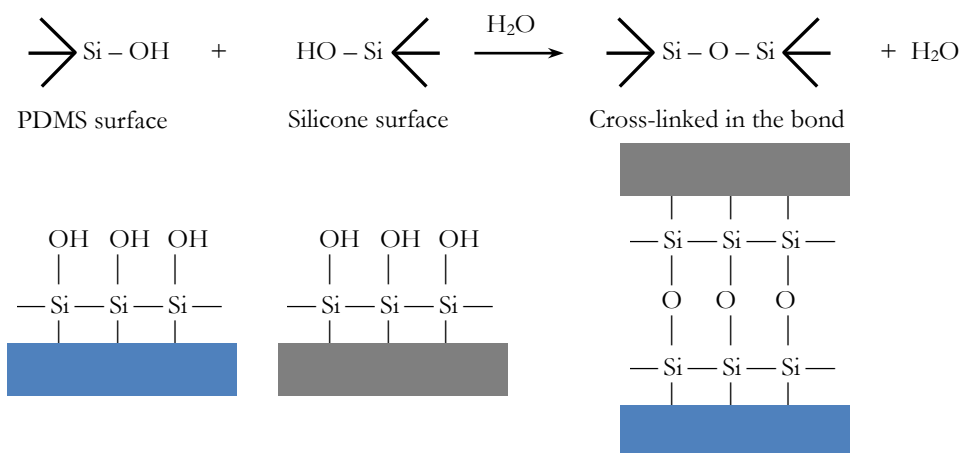


Figure 2.24. The mechanism of forming covalent siloxane bonds between two activated surfaces of PDMS and silicone by oxygen plasma treatment

The silanol groups change the surface properties of PDMS from being hydrophobic to hydrophilic. The two activated surfaces must be put in contact immediately after turning off plasma, because of the unstable surfaces after activated. In literature, many mechanisms have been proposed for hydrophobicity recovery of PDMS elastomer after exposed to plasma, possibilities including:

- Migration of low molar mass species from the bulk to the surface
- Reorientation of polar groups at the surface into the bulk
- Condensation of the silanol (Si—OH) groups at the surface
- External contamination of the surface
- Change of surface roughness
- Loss of volatile species to the atmosphere

Of these proposed mechanisms, there is a consensus that migration of low molar mass of PDMS to the surface is the dominant mechanism. The oxidation to a SiO_x surface layer retards the migration of low molar mass PDMS. However, cracking of the SiO_x layer enhances the rate of hydrophobic recovery.

b. Reversible bonding

In specific applications, the development of a reversible packaging, which enables to reuse the microfluidic chip several times, is very attractive, especially when integrated components (e.g. electrodes for electrochemical detection, microcoils for magnetic trapping or analysis, etc.) have been required a complex and expensive

microfabrication process. Indeed, the reversible packaging allows the PDMS cap removal for a better cleaning and/or channel replacement.

Few reversible packaging methods allowing PDMS microfluidic chip to work at quite high pressure have been already published. The simplest one is to fasten the contact between the cap and the device wafer with a mechanical strength thanks to two clamps (Plexiglas®) tightened by screws [98, 99], as shown in Figure 2.25.

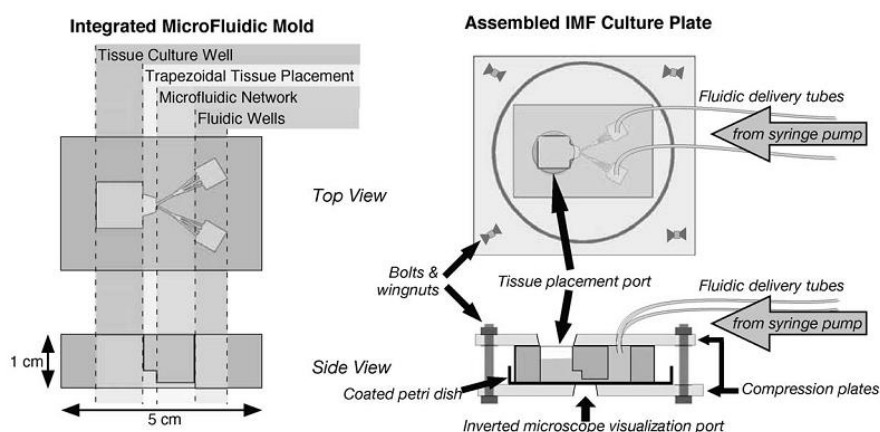


Figure 2.25. Schematic view of integrated microfluidic mold and assembled IMF tissue plate. (Left - figure)

The integrated microfluidic mold is cast from the silicone elastomer PDMS. The mold dimensions are approximately 3 cm×5cm×1 cm. Regions of interest within the mold are indicated above the schematic. (Right - figure) The assembled IMF tissue culture plate. Two Plexiglas plates compress an IMF mold onto a coated 60 mm petri dish. Culture media is delivered from a syringe pump through the fluidic delivery tubes into the microfluidic network, [99].

In addition to the specific design of the mechanical clamps, channel deformation can appear when a hard press is applied onto the cap. Packaging by aspiration through a dedicated crossing channel network patterned in the cap suffers from the same drawback [100]. In addition, using a vacuum system implies that the applied pressure needs to be well regulated. Magnetic field strength can be used to clamp both parts of the microfluidic chip thanks to magnets or embedded iron powder in PDMS. Rafat et al. [101] reported a working pressure up to 145 kPa but this technique is not compatible with microfluidic chips using magnetic beads inside the channel.

Another way is to seal the PDMS microfluidic chip with an adhesive layer or special double side tape [102], as shown in Figure 2.26. Choong S.C. et al. 2005 [103] used a bio/chemical compatible tape to bond the channel cap to the bottom substrate. The tape enhances the bonding strength (the pressure inside channel is up to 100 kPa) and the cap is easily removed from the substrate.

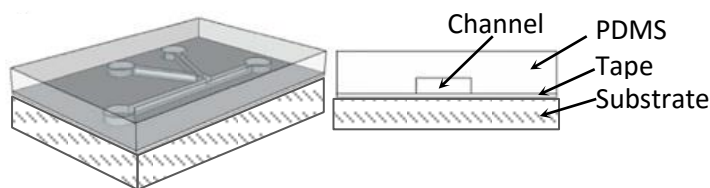


Figure 2.26. The reversible bonding PDMS chip with adhesive tape

The PDMS bonding on different substrates combining a plasma and an adhesive layer (Dimethyl-methylphenylmethoxy siloxane, DMPMS) between the channel cap and the bottom substrate has previously been performed by Vézy et al. 2011 [104]. This technique allows chips reusing and working in high pressures with no leakage.

2.5 Conclusions

The rapid development of microfluidics in literature in biochemical assays was a motivation for researchers and manufacturers in researching and applying new microfluidic devices, which adapt to fast and portable analyzing devices. Basing on the traditional ELISA technique, the bead-based immunoassay has become a reliable process in early diagnostic many diseases in medicine. Combining the MEMS and chemical, biological and medical analysis, integrated microfluidics is approaching a fully-automated Lab-on-a-Chip device.

Based on the advantages of typical microfluidics, this study in this thesis will focus on microfluidic device which used embedded microcoils. This microfluidic device will be designed in order to be used for immunoassay and for manipulating magnetic beads.

REFERENCES

- [1] N. Blow, Microfluidics: in search of a killer application, *Nat Meth*, 4 (2007) 665-670.
- [2] R.S. Yalow, S.A. Berson, IMMUNOASSAY OF ENDOGENOUS PLASMA INSULIN IN MAN, *The Journal of Clinical Investigation*, 39 (1960) 1157-1175.
- [3] M. Honda, S. Yamamoto, M. Cheng, K. Yasukawa, H. Suzuki, T. Saito, Y. Osugi, T. Tokunaga, T. Kishimoto, Human soluble IL-6 receptor: its detection and enhanced release by HIV infection, *The Journal of Immunology*, 148 (1992) 2175-2180.
- [4] L.-S. Wang, Y.Y. Leung, S.-K. Chang, S. Leight, M. Knapik-Czajka, Y. Baek, L.M. Shaw, V.M.Y. Lee, J.Q. Trojanowski, C.M. Clark, Comparison of xMAP and ELISA Assays for Detecting Cerebrospinal Fluid Biomarkers of Alzheimer's Disease, *Journal of Alzheimer's Disease*, 31 (2012) 439-445.
- [5] E.A. Wayner, S.-I. Quek, R. Ahmad, M.E. Ho, M.A. Loprieno, Y. Zhou, W.J. Ellis, L.D. True, A.Y. Liu, Development of an ELISA to detect the secreted prostate cancer biomarker AGR2 in voided urine, *The Prostate*, 72 (2012) 1023-1034.
- [6] N. Scholler, M. Crawford, A. Sato, C.W. Drescher, K.C. O'Briant, N. Kiviat, G.L. Anderson, N. Urban, Bead-Based ELISA for Validation of Ovarian Cancer Early Detection Markers, *Clinical Cancer Research*, 12 (2006) 2117-2124.
- [7] E. Engvall, P. Perlmann, Enzyme-linked immunosorbent assay (ELISA) quantitative assay of immunoglobulin G, *Immunochemistry*, 8 (1971) 871-874.
- [8] B.K. Van Weemen, A.H.W.M. Schuurs, Immunoassay using antigen—enzyme conjugates, *FEBS Letters*, 15 (1971) 232-236.
- [9] A. Voller, The enzyme-linked immunosorbent assay (ELISA) (theory, technique and applications), *Ric Clin Lab*, 8 (1978) 289-298.
- [10] A. Voller, A. Bartlett, D.E. Bidwell, Enzyme immunoassays with special reference to ELISA techniques, *J Clin Pathol*, 31 (1978) 507-520.
- [11] R. de la Rica, M.M. Stevens, Plasmonic ELISA for the ultrasensitive detection of disease biomarkers with the naked eye, *Nat Nano*, 7 (2012) 821-824.
- [12] H. Kuramitz, Magnetic microbead-based electrochemical immunoassays, *Anal Bioanal Chem*, 394 (2009) 61-69.
- [13] C.-J. Liu, K.-Y. Lien, C.-Y. Weng, J.-W. Shin, T.-Y. Chang, G.-B. Lee, Magnetic-bead-based microfluidic system for ribonucleic acid extraction and reverse transcription processes, *Biomedical Microdevices*, 11 (2009) 339-350.
- [14] A.C. Ng, U. Uddayasankar, A. Wheeler, Immunoassays in microfluidic systems, *Anal Bioanal Chem*, 397 (2010) 991-1007.
- [15] C. Wyatt Shields Iv, C.D. Reyes, G.P. Lopez, Microfluidic cell sorting: a review of the advances in the separation of cells from debulking to rare cell isolation, *Lab on a chip*, 15 (2015) 1230-1249.
- [16] K. Sung Kim, J.-K. Park, Magnetic force-based multiplexed immunoassay using superparamagnetic nanoparticles in microfluidic channel, *Lab on a chip*, 5 (2005) 657-664.
- [17] R. Gottheil, N. Baur, H. Becker, G. Link, D. Maier, N. Schneiderhan-Marra, M. Stelzle, Moving the solid phase: a platform technology for cartridge based sandwich immunoassays, *Biomedical Microdevices*, 16 (2014) 163-172.
- [18] E.K. Sackmann, A.L. Fulton, D.J. Beebe, The present and future role of microfluidics in biomedical research, *Nature*, 507 (2014) 181-189.
- [19] M.J.E. Golay, Vapor Phase Chromatography and Telegrapher's Equation, *Analytical Chemistry*, 29 (1957) 928-932.
- [20] S.C. Terry, J.H. Jerman, J.B. Angell, A gas chromatographic air analyzer fabricated on a silicon wafer, *Electron Devices, IEEE Transactions on*, 26 (1979) 1880-1886.
- [21] E. Bassous, H.H. Taub, L. Kuhn, Ink jet printing nozzle arrays etched in silicon, *Applied Physics Letters*, 31 (1977) 135-137.
- [22] K.E. Petersen, K.E. Petersen, Fabrication of an integrated, planar silicon ink-jet structure, *Electron Devices, IEEE Transactions on*, 26 (1979) 1918-1920.
- [23] A. Manz, N. Graber, H.M. Widmer, Miniaturized total chemical analysis systems: A novel concept for chemical sensing, *Sensors and Actuators B: Chemical*, 1 (1990) 244-248.
- [24] D.J. Beebe, G.A. Mensing, G.M. Walker, Physics and applications of microfluidics in biology, *Annual Review of Biomedical Engineering*, 4 (2002) 261-286.
- [25] A.E. Kamholz, E.A. Schilling, P. Yager, Optical Measurement of Transverse Molecular Diffusion in a Microchannel, *Biophysical Journal*, 80 (2001) 1967-1972.
- [26] A. Atwe, A. Gupta, R. Kant, M. Das, I. Sharma, S. Bhattacharya, A novel microfluidic switch for pH control using Chitosan based hydrogels, *Microsystem Technologies*, 20 (2014) 1373-1381.
- [27] A.E. Kamholz, B.H. Weigl, B.A. Finlayson, P. Yager, Quantitative Analysis of Molecular Interaction in a Microfluidic Channel: The T-Sensor, *Analytical Chemistry*, 71 (1999) 5340-5347.

- [28] D.C. Duffy, H.L. Gillis, J. Lin, N.F. Sheppard, G.J. Kellogg, Microfabricated Centrifugal Microfluidic Systems: Characterization and Multiple Enzymatic Assays, *Analytical Chemistry*, 71 (1999) 4669-4678.
- [29] J. Kameoka, H.G. Craighead, H. Zhang, J. Henion, A Polymeric Microfluidic Chip for CE/MS Determination of Small Molecules, *Analytical Chemistry*, 73 (2001) 1935-1941.
- [30] B.A. Otieno, C.E. Krause, A. Latus, B.V. Chikkaveeraiah, R.C. Faria, J.F. Rusling, On-line protein capture on magnetic beads for ultrasensitive microfluidic immunoassays of cancer biomarkers, *Biosensors and Bioelectronics*, 53 (2014) 268-274.
- [31] M.E. Piyasena, S.W. Graves, The intersection of flow cytometry with microfluidics and microfabrication, *Lab on a chip*, 14 (2014) 1044-1059.
- [32] D. Figeys, S.P. Gygi, G. McKinnon, R. Aebersold, An Integrated Microfluidics-Tandem Mass Spectrometry System for Automated Protein Analysis, *Analytical Chemistry*, 70 (1998) 3728-3734.
- [33] T. Geng, R.A. Mathies, Minimizing inhibition of PCR-STR typing using digital agarose droplet microfluidics, *Forensic Science International: Genetics*, 14 (2015) 203-209.
- [34] A.H.J. Yang, K. Hsieh, A.S. Patterson, B.S. Ferguson, M. Eisenstein, K.W. Plaxco, H.T. Soh, Accurate Zygote-Specific Discrimination of Single-Nucleotide Polymorphisms Using Microfluidic Electrochemical DNA Melting Curves, *Angewandte Chemie*, 126 (2014) 3227-3231.
- [35] S.K.W. Dertinger, D.T. Chiu, N.L. Jeon, G.M. Whitesides, Generation of Gradients Having Complex Shapes Using Microfluidic Networks, *Analytical Chemistry*, 73 (2001) 1240-1246.
- [36] J.A. Kim, M. Kim, S.M. Kang, K.T. Lim, T.S. Kim, J.Y. Kang, Magnetic bead droplet immunoassay of oligomer amyloid β for the diagnosis of Alzheimer's disease using micro-pillars to enhance the stability of the oil-water interface, *Biosensors and Bioelectronics*, 67 (2015) 724-732.
- [37] R. Gómez-Sjöberg, A.A. Leyrat, D.M. Pirone, C.S. Chen, S.R. Quake, Versatile, Fully Automated, Microfluidic Cell Culture System, *Analytical Chemistry*, 79 (2007) 8557-8563.
- [38] J. Pan, A.L. Stephenson, E. Kazamia, W.T.S. Huck, J.S. Dennis, A.G. Smith, C. Abell, Quantitative tracking of the growth of individual algal cells in microdroplet compartments, *Integrative Biology*, 3 (2011) 1043-1051.
- [39] N.-T. Nguyen, S.T. Wereley, fundamentals and applications of microfluidics, 2 ed., ARTECH HOUSE, INC., 2006.
- [40] D.L. Englert, M.D. Manson, A. Jayaraman, Flow-Based Microfluidic Device for Quantifying Bacterial Chemotaxis in Stable, Competing Gradients, *Applied and Environmental Microbiology*, 75 (2009) 4557-4564.
- [41] H. Lee, Y. Liu, R.M. Westervelt, D. Ham, IC/Microfluidic hybrid system for magnetic manipulation of biological cells, *Ieee Journal of Solid-State Circuits*, 41 (2006) 1471-1480.
- [42] E. Finehout, W.-C. Tian, *Microfluidics for Biological Applications*, 1 ed., Springer US, 233 Spring Street, New York, NY 10013, USA, 2009.
- [43] C.-M. Ho, Y.-C. Tai, Micro-electro-mechanical-systems (MEMS) and fluid flows, *Annual Review of Fluid Mechanics*, 30 (1998) 579-612.
- [44] T. Bayraktar, S.B. Pidugu, Characterization of liquid flows in microfluidic systems, *International Journal of Heat and Mass Transfer*, 49 (2006) 815-824.
- [45] J.O.C. Jones, An Improvement in the Calculation of Turbulent Friction in Rectangular Ducts, *Journal of Fluids Engineering*, 98 (1976) 173-180.
- [46] S.R. Dave, X. Gao, Monodisperse magnetic nanoparticles for biodetection, imaging, and drug delivery: a versatile and evolving technology, *Wiley Interdisciplinary Reviews: Nanomedicine and Nanobiotechnology*, 1 (2009) 583-609.
- [47] M. Mahmoudi, S. Sant, B. Wang, S. Laurent, T. Sen, Superparamagnetic iron oxide nanoparticles (SPIONs): Development, surface modification and applications in chemotherapy, *Advanced Drug Delivery Reviews*, 63 (2011) 24-46.
- [48] A.L. Daniel-da-Silva, T. Trindade, *Biofunctional Composites of Polysaccharides Containing Inorganic Nanoparticles*, 2011.
- [49] L. Janssen, F. Sobott, P.P. De Deyn, D. Van Dam, Signal loss due to oligomerization in ELISA analysis of amyloid-beta can be recovered by a novel sample pre-treatment method, *MethodsX*, 2 (2015) 112-123.
- [50] L. Wu, X. Qu, Cancer biomarker detection: recent achievements and challenges, *Chemical Society Reviews*, (2015).
- [51] J.C. Jr, T. P, W. M, e. al, *Immunobiology: The Immune System in Health and Disease*, 5th ed., Garland Science, New York, 2001.
- [52] S. Puertas, P. Batalla, M. Moros, E. Polo, P. del Pino, J.M. Guisán, V. Grazú, J.M. de la Fuente, Taking Advantage of Unspecific Interactions to Produce Highly Active Magnetic Nanoparticle-Antibody Conjugates, *ACS Nano*, 5 (2011) 4521-4528.
- [53] B. Lu, M.R. Smyth, R. O'Kennedy, Tutorial review. Oriented immobilization of antibodies and its applications in immunoassays and immunosensors, *Analyst*, 121 (1996) 29R-32R.

- [54] D. Falconnet, J. She, R. Tornay, E. Leimgruber, D. Bernasconi, L. Lagopoulos, P. Renaud, N. Demierre, P. van den Bogaard, Rapid, Sensitive and Real-Time Multiplexing Platform for the Analysis of Protein and Nucleic-Acid Biomarkers, *Analytical Chemistry*, 87 (2015) 1582-1589.
- [55] B. Teste, J. Vial, S. Descroix, T. Georgelin, J.-M. Siaugue, J. Petr, A. Varenne, M.-C. Hennion, A chemometric approach for optimizing protein covalent immobilization on magnetic core-shell nanoparticles in view of an alternative immunoassay, *Talanta*, 81 (2010) 1703-1710.
- [56] N. Soh, H. Nishiyama, Y. Asano, T. Imato, T. Masadome, Y. Kurokawa, Chemiluminescence sequential injection immunoassay for vitellogenin using magnetic microbeads, *Talanta*, 64 (2004) 1160-1168.
- [57] J. Xu, W. Yin, Y. Zhang, J. Yi, M. Meng, Y. Wang, H. Xue, T. Zhang, R. Xi, Establishment of magnetic beads-based enzyme immunoassay for detection of chloramphenicol in milk, *Food Chemistry*, 134 (2012) 2526-2531.
- [58] S. Schreier, G. Doungchawee, D. Triampo, P. Wangroongsarb, R.A. Hartskeerl, W. Triampo, Development of a magnetic bead fluorescence microscopy immunoassay to detect and quantify *Leptospira* in environmental water samples, *Acta Tropica*, 122 (2012) 119-125.
- [59] M. Eguílaz, M. Moreno-Guzmán, S. Campuzano, A. González-Cortés, P. Yáñez-Sedeño, J.M. Pingarrón, An electrochemical immunosensor for testosterone using functionalized magnetic beads and screen-printed carbon electrodes, *Biosensors and Bioelectronics*, 26 (2010) 517-522.
- [60] J. Wen, S. Zhou, J. Chen, Colorimetric detection of *Shewanella oneidensis* based on immunomagnetic capture and bacterial intrinsic peroxidase activity, *Sci. Rep.*, 4 (2014).
- [61] M. Herrmann, T. Veres, M. Tabrizian, Enzymatically-generated fluorescent detection in micro-channels with internal magnetic mixing for the development of parallel microfluidic ELISA, *Lab on a chip*, 6 (2006) 555-560.
- [62] D. Holmes, J.K. She, P.L. Roach, H. Morgan, Bead-based immunoassays using a micro-chip flow cytometer, *Lab on a chip*, 7 (2007) 1048-1056.
- [63] C.-C. Lin, J.-H. Wang, H.-W. Wu, G.-B. Lee, Microfluidic Immunoassays, *Journal of the Association for Laboratory Automation*, 15 (2010) 253-274.
- [64] S.-H. Song, H.-L. Lee, Y.H. Min, H.-I. Jung, Electromagnetic microfluidic cell labeling device using on-chip microelectromagnet and multi-layered channels, *Sensors and Actuators B: Chemical*, 141 (2009) 210-216.
- [65] M. Berenguel-Alonso, X. Granados, J. Faraudo, J. Alonso-Chamarro, M. Puyol, Magnetic actuator for the control and mixing of magnetic bead-based reactions on-chip, *Anal Bioanal Chem*, 406 (2014) 6607-6616.
- [66] T. Zhu, D. Lichlyter, M. Haidekker, L. Mao, Analytical model of microfluidic transport of non-magnetic particles in ferrofluids under the influence of a permanent magnet, *Microfluidics and Nanofluidics*, 10 (2011) 1233-1245.
- [67] M.D. Tarn, R.F. Fakhrullin, V.N. Paunov, N. Pamme, Microfluidic device for the rapid coating of magnetic cells with polyelectrolytes, *Materials Letters*, 95 (2013) 182-185.
- [68] N. Pamme, Magnetism and microfluidics, *Lab on a chip*, 6 (2006) 24-38.
- [69] R. Rong, C. Jin-Woo, H.A. Chong, An on-chip magnetic bead separator for biocell sorting, *Journal of Micromechanics and Microengineering*, 16 (2006) 2783.
- [70] R. Fulcrand, A. Bancaud, C. Escriba, Q. He, S. Charlot, A. Boukabache, A.-M. Gué, On chip magnetic actuator for batch-mode dynamic manipulation of magnetic particles in compact lab-on-chip, *Sensors and Actuators B: Chemical*, 160 (2011) 1520-1528.
- [71] C.-Y. Lee, Z.-H. Chen, H.-T. Chang, C.-Y. Wen, C.-H. Cheng, Design and fabrication of novel micro electromagnetic actuator, *Microsystem Technologies*, 15 (2009) 1171-1177.
- [72] J.W. Choi, K.W. Oh, J.H. Thomas, W.R. Heineman, H.B. Halsall, J.H. Nevin, A.J. Helmicki, H.T. Henderson, C.H. Ahn, An integrated microfluidic biochemical detection system for protein analysis with magnetic bead-based sampling capabilities, *Lab on a chip*, 2 (2002) 27-30.
- [73] Z. Yushan, M. Sawan, A microsystem for magnetic immunoassay towards protein toxins detection, in: *Circuits and Systems (ISCAS)*, 2014 IEEE International Symposium on, 2014, pp. 225-228.
- [74] Z. Yushan, M. Sawan, Planar Microcoil Array Based Temperature-Controllable Lab-on-Chip Platform, *Magnetics*, IEEE Transactions on, 49 (2013) 5236-5242.
- [75] C. Chen-Chia, H. Shih-Hsun, S. Chen-Hsiang, Y. Chih-Chyau, W. Chien-Ming, H. Chun-Ming, S. Jeng-Tzong, Multi-layer planar micro-coils chip as actuators and heaters for biological applications, in: *Biomedical Circuits and Systems Conference (BioCAS)*, 2012 IEEE, 2012, pp. 392-395.
- [76] A. Beyzavi, N.-T. Nguyen, Modeling and optimization of planar microcoils, *Journal of Micromechanics and Microengineering*, 18 (2008) 095018.
- [77] K. Smistrup, P.T. Tang, O. Hansen, M.F. Hansen, Microelectromagnet for magnetic manipulation in lab-on-a-chip systems, *Journal of Magnetism and Magnetic Materials*, 300 (2006) 418-426.
- [78] M. Woytasik, J. Moulin, E. Martincic, A.-L. Coutrot, E. Dufour-Gergam, Copper planar microcoils applied to magnetic actuation, *Microsystem Technologies*, 14 (2007) 951-956.

- [79] S.-H. Song, B.-S. Kwak, J.-S. Park, W. Kim, H.-I.L. Jung, Novel application of Joule heating to maintain biocompatible temperatures in a fully integrated electromagnetic cell sorting system, *Sensors and Actuators A: Physical*, 151 (2009) 64-70.
- [80] Y.-H. Lin, P.-Y. Peng, Semiconductor sensor embedded microfluidic chip for protein biomarker detection using a bead-based immunoassay combined with deoxyribonucleic acid strand labeling, *Analytica Chimica Acta*, (2015).
- [81] J.-W. Choi, C.H. Ahn, S. Bhansali, H.T. Henderson, A new magnetic bead-based, filterless bio-separator with planar electromagnet surfaces for integrated bio-detection systems, *Sensors and Actuators B: Chemical*, 68 (2000) 34-39.
- [82] K. Ren, J. Zhou, H. Wu, Materials for Microfluidic Chip Fabrication, *Accounts of Chemical Research*, 46 (2013) 2396-2406.
- [83] A.D. Stroock, G.M. Whitesides, Controlling Flows in Microchannels with Patterned Surface Charge and Topography, *Accounts of Chemical Research*, 36 (2003) 597-604.
- [84] J.C. McDonald, G.M. Whitesides, Poly(dimethylsiloxane) as a Material for Fabricating Microfluidic Devices, *Accounts of Chemical Research*, 35 (2002) 491-499.
- [85] S. Hironobu, M. Hirokazu, K. Satoshi, S. Shuichi, An all SU-8 microfluidic chip with built-in 3D fine microstructures, *Journal of Micromechanics and Microengineering*, 16 (2006) 2318.
- [86] Y. Zheng, W. Dai, D. Ryan, H. Wu, Fabrication of freestanding, microperforated membranes and their applications in microfluidics, *Biomicrofluidics*, 4 (2010) 036504.
- [87] H. Becker, C. Gärtner, Polymer microfabrication technologies for microfluidic systems, *Anal Bioanal Chem*, 390 (2008) 89-111.
- [88] A.W. Martinez, S.T. Phillips, M.J. Butte, G.M. Whitesides, Patterned Paper as a Platform for Inexpensive, Low-Volume, Portable Bioassays, *Angewandte Chemie International Edition*, 46 (2007) 1318-1320.
- [89] A.W. Martinez, S.T. Phillips, E. Carrilho, S.W. Thomas, H. Sindi, G.M. Whitesides, Simple Telemedicine for Developing Regions: Camera Phones and Paper-Based Microfluidic Devices for Real-Time, Off-Site Diagnosis, *Analytical Chemistry*, 80 (2008) 3699-3707.
- [90] J.C. McDonald, D.C. Duffy, J.R. Anderson, D.T. Chiu, H. Wu, O.J. Schueller, G.M. Whitesides, Fabrication of microfluidic systems in poly(dimethylsiloxane), *Electrophoresis*, 21 (2000) 27-40.
- [91] J. Lee, J. Kim, H. Kim, Y.M. Bae, K.H. Lee, H.J. Cho, Effect of thermal treatment on the chemical resistance of polydimethylsiloxane for microfluidic devices, *Journal of Micromechanics and Microengineering*, 23 (2013) 035007.
- [92] K.-Y. Lien, C.-J. Liu, Y.-C. Lin, P.-L. Kuo, G.-B. Lee, Extraction of genomic DNA and detection of single nucleotide polymorphism genotyping utilizing an integrated magnetic bead-based microfluidic platform, *Microfluidics and Nanofluidics*, 6 (2009) 539-555.
- [93] A.H. Diercks, A. Ozinsky, C.L. Hansen, J.M. Spotts, D.J. Rodriguez, A. Aderem, A microfluidic device for multiplexed protein detection in nano-liter volumes, *Anal Biochem*, 386 (2009) 30-35.
- [94] Y. Liu, A.K. Singh, Microfluidic platforms for single-cell protein analysis, *J Lab Autom*, 18 (2013) 446-454.
- [95] M. Pla-Roca, D. Juncker, PDMS microfluidic capillary systems for patterning proteins on surfaces and performing miniaturized immunoassays, *Methods Mol Biol*, 671 (2011) 177-194.
- [96] S. Neethirajan, I. Kobayashi, M. Nakajima, D. Wu, S. Nandagopal, F. Lin, Microfluidics for food, agriculture and biosystems industries, *Lab on a chip*, 11 (2011) 1574-1586.
- [97] M.A. Unger, H.-P. Chou, T. Thorsen, A. Scherer, S.R. Quake, Monolithic Microfabricated Valves and Pumps by Multilayer Soft Lithography, *Science*, 288 (2000) 113-116.
- [98] A. Khademhosseini, J. Yeh, G. Eng, J. Karp, H. Kaji, J. Borenstein, O.C. Farokhzad, R. Langer, Cell docking inside microwells within reversibly sealed microfluidic channels for fabricating multiphenotype cell arrays, *Lab on a chip*, 5 (2005) 1380-1386.
- [99] J.H. Wittig Jr, A.F. Ryan, P.M. Asbeck, A reusable microfluidic plate with alternate-choice architecture for assessing growth preference in tissue culture, *Journal of Neuroscience Methods*, 144 (2005) 79-89.
- [100] M. Le Berre, C. Crozatier, G. Velte Casquillas, Y. Chen, Reversible assembling of microfluidic devices by aspiration, *Microelectronic Engineering*, 83 (2006) 1284-1287.
- [101] M. Rafat, D.R. Raad, A.C. Rowat, D.T. Auguste, Fabrication of reversibly adhesive fluidic devices using magnetism, *Lab on a chip*, 9 (2009) 3016-3019.
- [102] C.S. Thompson, A.R. Abate, Adhesive-based bonding technique for PDMS microfluidic devices, *Lab on a chip*, 13 (2013) 632-635.
- [103] S.C. Choong, L. Xie, Y. Levent, H.M. Ji, J. Li, Y. Chen, P. Damaruganath, W.C. Hui, M.K. Iyer, Disposable Polydimethylsiloxane Package for 'Bio-Microfluidic System', in: 55th Electronic Components and Technology Conference (ECTC), Lake Buena Vista FL USA, 2005, pp. 617 - 621.
- [104] C. Vézy, N. Haddour, N.M. Dempsey, F. Dumas-Bouchiat, M. Frenéa-Robin, Simple method for reversible bonding of a polydimethylsiloxane microchannel to a variety of substrates, *Micro & Nano Letters*, 6 (2011) 871.

CHAPTER 3. MICROCOILS DESIGN AND FABRICATION

- *Magnetic field theory for planar coils*
 - *2D Modelling planar coils using FE simulation with ANSYS® v12.1 software*
 - *Criteria for the design of microcoils (shape, turn number, dimension, wire parameters: high, wide and space) Coils fabrication and characterization*
-

In this chapter, a model of coil is built to carry out magnetic field simulation using FE¹ method thanks to ANSYS® v12.1 software². The criteria for designing planar microcoils are an optimal magnetic field obtained with low power consumption, *i.e.* high power efficiency is chosen in order to decrease coil heating in the microfluidic chips. Figures of merits (or merit factors) such as the magnetic field generated for a given power loss are defined. The effective coil for magnetic beads trapping is found to be with narrow wires and large number of turns. Furthermore, the known efficient trapping area close to the coil surface (around 20 μm) is observed.

¹ Finite element

²A product of ANSYS®, Inc.

3.1. Introduction

This chapter is focused on the design of microcoils dedicated to magnetic beads trapping in microfluidic channels for integrated biochips. Among all the possible techniques able to trap magnetic beads described in previous chapter, microcoils offer the possibility to be integrated into tiny biochips. Their integration is not straightforward, since temperature issues need to be solved prior to integration.

We propose in this chapter to investigate the design of the trapping coils with the objective to obtain the maximum ratio of trapping efficiency to dissipated power, possibly allowing keeping the temperature of the microchannel in the range of 30 to 40°C, biocompatible temperature value.

As in many cases [1-3], simulation software has been used for design purposes. Digital models allow to change the design parameters (radius, turn numbers, space between wire coil, width and height of wire, materials information, etc.) and to observe the effect of the changes without the need of resource consuming extensive manufacturing.

Finite Element Modelling (FEM) software, Ansys® v12.1, is used in this work. The map of the magnetic field generated by a microcoil is calculated and extracted along several directions away from the microcoil. The intensity of the generated magnetic force is used as a primary indicator of the force exerted on magnetic nano-beads in the vicinity of the microcoil. The power loss, *i.e.* the temperature elevation consequence of the magnetic attraction is calculated. Merit factors indicating the magnetic field intensity per unit current and per unit power loss are also calculated.

Together with design issues, the choice of the fabrication process is of crucial importance to attain high trapping and thermal performance. The microcoil fabrication process is presented here as a follow-up of the design step. It has been thought with the aim of:

- Placing a microchannel as close as possible to the coil surface. A three-mask level process allows the central electrical connection report. The entire coil surface is free to be covered by a microchannel.
- Using thick microcoil conductors: copper electroplating in thick photoresist mold, *i.e.* micro-molding process, allows the realization of 10-20 μm thick conductors.

3.2. Magnetic field/force theory

3.2.1. Magnetic field of straight and finite wire

A conducting wire carrying a current, I , produces a magnetic field \mathbf{H} . The strength and direction of the field \mathbf{H} depend on r , the distance from current to a point P. The magnetic field at any point P due to the current can be calculated by adding up the magnetic field contributions, $d\mathbf{H}$, from small segments of the wire $d\ell$,

Figure 3.1.(a).

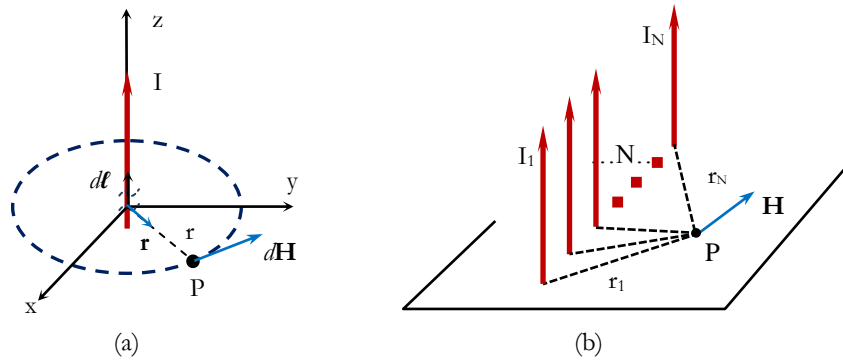


Figure 3.1. (a). Magnetic field \mathbf{H} at point P due to a current-carrying element $I d\ell$. (b). Total magnetic field \mathbf{H} at point P due to N parallel current-carrying element I

The Biot–Savart law (for infinite/straight wire) gives an expression for the magnetic field contribution, $d\mathbf{H}$, from the current source, $I d\ell$, [4]:

$$d\mathbf{H} = \frac{1}{4\pi} \frac{I d\ell \times \mathbf{r}}{r^2} \quad (3_1)$$

where I is the current flowing in the wire; r is the distance from the wire to point P; \mathbf{r} is the corresponding unit vector.

Adding up these contributions to find the magnetic field, which is generated by one straight wire, at the point P requires integrating over the current source:

$$\mathbf{H} = \int_{\text{wire}} d\mathbf{H} \quad (3_2)$$

For N straight wires, Figure 3.1. (b), \mathbf{H} can be defined:

$$\mathbf{H} = \sum_{i=1}^N \mathbf{H}_i \quad (3_3)$$

and the magnetic field strength is calculated by:

$$H = \sum_{i=1}^N H_i \quad (3_4)$$

By considering a circular loop of radius r , the symmetry can simplify the calculations. For example in planar coils such as in Figure 3.2, the distance of the point P to the wire is constant and equal to r . The magnetic field strength in the center of the circular loop can be calculated using equation (3_1):

$$H = \frac{I}{4\pi r^2} \frac{d\ell}{2r} = \frac{I}{2r} \quad (3_5)$$

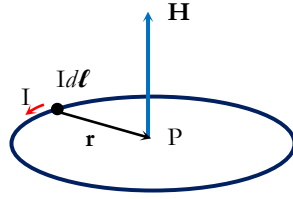


Figure 3.2. Magnetic field H inducing by circular loop at point P

In case of rectangular or square coils, the distance to the considered point is not constant, Figure 3.3.

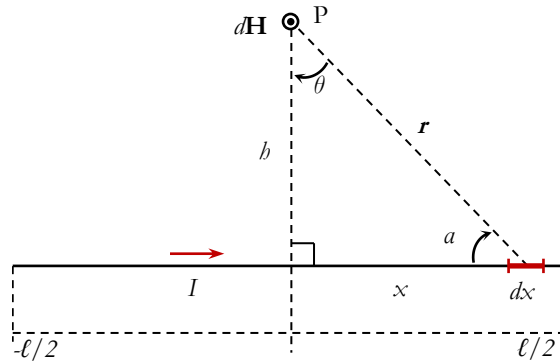


Figure 3.3. Magnetic field H at point P inducing by non-finite straight wire

The elementary magnetic field dH produced by a small section dx of the wire is:

$$dH = \frac{1}{4\pi} \frac{I \cos(\theta) dx}{r^2} = \frac{1}{4\pi} \frac{I \cos(\theta) d\theta}{r^2} \quad (3_6)$$

In the equation (3_6), the distance b from conductor wire to the point P can be expressed by:

$$x = b \cdot \tan \theta \quad (3_7)$$

This leads to:

$$\frac{dx}{d\theta} = \frac{h}{\cos^2 \theta} = \frac{r^2}{h} \quad (3_8)$$

The magnetic field produced by a portion of single wire of square turn can be calculated using equation (3_1).

$$H = \int_{-\ell/2}^{\ell/2} dH = 2 \int_0^{\ell/2} dH = \frac{1}{4\pi} \frac{I}{h} \int_0^{\theta_0} \cos \theta d\theta \quad (3_9)$$

with $\theta_0 = \text{Arctan}\left(\frac{\ell}{2h}\right)$, side length of square turn is ℓ , as shown in Figure 3.3.

Finally, a non-infinite straight wire produces a magnetic field:

$$H = \frac{I}{2\pi h} \sin \theta_0 \quad (3_{10})$$

It can be seen from equation (3_10) that the magnitude of the magnetic field is inversely proportional to the distance of the point to the wire, as well as for infinite wires.

The sine term of the equation (3_10) is represented at Figure 3.4:

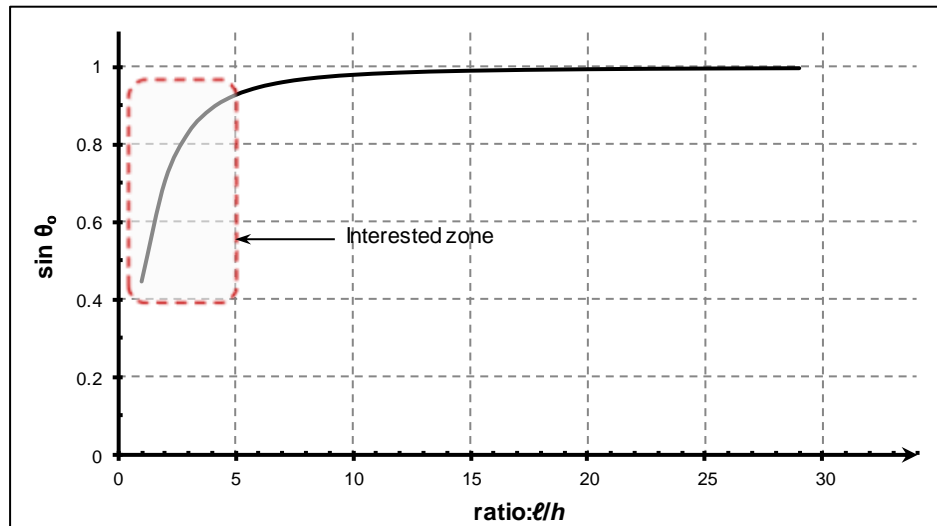


Figure 3.4. The effect of ration ℓ/h on $\sin \theta_0$, which defines roughly the respective dimensions of coils and corresponds to the magnetic field H ; where $\theta_0 = \arctan(\ell/2h)$ and considered $h = 1$ unit

In Figure 3.4, the relationship of the wire length (ℓ) and the distance (h) of this wire to the point P for calculating magnetic field are defined in following equation:

$$\sin\left(\arctan\left(\frac{\ell}{2h}\right)\right) = \frac{\ell}{\sqrt{4h^2 + \ell^2}} \quad (3_{-11})$$

The curve, Figure 3.4, shows that for a given length of the wire (ℓ), if the distance (h) is kept lower than 5 times the length of the wire, the magnetic field produced is almost the same than for infinite wires. This result can be used to define roughly the respective dimensions of coils and microchannels.

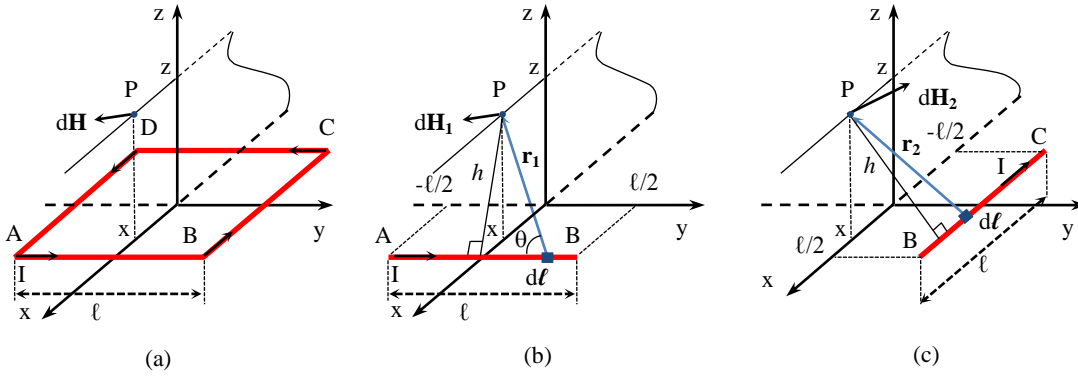


Figure 3.5. (a). Magnetic field $d\mathbf{H}$ at point P due to a current-carrying element $I d\ell$ in square loop. (b) and (c) the calculation of the component magnetic field $d\mathbf{H}_1$ and $d\mathbf{H}_2$ at point P.

The similar calculation for the three magnetic field components \mathbf{H}_2 , \mathbf{H}_3 and \mathbf{H}_4 allows the total magnetic field \mathbf{H} to be defined:

$$\mathbf{H} = \mathbf{H}_1 + \mathbf{H}_2 + \mathbf{H}_3 + \mathbf{H}_4 \quad (3_{-12})$$

In the case of multiple turns of a coil, the magnetic field is defined as the vector sum of each wire segment component generated magnetic field \mathbf{H}_i .

The relationship between the magnetic field and the magnetic flux density \mathbf{B} is given by:

$$\mathbf{B} = \mu_0 \mathbf{H} (1 + \chi_m) = \mu_0 \mu_r \mathbf{H} \quad (3_{-13})$$

where χ_m is the magnetic susceptibility of material, μ_0 is the permeability of free space: $\mu_0 = 4\pi \times 10^{-7} \text{ T}\cdot\text{m/A}$. In the case of vacuum, water or air, $\mu_r = 1 + \chi_m = 1$.

The coils models under study present complex coils shapes or large number of turns. The computation of the magnetic field generated in each point of the space for random geometries becomes a heavy task. A finite element modelling software is then of great help to calculate the magnetic field in the case of complex structures.

Furthermore, all previous equations consider the magnetic permeability μ of all materials in space equal to the vacuum one μ_0 . When magnetic materials (i.e. materials with $\mu > \mu_0$) are present, the lines of the magnetic field are strongly affected by their presence and the magnetic field at any point in space (surrounding wires) cannot be calculated without simulation software but for simple geometries.

3.2.2. Magnetic force: theory

When a magnetic micro/nano bead is placed into a magnetic field, the electrons spins can take different orientation. The bead acts then as a “small permanent magnet”. The “small permanent magnet” could be also obtained by a small equivalent current loop. The magnetic moment \mathbf{m} is a vector magnitude that represents the magnetic property of a magnetic source. This source can be a magnetic material submitted to an external field, a current loop or a permanent magnet. The magnetic moment is:

$$\mathbf{m} = V\mu_0\mathbf{M} = V\mu_0\chi\mathbf{H} \text{ (T)} \quad (3_14)$$

where V is the volume of the bead and \mathbf{M} its magnetization.

When the bead is placed in a magnetic field, a force is exerted onto it. The magnetic force acting on a magnetic bead can be determined [5] by equation:

$$\mathbf{F}_m = \frac{1}{\mu_0} \nabla(m \cdot \mathbf{B}) \approx \frac{1}{\mu_0} (m \cdot \nabla) \mathbf{B} \quad (3_15)$$

In case of beads' spherical geometry and nano-scale size, the magnetic moment of magnetic bead does not vary in space ($\nabla \cdot \mathbf{m} = 0$).

Using this relation and the equation (3_13), the equation (3_15) is re-written in the air (for one current loop):

$$\mathbf{F}_m = \frac{V\chi}{\mu_0} (\mathbf{B} \cdot \nabla) \mathbf{B} \quad (3_16)$$

where V is the volume of the magnetic bead, χ is the susceptibility of the magnetic component of the bead.

Along to x, y and z axis, this force can be written for each axis component:

$$\left. \begin{aligned} \mathbf{F}_{m,x} &= \frac{V\chi}{\mu_0} \left(B_x \frac{\partial}{\partial x} + B_y \frac{\partial}{\partial y} + B_z \frac{\partial}{\partial z} \right) B_x \\ \mathbf{F}_{m,y} &= \frac{V\chi}{\mu_0} \left(B_x \frac{\partial}{\partial x} + B_y \frac{\partial}{\partial y} + B_z \frac{\partial}{\partial z} \right) B_y \\ \mathbf{F}_{m,z} &= \frac{V\chi}{\mu_0} \left(B_x \frac{\partial}{\partial x} + B_y \frac{\partial}{\partial y} + B_z \frac{\partial}{\partial z} \right) B_z \end{aligned} \right\} \quad (3_17)$$

From equation(3_17), the useful component for trapping is the force along z axis. Eq. 3_17 shows that the trapping force intensity results from the product of the magnitude by the variation of the magnetic field. Then, the gradient and magnitude of magnetic field should be both high. Indeed, having a strong magnetic field in a small space (such as the space occupied by a microcoil) means a strong gradient around the microcoil. Thus, for microcoils design considerations, these two previous conditions can be represented by a single condition: the generated magnetic field must be as strong as possible. The maximum magnitude of magnetic field can be used as a reliable indicator of the microcoils' trapping ability.

We propose here to define the magnetic field magnitude as a primary indicator. Several configurations of microcoils that allow obtaining a given magnetic field can be designed. In these designs, some merit factors can be defined, such as the maximum magnetic field obtained by unit current, by unit current density or by unit power loss. These merit factors reflect the ability of coil geometry to generate the magnetic field in its vicinity for a given induced heat.

3.3. Magnetic field simulation and calculation

FEM software (ANSYS® v.12.1.) was used to calculate the magnetic field generated by microcoils. For comprehensive results, the calculated results of the magnetic field was extracted along lines perpendicular to the coil's plane and along lines parallel to the coil's plane at some fixed distances above copper wires. A parametric study of the variations in magnetic field (B) over the coil surface when changing turn number (N), diameter of coils, parameters of copper tracks and space between two tracks as well as the maximum (optimal) value of B on each coil was driven.

3.3.1. FE simulation of microcoils

Because representing 3D complex geometries in FEM software has a very important cost in terms of calculation time and effort, 2D simulations were made.

The hypothesis that the region of interest, *i.e.* the microfluidic channel is smaller than the radius of the microcoil, has to be made to avoid the influence of edge effect that are not taken into account in the simulations. The study of the magnetic field can then be reduced to a longitudinal cut of the microcoil. As a counterpart, the simulations are lighter and allow representing each single wire of the coil, thus giving access to the variations of the magnetic field near of each single wire of the simulated coils.

For symmetry reasons, only one half of a longitudinal cut was represented (Figure 3.6). 2D simulations were carried out, which is equivalent to assuming that the length of each segment is infinite compared to the working distance. In this case, the results obtained are valid whether the coil shape is circular or square, provided the length of the segments is high against the dimensions of interest.

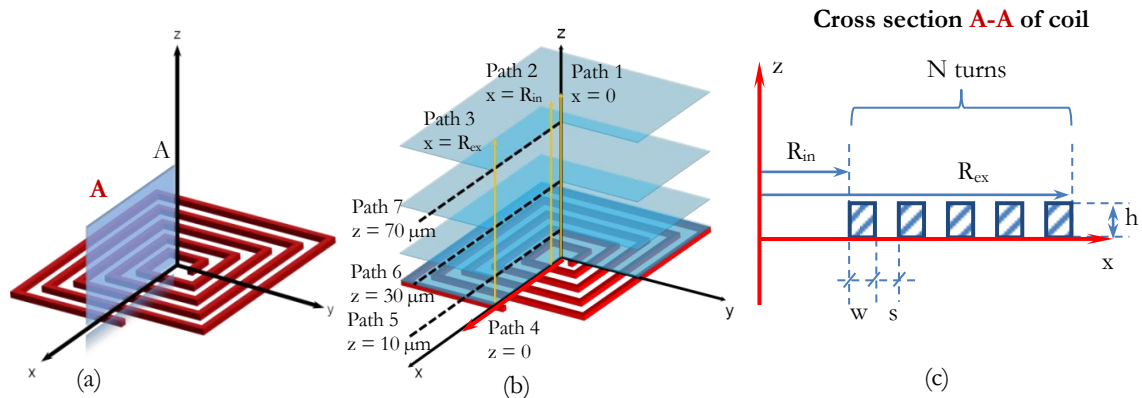


Figure 3.6. Simulation model: (a). Coil model; (b). Magnetic calculation at the positions that will be shown in simulation results; (c). Detail parameters of coil model at cross section A-A. w = width of Cu wire; s = space between two Cu wires; R_{in} : inner radius of coil; R_{ex} : outer radius of coil.

Figure 3.6.a shows a view of a square coil; The A-x-z plane cut was represented in ANSYS® in order to simulate the magnetic field in this plane. Figure 3.6.b shows the position of the paths used to quantify the modulus of the flux density. Figure 3.6.c shows the geometric parameters of the coil.

The magnetic flux density is calculated for:

- Paths (from 1 to 3) along the z-axis at three different positions in x-axis: center ($x = 0$), inner wire ($x = R_{in}$) and outer wire ($x = R_{ex}$) of the coil.
- Paths (from 4 to 7) along the x-axis at different distances from the wire surface (Cu). $z = 0; 10; 30; 70 \mu\text{m}$.

Table 3-1 shows the parameters used for the simulations and the used values. The values were chosen taking into account technological constraints related to cleanroom fabrication.

Table 3-1. Input parameters and explored values for magnetic field simulation

Input parameters for calculation	Simulated values
w (width of Cu wire)	10, 15, 20, 25, 30, 35, 40, 45, 50 μm
s (separation between 2 Cu wires)	10 μm
h (height of Cu wire)	15 μm
N (number of turns)	10, 15, 20, 25, 30, 35, 40
R_{ex} (outer radius of the coil)	500, 750 and 1000 μm
J (Current density)	1.10^9 A/m^2 (kept constant)

3.3.2. Simulation results

a. General considerations on the magnitude and shape of the magnetic field

The first view of simulation is shown in the Figure 3.7, which presents the magnetic flux density extracted along a cut of the coil from the center. It can be seen that the magnetic flux density (*i.e.* the trapping force) decreases as the distance to the coil surface is higher. Figure 3.8 shows the simulation results of the magnetic flux on all paths (from path 1 to 7) on the above surface of the square microcoil corresponding to parameters: $R_{\text{ex}} = 500 \mu\text{m}$, $N = 20$ turns, $w = 10 \mu\text{m}$, $s = 10 \mu\text{m}$ and $h = 15 \mu\text{m}$.

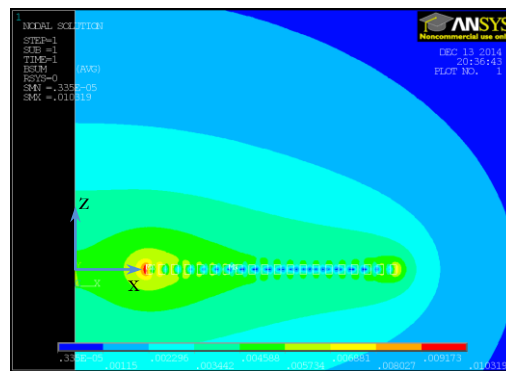


Figure 3.7. Simulated magnetic flux density (B) for a coil with $R_{\text{ex}} = 500 \mu\text{m}$, $N = 20$ turns, $w = 10 \mu\text{m}$, $h = 15 \mu\text{m}$

As predicted by equation (3_1) the B modulus decreases when the distance to the conductors increases. A $1/x$ shape can be roughly observed at Figure 3.8.a. The trapping capability of the coil is higher close to the coil's surface. Consequently, as the coil cannot be directly in contact with the liquid flowing in the microchannel, the

necessary protective layer must be fabricated as thin as possible. Furthermore, the trapping capability into a microchannel is very different on the space above or on the bottom of the channel, as it has been observed in [3].

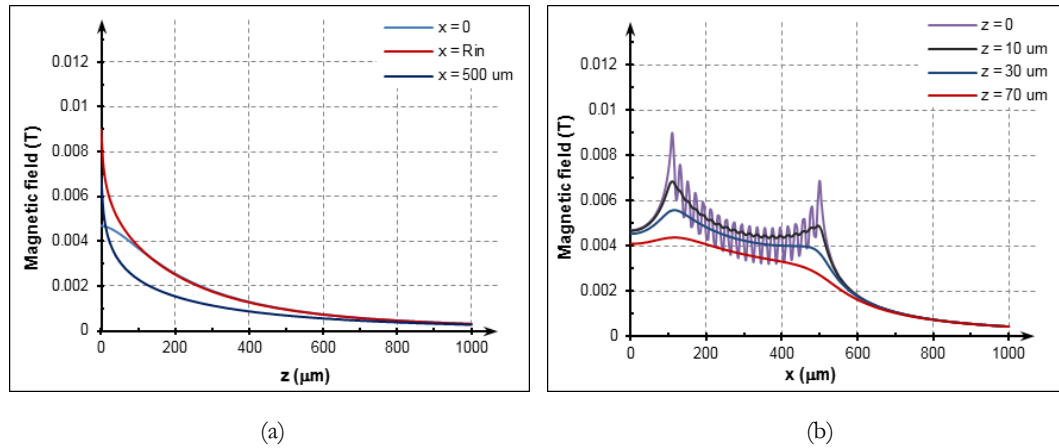


Figure 3.8. The profile of magnetic flux (B) of coils at path 4, 5, 6, 7 (a) and 1, 2, 3 (b)

Figure 3.8.b shows the B modulus ripple at paths 4, 5, 6 and 7 parallel to the coil surface. As it could be expected, the B modulus decreases at higher distances from the coil's surface, as well as outside the coil area ($x > 500 \mu\text{m}$). The intensity of B shows a strong ripple at a distance $z \approx 10 \mu\text{m}$ or lower due to the very close proximity of the coil's conductors. At distances higher than $10 \mu\text{m}$, the B modulus decreases and peaks disappear.

Other coils geometries (changing the turn numbers (N), radius (R_{ex}), width of copper wire (w), etc.) were simulated and gave similar distribution of the magnetic field modulus, Figure 3.9. In all cases, a fast decrease of B modulus can be observed when the distance to the surface increases. Furthermore, in the first μm above the coil surface, the B modulus is higher and shows a strong ripple: according to equation (3_17), these two effects combine to improve the trapping efficiency of the coil.

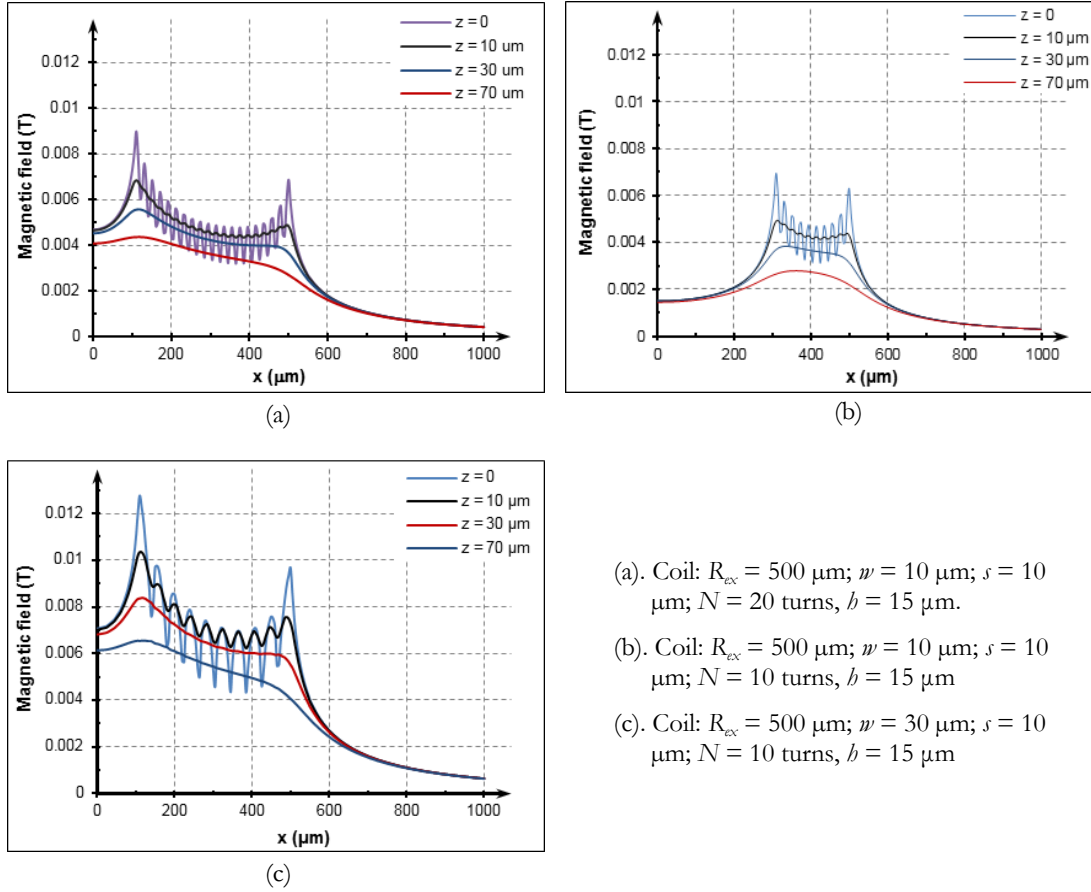


Figure 3.9. Profiles of magnetic flux (B) of coils at path 4, 5, 6, 7 of three coils with different parameters; the graphs (a) and (b) give the changes of B modulus when the number of turn is changed; the graphs (a) and (c) give the changes of B when the width of conductors is changed

Figure 3.9 also shows the influence of the wires width on the magnetic field ripple. Figure 3.9.a and b are obtained with $10 \mu\text{m}$ wide wires and Figure 3.9.c is obtained with $30 \mu\text{m}$ wide wire. A stronger ripple is observed at the top of the coil and at $10 \mu\text{m}$ distance, suggesting a favorable influence on trapping. Despite this advantage in the few μm above the coil, no difference can be observed at $30 \mu\text{m}$ distance, suggesting that for deep channels of more than some tens of μm , the width of the wire has no influence: trapping in the top of a deep microchannel is not improved with wide wires.

A set of simulations was carried out for different coils geometries. The general shape of B modulus is the same as observed in Figure 3.9. and Figure 3.10 shows a schematic view of B modulus. Increasing the number of turns for given dimensions of conductor width, thickness and space between conductors result in an increase of the mean value of B modulus, as well as the mean force value exerted on a bead in the channel. Furthermore, the ratio between the maximum value of B modulus and the minimum magnitude attained on the coil surface is also increased.

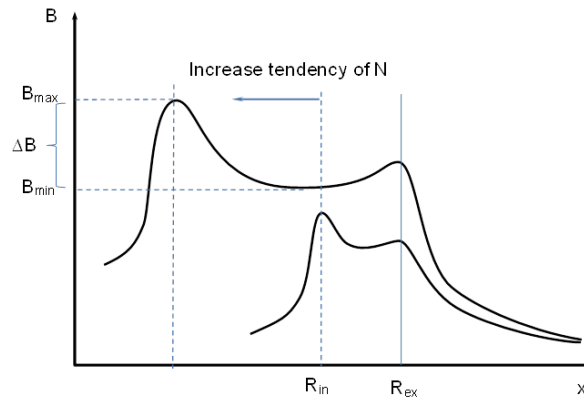


Figure 3.10. General shape of B modulus for coils having the same diameter, but different number of turns

These results show that the trapping will occur preferably on the surface of the coil's windings. The trapping of the beads can occur mainly at the edges of the coil or on its entire surface, depending on the magnetic field homogeneity. A magnitude that represents the homogeneity of trapping capability is the ratio B_{\max}/B_{\min} . Figure 3.11 shows the B_{\max}/B_{\min} ratio as a function of the number of turns for several coils of the same outer radius ($R_{\text{ex}}=500 \mu\text{m}$).

In order to homogeneously trap on the coil's entire surface, a high value of B is desired on the whole chip: the B_{\max}/B_{\min} ratio should then be as low as possible.

However, this homogeneous trapping demand leads to reduce the number of turns of the coil, and so to decrease the maximum magnetic field obtained, as shown in Figure 3.10 and Figure 3.11: homogeneously trapping also means a lower trapping capability.

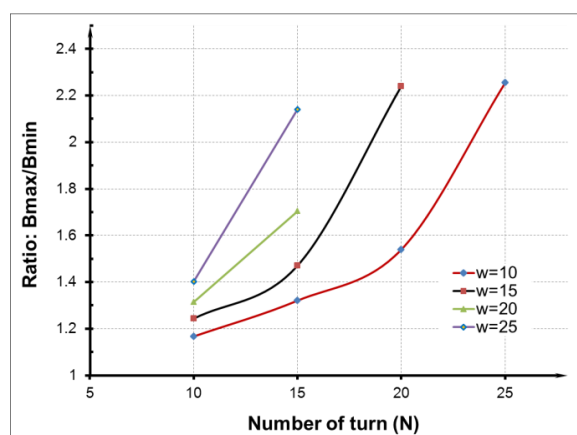


Figure 3.11. Homogeneity of the magnetic induction: B_{\max}/B_{\min}

b. Coil geometry effect on the power loss and heating

For given inner and outer radius of the coil (R_{in} and R_{ex}), the number of turns, the spacing and conductor's width can be different (Figure 3.12.a). Although the effect on

power loss may not be significant in macroscopic coils, the technological limits of microcoils, which are determined by lithography resolution and deposition or plating technologies, drive to a significant minimum spacing between conductors (higher than several micrometers, which is a significant percentage of the copper width for small wires). The surface filled by copper is represented by the filling ratio:

$$r = \frac{N \cdot w}{R_{\text{ex}}} \cdot 100\% \quad (3_18)$$

We chose here to have a space between conductors of $s = 10 \mu\text{m}$, which corresponds to a safe lower limit when using thick copper micromolding. For given spacing and width of the conductors, the filling ratio increases with N . Its higher limit is given by the ratio of the width of the conductors (w) to the sum of the width and spacing of the conductors ($s + w$).

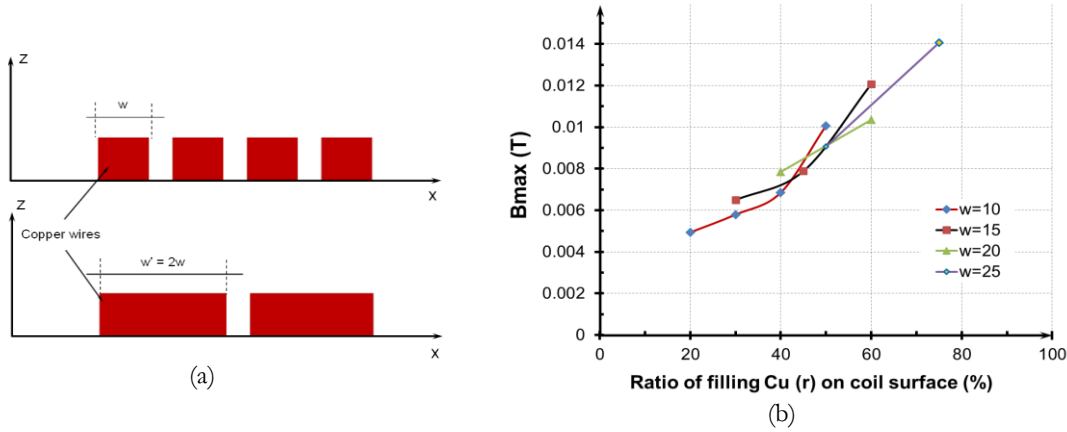


Figure 3.12. (a). Different widths of the conductors, (b). Effect of filling ratio on B_{max} value ($R_{\text{ex}} = 500 \mu\text{m}$).

Figure 3.12.b shows the maximum modulus of flux density B_{max} generated with coils for different conductors' width and turn number (w and N) at path 5 ($z = 10 \mu\text{m}$). In this figure, the B_{max} increases with the rise of N at a given w value. The obtained filling ratio values are between 20% and 75%.

As the simulation input was chosen to be the current density, the product of the number of turns by current flowing through the coil ($N \cdot I$) is then proportional for a given number of turns to the width of the conductors. It can be observed at Figure 3.12.b that for a given coil configuration, the effective maximum flux density is roughly proportional to the filling factor.

The maximum B modulus is obtained with the highest filling ratio (around 75%), which means that a design rule for trapping coils can be to make coils with conductors' width larger than the spacing between conductors:

$$w \gg s \quad (3_{19})$$

Figure 3.12.b shows that the maximum B modulus is not always obtained for a wider conductor: the coil with $w = 20 \mu\text{m}$ allows a B_{max} of 10 mT but $w = 15 \mu\text{m}$ allows a B_{max} of 12 mT. When w is high, a space kept in the center of the coil cannot be filled with a conductor. The upper limit of the filling ratio is then not reached and the B modulus is lower than for another configuration that seemed better in a first approach.

Despite the high interest for power efficiency to maximize the width of the wires, it can be pointed out that when conductors are very wide, leading to a coil with very few turns, the current density is not constant along the conductor's section, leading to higher power dissipation than for lower widths. The optimal number of turns is then given by a trade-off between the maximization of the filling factor while keeping the current density equal in the conductors section.

c. Power consumption and merit factors

The power loss by Joule effect in the coil is known to be:

$$P = R.I^2 = V_{\text{Cu}} \cdot \rho_{\text{Cu}} \cdot J^2 \quad (3_{20})$$

where I is the current flowing through the coil, J is the current density, ρ_{Cu} is the resistivity of copper and V_{Cu} is the total volume of copper.

Figure 3.13 shows the variation of power consumption in coils ($R_{\text{ex}} = 500 \mu\text{m}$) as a function of the turn number for several widths of copper conductors.

Previous paragraph showed (Figure 3.12) that the B_{max} is highest when N and w values are maximized. Furthermore, a strong increase of B_{max} is obtained when filling ratio is higher than 60%. The power consumption represented at Figure 3.13 shows that for given outer radius and width of the conductors, increasing the filling ratio (i.e. increasing N) only slightly increases the power losses. For example, when $w = 10 \mu\text{m}$, designing 20 or 25 turns give almost no change on the power losses, while fig 3.9 showed that the value of B_{max} is still increased when the number of turns is higher: both B_{max} and power consumption criteria induce to choose the highest filling ratio.

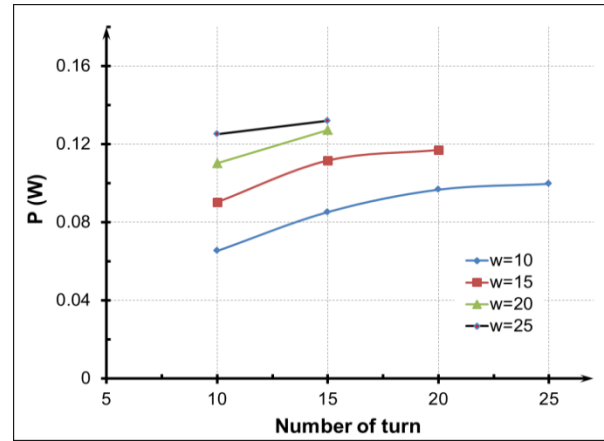


Figure 3.13. The power consumptions (P) in coil with different turn number and width of Cu wire ($R_{ex} = 500 \mu\text{m}$).

To estimate comprehensively the relationship of magnetic field and power consumption, the current merit factor $M_i = B_{\text{max}}/I$ and the power merit factor $M_p = B_{\text{max}}/P$ can be used to quantify the ability of coils to produce a magnetic field for a given amount of current and a given amount of power loss, i.e. heating of the coil, as shown in Figure 3.14.

The M_i merit factor curves (Figure 3.14.a) seems to indicate that the configuration of the coils giving a higher magnetic flux density is obtained maximizing the number of turns of the coils, i.e. leaving no empty space in the center of the coil. Furthermore, M_i curves show that the best configuration is obtained with thin wires.

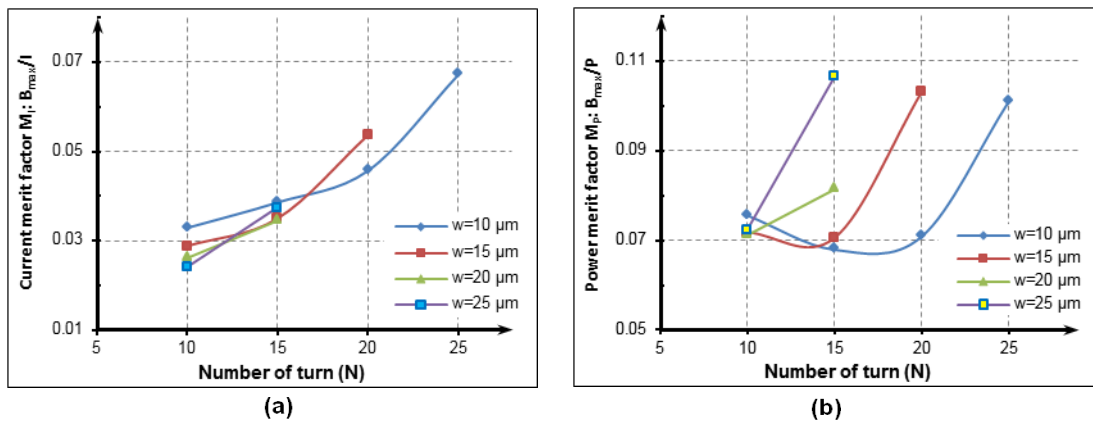


Figure 3.14. Current and power merit factors M_i and M_p of coils with $R_{ex} = 500 \mu\text{m}$; $s = 10 \mu\text{m}$ and different turn numbers and wire widths. (a). Power merit factor M_i is calculated by the maximum generated magnetic field on each unit of injected current (I) in coils. (b). Power merit factor M_p is calculated by the maximum generated magnetic field on each unit of energy consumption;

The M_p merit factor curves (Figure 3.14.b) indicates that all the configurations of the coils can have a similar production of magnetic field provided the inner space of the coil is filled with conductors. A slight advantage can be observed for coils with

wider wires which can be attributed to the slight raise of the filling factor obtained in these cases. It should be pointed out that this conclusion could be modified if the width of the wires became high relatively to the coil's radius: if the wire's width increases much, the maximum theoretical filling factor cannot be obtained, hindering the final power merit factor M_p .

d. Conclusions:

Magnetic field generated by model planar microcoils has been calculated by ANSYS® software. These calculations show about a detailed panel of the 2D magnetic field generated by the coil at reference space positions (according to x -axis and z -axis).

Based on the analysis of B_{max} , B_{min} , M_i and M_p , some criteria for the coils design can be proposed: the coils should have large turn number in order to increase the magnitude of the induced magnetic field. For micro-machined coils, the spacing between 2 wires cannot be 0. The minimum width between wires can seriously hinder the magnetic field value obtained for a given power loss. Consequently, the wires should be much wider than the space between 2 wires (equation (3_19)).

The results show that to achieve the optimal value of B with lower energy consumption and high power efficiency, the surface of the wafer should be filled with the coils wires, i.e. no empty space should be left in the center of the coil. Furthermore, the width of the wires should be kept much higher than the space between two adjacent wires.

Other simulation results with different input parameters, as shown in Table 3-1, give the same trends. Full results are presented in detail in **Appendix 1**.

These results are the basic information to perform the microcoils fabrication based on the input parameters in calculating.

3.4. Planar coils fabrication and characterization

This part describes the coil fabrication processes (multi-layer fabrication) on silicon substrate. Coils are designed in millimeter and sub-millimeter dimensions. The coils are realized with a three layers process:

- Bottom track for connecting the center of coil to outer circuit
- Dielectric layer between the bottom track and thick coil wires

- The thick coil wires on the third layer.

3.4.1. Mask design

Due to space constraints, only some of the design previously simulated has been drawn on a mask for fabrication. It was chosen to draw the best power performing (high power merit factor) coils and some samples of medium performing coils in order to check the calculated behavior. Three masks have been designed using LASI¹ ver.7.0.86 software for the three levels process, all of them with dark field (Figure 3.15). The mask contains 12 chip of around 2.172 cm²; each chip has three coils which are arranged in line (Figure 3.15). To obtain a high resolution of the patterns, soda-lime masks have been manufactured (TOPPAN PHOTOMASK, Inc.).

The first mask level corresponds to the copper track for the center contact with the coil and outside circuit. Long connections tracks have been drawn in order to have enough space to add the microfluidic part of the chip. After the first layer, an insulating layer of SiO₂ is necessary to avoid short circuit of the thick coil wires. Thus, the second level of the mask corresponds to the windows that have to be opened through the insulating layer to enable the electrical contact between the Cu coil and the copper wire. In the third level the coils are designed. The coils contain from 15 to 46 turns, the coil-wire width ranges from 10 to 30 μm and the separation between two wires is 10 μm . The radiuses (R_{ex}) of all coils are 500, 750 and 1000 μm .

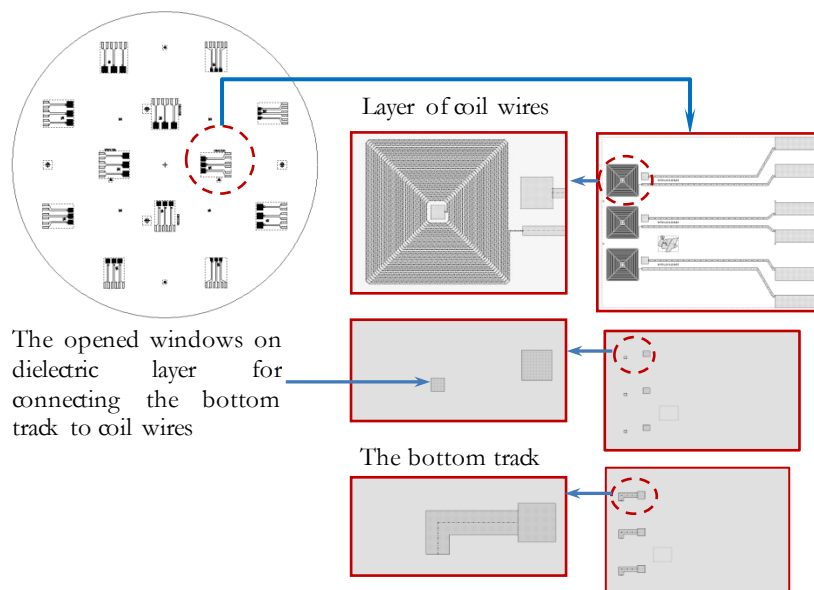


Figure 3.15. Description of mask layer design and coils arrangement

¹Layout Software for Individuals, <http://lasihome.com>

3.4.2. Fabrication process of coils

The coils are fabricated on 100nm SiO₂/Si substrates. Figure 3.16 shows the process of coil fabrication. A lift off process is used to fabricate the first layer of the coil that consists in a Cu track to connect the center of the coil: an AZ5214E photoresist (MicroChem®) is spun and pre-baked at 110°C for 55 s on a hot plate (1); the 1.5 µm thick photoresist layer is exposed in UV light using a dose of ~60mJ/cm². After the exposure, a post bake at 120°C for 2 min on hot plate is performed, followed by a flood exposure using a dose of 200 mJ/cm². Finally the photoresist is developed using diluted AZ developer (AZ - H₂O 1:1) (2).

A layer of Ti (10nm) and Cu (700nm) is sputtered by means of a Denton sputtering system (EPLORER Denton Vacuum® system) (3). The lift-off process is performed in acetone in order to obtain the Cu under track (4). A quick Cu etching step (wet etching) of 5 s is performed to round the edges of the Cu track. After that, a 500 nm-thick dielectric layer of SiO₂ is deposited by PECVD (STS PECVD System). Then, a 4 µm-thick layer of TI35ES photoresist is spun over the SiO₂ layer and the windows for creating the contact between bottom Cu track and wire center of coil are patterned by lithography (5). These windows are opened in the dielectric layer by reactive ionic etching (STS RIE system) (6). A sputtered seed layer of Ti (10nm)/Cu (100nm) as coil wire seed layer is deposited and a 20 µm thick AZ4562 photoresist (MicroChem®) is spin-coated and baked at 90°C for 1 h by applying a temperature ramp rate of 210°C/h from 20°C to 90°C (7). The photoresist is exposed using a dose of 350mJ/cm² and developed in AZ 400K developer (AZ 400K – H₂O 1:4) (8). Cu thick wires are obtained by electrodeposition in a sulfate bath with a current density of 30 mA/cm², controlled by potentiostat/galvanostat system (MetrohmAutolab), during 30 minutes in order to obtain a thickness of around 15-18 µm (9). Subsequently, the photoresist is removed (10) and the seed layer is etched by an argon ion beam etching (IBE Roth & Rau IonSys 500) (11). Finally, the wafer containing coils is diced in suitable pieces for assembling microfluidic chip step.

Figure 3.17 (a) is a general view of a diced chips with 2 pairs of 3 coils.

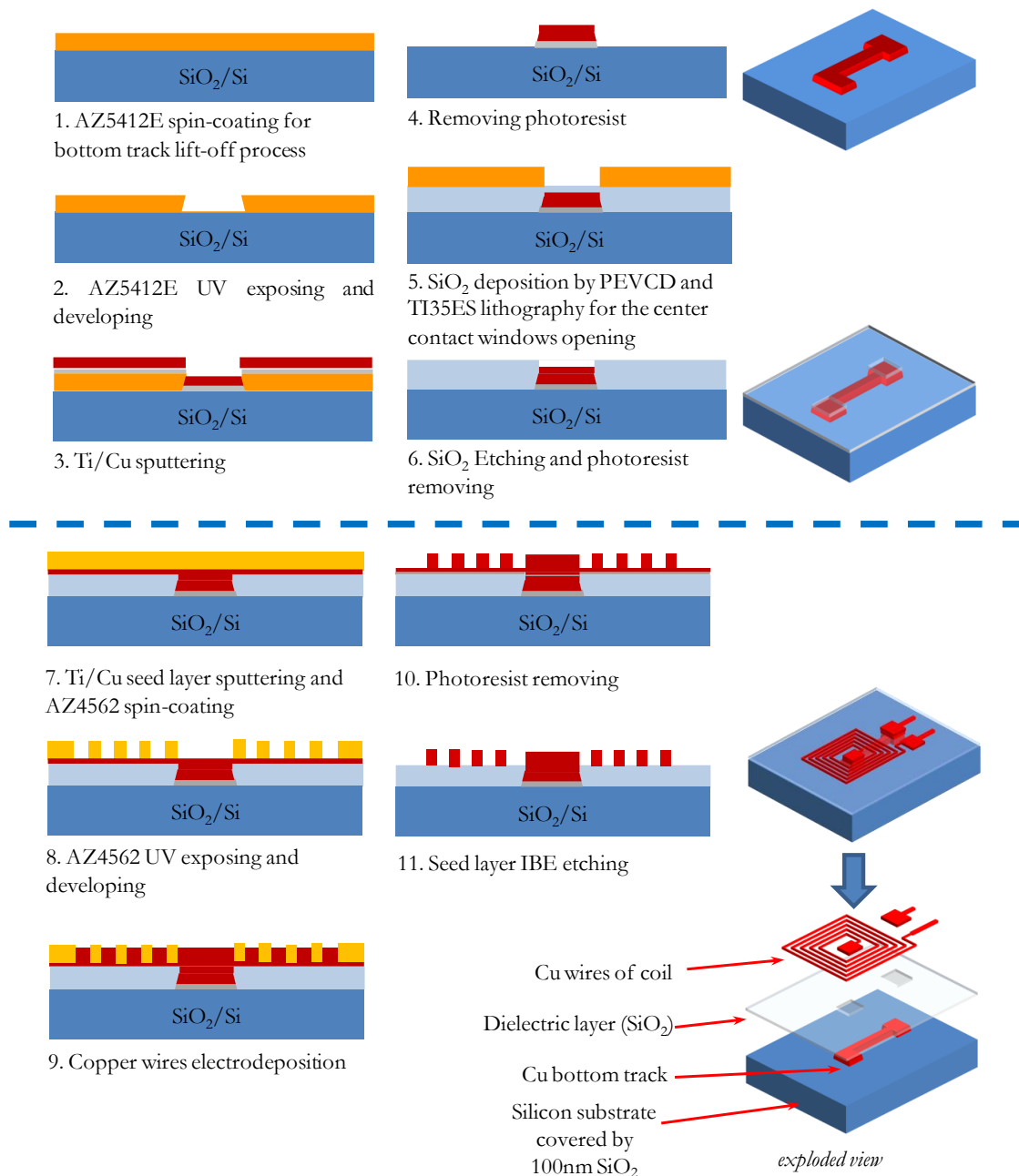


Figure 3.16. Fabrication process of microcoil by multi-layer microfabrication technique

Profile measurements are done to check the thickness of the wire (DEKTAK 8, Veeco) and optical microscope images are taken to get an overview of the coils and to check the coil geometric parameters. An example of observation is presented on Figure 3.17 (b) where the under track designed for the connections can be seen.

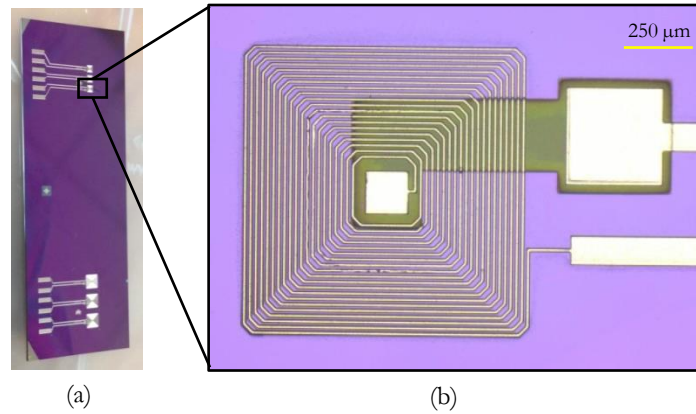


Figure 3.17. (a) Picture of coils after dicing, (b) Microscope images of the fabricated coil (1 mm wide, 20 turns, 10 μm wide of Cu wires, 10 μm wide of space between two wires)

For this coil, we measured a Cu wire of 10.8 μm wide and 10.7 μm high; a space between two wires of 9.1 μm . These parameters present minor differences to the mask's parameters: the width of conductors and the space between two conductors are 10 μm . These differences come from the lithography and the etching processes.

Complementary characterizations are made MEB. On the SEM images of Figure 3.18, the shape of wire's edges is clear and the result of etching process is very satisfactory.

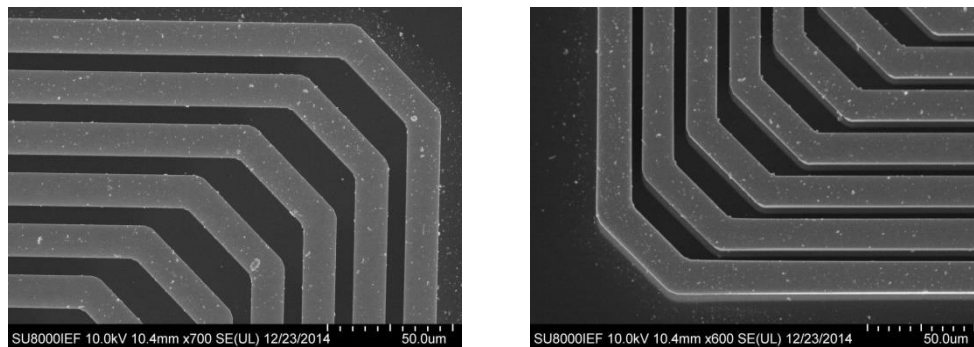


Figure 3.18. SEM images of coils (1 mm of size, 20 turns, 10 μm wide of Cu wires, 10 μm wide of space)

3.5. Conclusions

Magnetic field generated by model planar microcoils was calculated by ANSYS® software.

The calculation results show a detailed view about magnetic field of coil at some positions chosen to synthetically represent the magnetic field in the space in the vicinity of the coil. The simulations show that the magnetic field intensity on distance along z-axis decreases rapidly, roughly with a $1/z$ shape; furthermore, at a distance $>50\text{ }\mu\text{m}$ it is reduced of 50% or more. This result points out the crucial importance of the thickness of a protection layer on the microcoil when microcoil is integrated in microfluidic system: it must be as thin as technologically possible.

The power consumption (P) was calculated. Current and power merit factors were defined: they represent the ability of a coil to generate a magnetic field for a given current or power consumption. In addition, the results show that to achieve the optimal value of B with lower energy consumption and high power efficiency will reduce the working temperature of the coil.

General design rules were determined with these results: The surface of the wafer should be filled with the coils wires, i.e. no empty space should be left in the center of the coil. The width of the wires should be kept much higher than the space between 2 adjacent wires.

These general rules can apply to coils of any shapes. Nevertheless, this FE model is limited by the fact that 2D simulations have been used. Shape effect of the coils and 3D effects that can occur are then not taken into account. This limitation is specially true when wires are square or meander shaped. Corner shaped wires are likely to drastically increase the magnetic field variation, and then the attraction force. Further calculations are necessary to quantify shape effects. However, taking into account both the filling factor and the shape effect is a very computing resource consuming task and could not be realized in this work.

The fabrication process using 3 mask levels was designed and implemented. The coils windings are manufactured by thick (10-20 μm) copper electroplating. A buried lift-off of 700 nm thick copper is used for center wire connection with external connection pads. Microcoils were then fabricated and characterized with optimized geometric properties in order to verify the design results.

REFERENCES

- [1] R. Fulcrand, A. Bancaud, C. Escriba, Q. He, S. Charlot, A. Boukabache, A.-M. Gué, On chip magnetic actuator for batch-mode dynamic manipulation of magnetic particles in compact lab-on-chip, *Sensors and Actuators B: Chemical*, 160 (2011) 1520-1528.
- [2] A. García, J.A. Carrasco, J.F. Soto, F. Maganto, C. Morón, A method for calculating the magnetic field produced by a coil of any shape, *Sensors and Actuators A: Physical*, 91 (2001) 230-232.
- [3] A. Beyzavi, N.-T. Nguyen, Modeling and optimization of planar microcoils, *Journal of Micromechanics and Microengineering*, 18 (2008) 095018.
- [4] Richard P. Feynman, Robert B. Leighton, M. Sands, *The Feynman Lectures on Physics*, New Millennium ed., Basic Books, New York, 2010.
- [5] M.A.M. Gijs, Magnetic bead handling on-chip: new opportunities for analytical applications, *Microfluidics and Nanofluidics*, 1 (2004) 22-40.

CHAPTER 4. FABRICATION OF MICROFLUIDIC CHIPS AND APPLICATIONS

- *Describing the fabrication process of microfluidic chip with integrated microcoils: The fabrication process of PDMS channel and packaging process chip.*
 - *The application of microfluidic chips in trapping magnetic micro/nano beads at low temperature ($<37^{\circ}\text{C}$)*
 - *Application of these chips in grafting antibodies IgGs on beads surface and valuating by IgG-FITC-conjugated.*
-

In this chapter, the microfluidic chip is finalized in two main steps: PDMS channel fabrication (channel design, replica molding and PDMS prototyping) and chip assembling (packaging process and mounting chip to PCB motherboard). In addition, a multi-valve switch is designed and fabricated in order to control the liquid flows in the immunoassay process inside microfluidic chip. In the packaging process, techniques of reversible packaging are developed in order to re-use bottom substrate, which contains microcoils. Before the bonding step, an optimal thin layer is chosen to protect coils from liquid interaction while keeping bottom of channel close to the coils' surface.

The microfluidic chip is used for magnetic beads trapping experiments, temperature measurement, and IgG antibodies immobilization inside channel. The effects of applied current in the coil and trapping time are studied on the trapping efficiency and temperature rise. The IgGs immobilization is performed inside channel based on several steps: activating surface of carboxyl-beads, grafting primary IgG-antibody on activated beads' surface and validating the grafted of primary antibody layer by coupling it with IgG-FITC-conjugated.

4.1. Introduction

This chapter presents the way to integrate the coils in the microfluidic chip and the proof of device usability for immunoassay and biological detection.

Even if PDMS is the most common material for microchannel fabrication, it presents some disadvantages with bio-components [1, 2] (surface adsorption). To limit this effect, a surface treatment of the PDMS channels is applied to obtain a hydrophilic surface that will block the non-specific adsorption. The treatment process is performed with Poly(Ethylene Oxide) – PEO combined with oxygen plasma pre-treatment.

Finally, results of the microfluidic chip application in biochemical grafting of nanobeads will be shown. The experiment consists of building the sandwich structure of bead-IgG¹-FITC² with a protocol validated in micro test tubes.

¹ IgG: Antibody from mouse serum

² FITC: Fluorescein isothiocyanate conjugation kit from Sigma Aldrich®.

4.2. Microfluidic chips fabrication

The microfluidic chip is mainly constituted microcoils on bottom substrate and cap in PDMS with microchannel.

We present here the channel design, its fabrication and its assembling steps with the bottom substrate by using specific packaging techniques, and a specific multi-valve switch used to control the flow inside the channel.

4.2.1. PDMS channel

The PDMS channel is fabricated with the common PDMS replica molding process. The channel design is drawn by Inkscape¹ software. Then, the mask for molding the channel is printed on polymer transparent sheet. This method is easy, fast and cheap when very high resolution of mask is not required.

a. Design of PDMS channel network

The Figure 4.1 shows the first channel design type develop for the application.

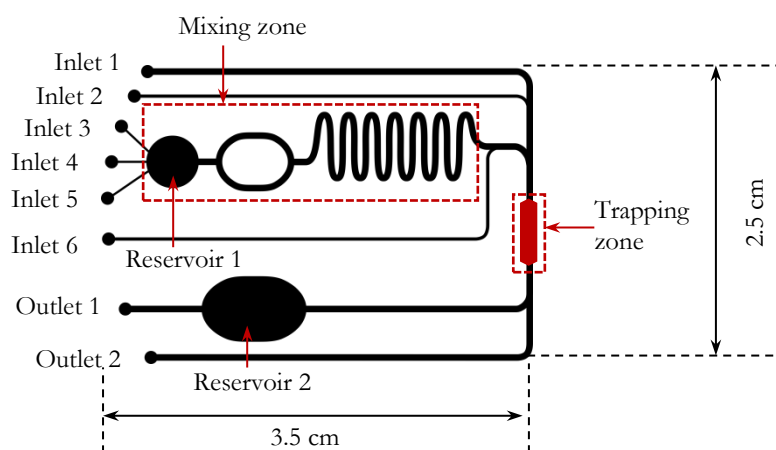


Figure 4.1: Design of channel network

This channel design includes three parts:

- *Inlet and outlet part:* There are six inlets for six different solutions. The inlets 3, 4 and 5 are designed for injecting three solutions together (to active beads, see page 21). The inlets 1, 2 and 6 are used for solutions from which we want to limit the interaction with other one while they flow inside channel. There are two outlets for two types of leaving reacted substances: one for normal outlet (outlet 2) and the other (outlet 1) for the case the reacted substances need to be kept in the inside reservoir (reservoir 2) for a while.

¹ A free software of Inkscape Team, www.inkscape.org

in 5 minutes, and finally, the mold is rinsed with isopropanol and dried with nitrogen flow (Figure 4.3.c).

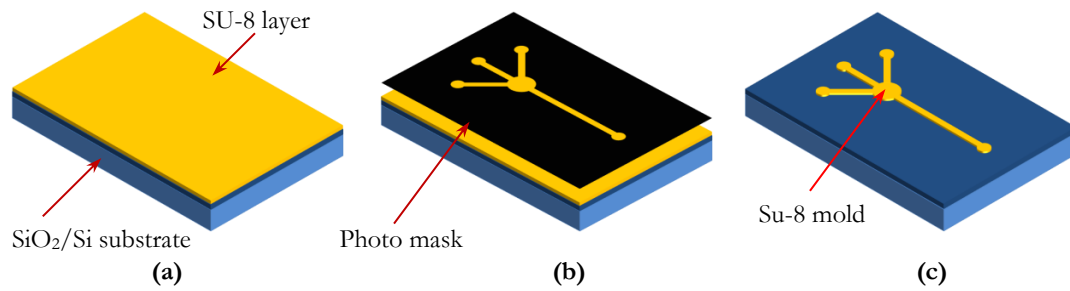


Figure 4.3. SU-8 3050 photoresist molding process

PDMS rapid prototyping by replica molding, (Figure 4.4): fresh PDMS is prepared by mixing uniformly two components: silicone elastomer base and curing agent (Sylgard® 184 silicone elastomer kit, purchased from Dow Corning Corp.) at a ratio 10:1 (wt./wt.). After mixing, the mixture is degassed in a vacuum chamber. Then, the fresh PDMS is poured onto the master mold, and cured in oven at 90°C for 1 hour or at 75°C for 2 hours (a). Subsequently, the embossed channel is carefully released from the SU-8 mold (b) and cut in the suitable shape. Finally, inlets and outlets of channel are drilled directly by PDMS tool kits (c).

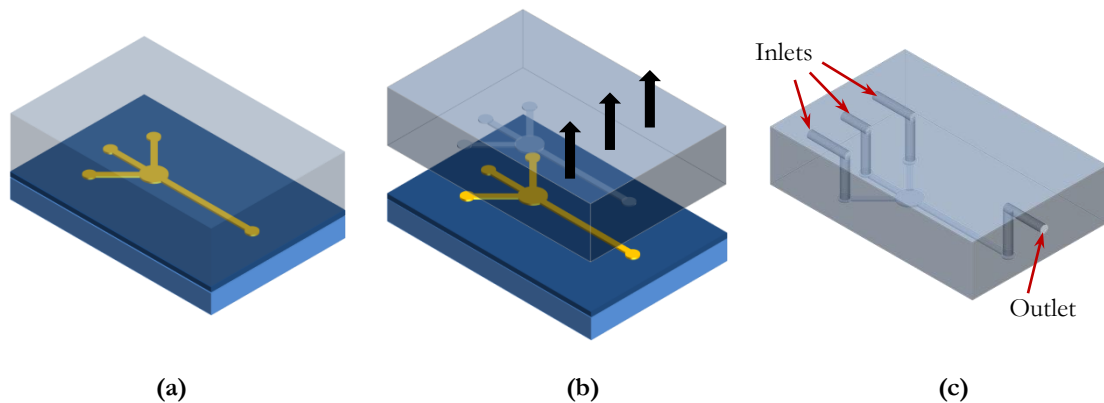


Figure 4.4. PDMS rapid prototyping process by replica molding

Optical microscope is used to characterize the geometry of channel mold and PDMS channel. Figure 4.5 shows the geometry of the SU-8 mold (250 μm wide and 50 μm high) after fabricating. Because of the limited resolution of channel photomask, the sharpness quality of mold and channel is not very high.

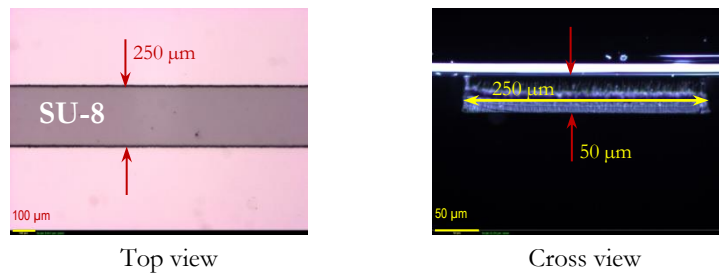


Figure 4.5. Optical microscope images of SU-8 mold

Figure 4.6 shows the microscope images of PDMS channel, which has been casted using SU-8 mold. Figure 4.7 shows photos of two types of the PDMS channel based on the two channel designs that were described in the previous part.

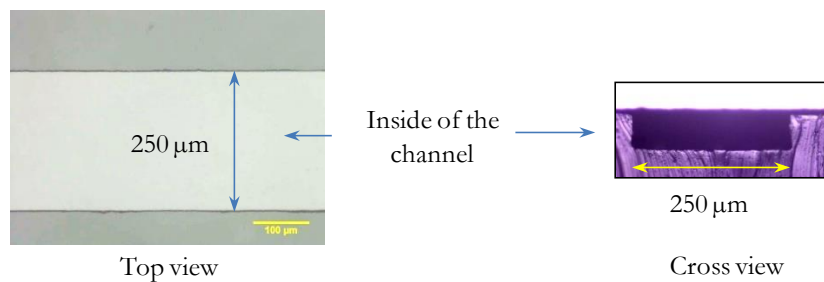


Figure 4.6. Optical microscope images of PDMS channel

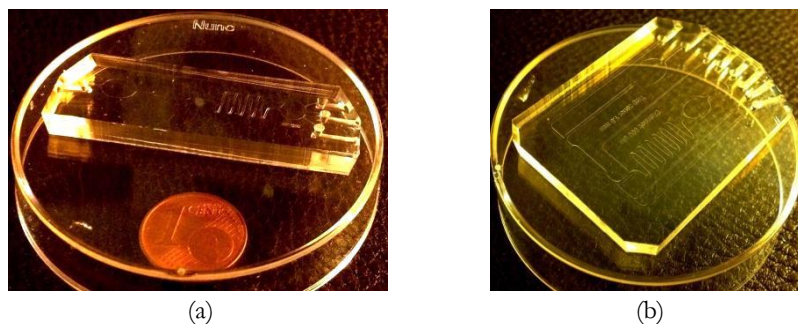


Figure 4.7. Photos of fabricated PDMS channels: (a). Channel with three inlets and one outlet; (b). Channel with six inlets and two outlets

4.2.2. Valves switch

Because the volume of channel is very small (about few microliters), the stability of flow inside channel is very sensitive with small actions such as un-plugging tube to replace liquids in each steps of experiment. To manage liquid flows injection from syringe pump to the channel with many inlets, a specific multi-valve switch has been designed and fabricated.

This valve is very useful to stop the flow, to change the injected liquid in channel and to control the flow during the experiment process and injecting multi flows together. Homemade with simple materials, even if it has not absolute precision and

fast responding time in operation as these commercial products (i.e. the flow switch of Elveflow® or Fluigent®)⁽¹⁾, cheap and well adapted to our experiment.

a. Design of multi-valves switch

The valves are constituted of 3 main parts: one flexible part in PDMS containing channels and 2 Plexiglas clamps, Figure 4.8. The valves are operated by handling a serial of screws, each screw applying a mechanical strength on a flexible membrane controlling the flow inside the channel, Figure 4.8 (1).

Two clamps help to fix the PDMS valve channels and support screws in operating functions of valve. One pair of clamps includes one bottom support, Figure 4.8 (2a), and one top support with positions for screws operation, Figure 4.8 (2b).

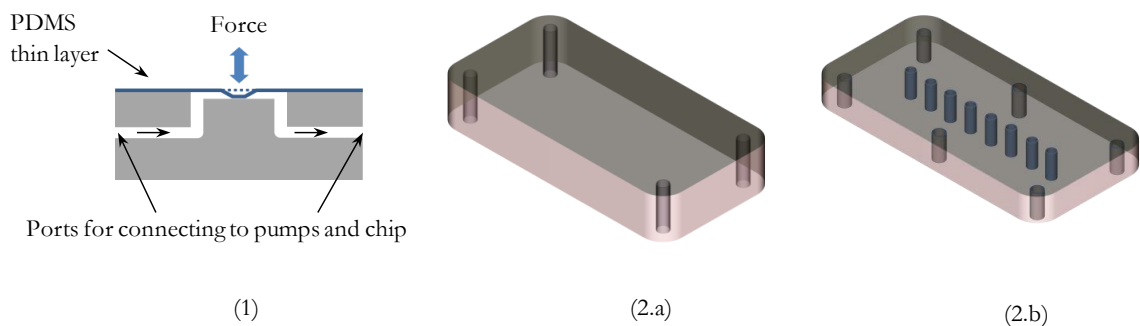


Figure 4.8. (1) Flexible channel valve principle and (2) description of clamps pair for fixing the valve channels

Two types of valve system are designed for the two channel networks, Figure 4.9. The first one, Figure 4.9 (a), is used for the channel design shown in Figure 4.1: there are six ports corresponding to six inlets of channel. The second one, Figure 4.9 (b), is used for the channel design shown in Figure 4.2: there are three main ports corresponding to the three inlets of channel. All solutions from pumps for experiment are connected to one of the two groups of “inlets of liquids”. The inlet of buffer supplier will usefully help to clean all channel and tubing part, which connects valve switch to channel.

⁽¹⁾ <http://www.elveflow.com>, and <http://www.fluigent.com>

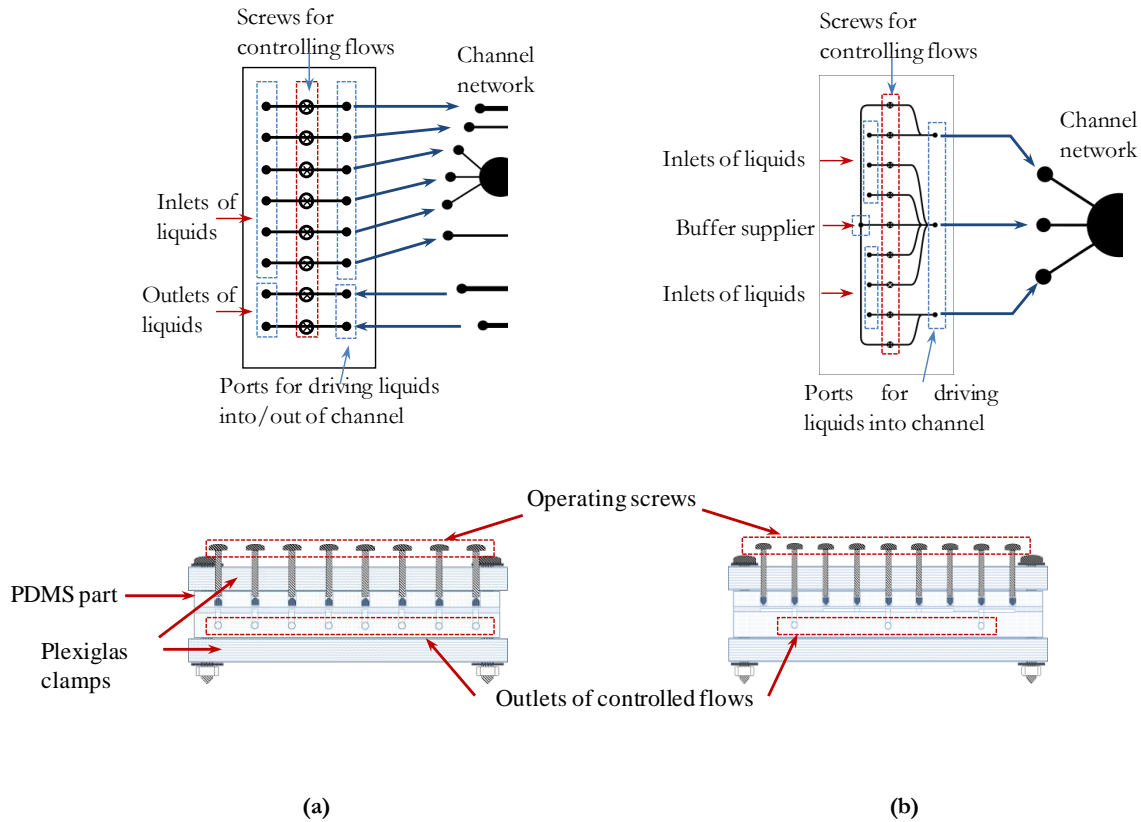


Figure 4.9. Descriptions of two types of the multi-valve controller top and crossed views; (a) Valve with separated on/off line; (b) Valve with three main ports for inlets and some combined flows

b. Multi-valve switch fabrication

These valve switches are fabricated in two steps: fabrication of PDMS part and fabrication of mechanical part (Plexiglas clamps). The Plexiglas clamps are machining and the PDMS channel valves present a PDMS thick layer containing the channel and a PDMS thin layer closing the channel, Figure 4.10.

Like PDMS channel cap, channel valves are obtain by replica molding on an SU-8 master mold (Figure 4.10 (1) to (4)). In the last step (5), channel valves are bond to a PDMS layer of 20 μm thick to close channel. This PDMS layer is obtained by spin-coating fresh PDMS (10:1 ratio) on silicon wafer coated with Teflon layer (C_xF_y) in order to easily peel off, [3, 4]. The layer is cured in oven at 75°C for 1 hour. The bonding of PDMS channel valve to that PDMS layer is performed by plasma treatment (1 minute, O_2 pressure of 0.4 mbar) and thermal treatment at 75°C for 1 hour, Figure 4.10 (5).

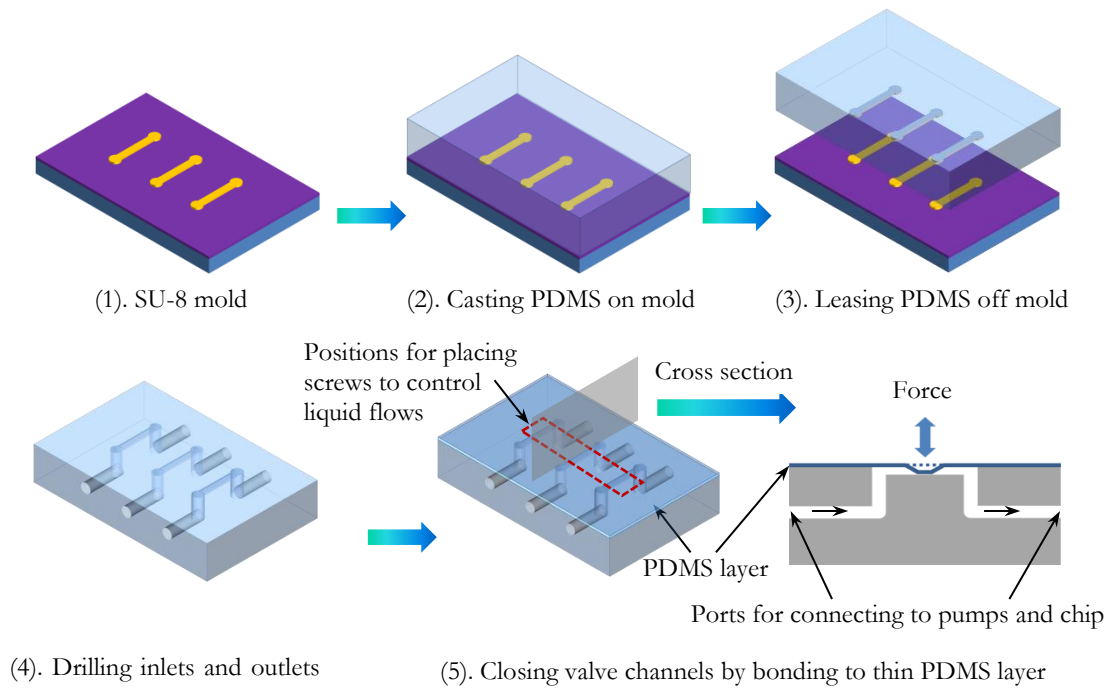


Figure 4.10. The fabrication process of the PDMS part of valve switches

Figure 4.11 show the valve switch and the connection of this switch to channel and syringe-pump system.

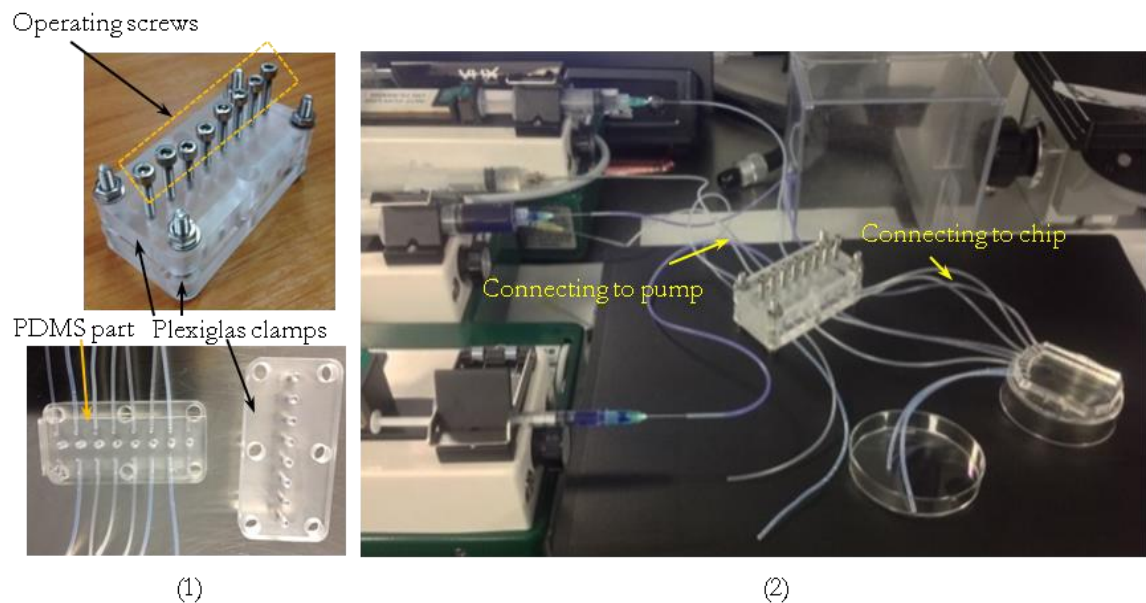


Figure 4.11. Valve switches (1) and switch connection with channel network and syringe pump system (2)

4.2.3. Microfluidic chip packaging

Before closing the microfluidic channel on the bottom substrate, a protective layer has to be applied on the coil surface to insure its wire electrical isolation. Our choice naturally turned to a thin spin-coated PDMS layer, PDMS to PDMS bonding been very easy. Indeed, by short oxygen plasma treatment combining with thermal

treatment [5, 6], very strong bonding force are obtained. This irreversible bonding can be applied in some fast and simple test of disposable chips [7, 8]. For instance, it has been used for closing the channel of the multi-valve switch seen before or for some primary experiments with the microfluidic chip. However, for our final device, a reversible bonding is desirable as it allows easy channel cleaning, even channel replacement and the possibility to re-use the bottom substrate. Indeed, this substrate contained the coils, which have required several fabrication steps.

In this part, two packaging techniques are presented: both with the specificity of allowing channel cap peel off from the bottom substrate. These two techniques have been characterized by leakage test and peeling cycle (methods presented in **Appendix 3**). Apart from their process steps, the main difference between these two techniques is the room where the peel off takes place: between the coils protective layer and the PDMS channel cap (Figure 4.12 (b)) or directly from the coil surface (Figure 4.12 (c)).

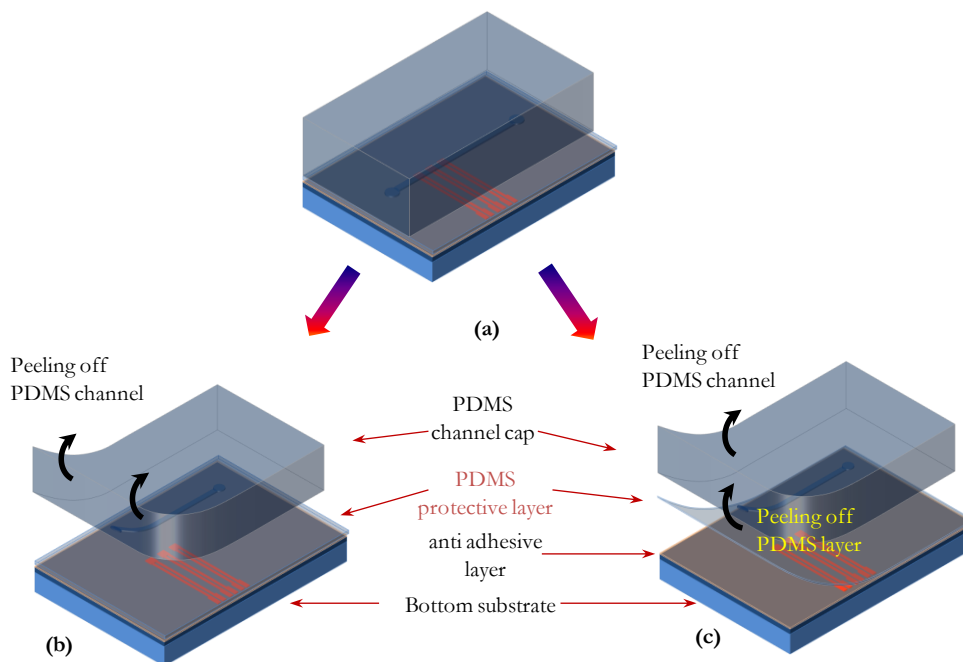


Figure 4.12. (a) Microfluidic chip with bonded channel⁽¹⁾; (b) PDMS channel able to peel off bottom substrate; (c) Both of channel cap and PDMS layer able to peel off bottom substrate after bonding

4.2.3.1. PDMS / PDMS reversible packaging based on stamping technique

The first reversible packaging technique has been developed by the stamping technique using Dimethyl-methylphenylmethoxy siloxane (DMPMS), a type of silicone conformal coating, as an adhesive layer on PDMS-coated substrates.

¹ The channel form illustrates only the fabrication process; it is not the real form of channel

This original process has been first developed on blank substrate and all detailed results are presented in a paper: “Reversible bonding by dimethyl-methylphenylmethoxy siloxane – based stamping technique for reusable poly(dimethylsiloxane) microfluidic chip”, (**Appendix 2**). In this paper, we demonstrate the feasibility of PDMS/PDMS and PDMS/glass reversible bonding using stamping technique with DMPMS. This technique is easy to perform as it needs only spin-coating and thermal curing steps, as shown in Figure 4.13. The bond strength is suitable for high working flow rate/pressure of liquid in channel (up to 500 $\mu\text{L}/\text{min}$ or 200 kPa). The cycle “peeling/bonding” of the cap can be repeated up to 5 times. In addition, a MTT cell proliferation assay has been performed and suggests the non-cytotoxicity of DMPMS.

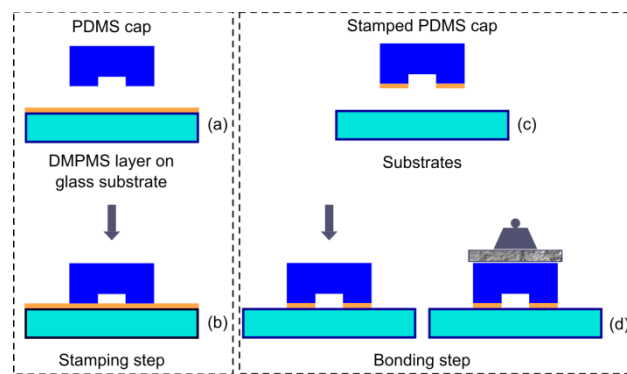


Figure 4.13. Bonding process by stamping technique: (a). Glass substrate with spin-coated DMPMS of $7\mu\text{m}$ -thick layer and cured PDMS cap; (b). PDMS cap is stamped onto DMPMS layer; (c). Stamped PDMS cap is put in contact with a bottom substrate: glass or cured PDMS/glass; (d). Oven thermal curing: sample with and without a load on top.

This first process has been applied for some basic experiments with the microfluidic chip. However, this process cannot be used for the final device as it avoids the complete replacement of the channel: the bottom surface of the channel been kept as the channel peel off occurs at the PDMS an interface with the DMPMS. Furthermore, we will see after that the PDMS channel surface has to be treated in order to avoid non-specific adsorption of fluorescent dyes.

4.2.3.2. Reversible packaging based on anti-adhesive under-layer

Figure 4.12 (c) describes the concepts of this second reversible bonding techniques. A Teflon-like anti-adhesive layer is spin-coated on the bottom substrate before spin-coating PDMS thin protective layer. The later layer permits an irreversible bonding step with the PDMS channel cap. After experiment, the channel cap and this

PDMS thin layer are easy to peel off from the anti-adhesive layer. Thus, the bottom substrate can be re-used many times with new and clean microchannels

This technique combines the high bonding strength of irreversible bonding PDMS to PMDS for the channel part and a low adhesion of the PDMS chip part to the bottom substrate thank to the anti-adhesive layer.

The bonding process is performed following those steps:

- *Bottom substrate preparation*, Figure 4.14: Firstly, the bottom substrate containing microcoils is covered by the anti-adhesive layer: CT-809M (CYTOP, AGC chemicals Europe, Ltd.) 1.5 μm thick layer is spin-coated (500 rpm/10 s + 3000 rpm/20 s) on the bottom substrate. Then, the layer is baked on hotplate at 100°C for 90 s and annealed in oven at 180°C for 1 hour. Secondly a 5 to 8 μm thick PDMS layer (the protective layer) is spin-coated (speed: 3000 to 4000 rpm for 60 s, acceleration: 1000 rpm/s). This fresh PDMS is obtained by mixing with the ratio 2.5:1 (wt:wt) of base and curing agent to obtain lower viscosity than normal ratio 10:1 and thus achieve thinner layer by spin-coating. Finally, PDMS layer is cured in oven at 75°C for 1 hour.

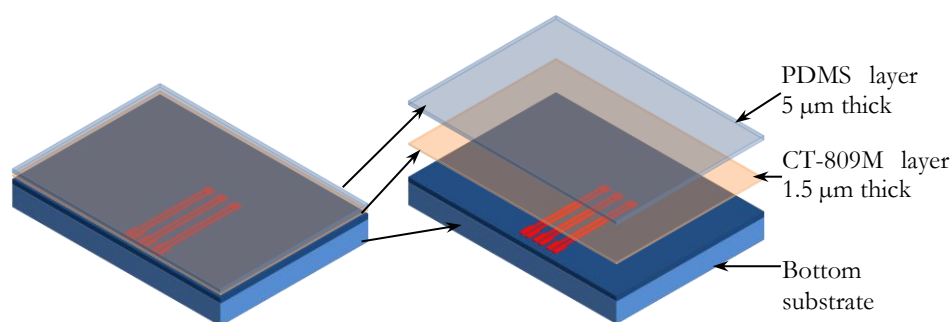


Figure 4.14. Bottom substrate preparation

- *Bonding step*, Figure 4.15: Both of PDMS channel cap and PDMS-covered bottom substrate (prepared above) are treated by oxygen plasma, at 160 W of power for 1 minute (Standard plasma system Pico, Diener electronic GmbH + Co.). After this plasma treatment, they are put in contact immediately after taking them out of plasma machine. It is noted that, the channel cap has to be align with the bottom substrate in order to place the coils just under the trapping zone. Adjustment of channel cap on substrate is making possible by adding a drop of ethanol on the surface just before putting them into contact. The layer of ethanol plays as a “temporary lubricant”. Finally, the bond is thermal treated in oven at 75°C for 1 hour, helping ethanol evaporation.

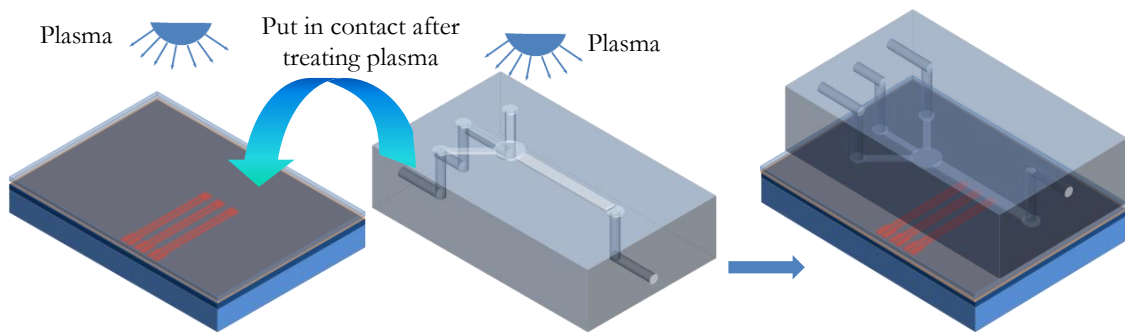


Figure 4.15. Bonding steps

After passing leakage test, both of channel cap and PDMS layer can be easily peeled off from the bottom substrate, as describing in Figure 4.16. The bonding process will be able to be performed again by only re-spin-coating PDMS layer and bonding channel cap to this layer.

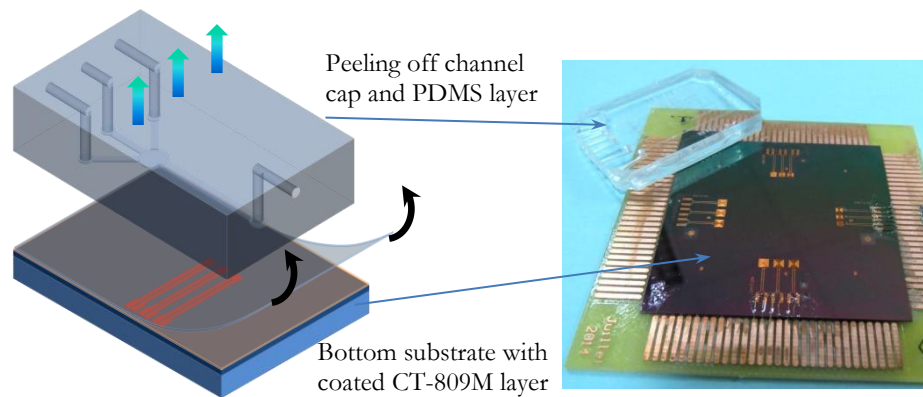


Figure 4.16. Peeling off PDMS channel cap and PDMS layer.

4.2.4. General conclusions in microfluidic chip fabrication:

A final microfluidic chip with embedded microcoils obtained after applying a packaging technique is shown in Figure 4.18. This chip is ready to be used in all experiments: characterization of heat generation and trapping magnetic beads, and immunoassay inside microfluidic chip.

Leakage tests show that all fabricated microfluidic chips resist to a pressure of 500 $\mu\text{L}/\text{min}$, without any leakage. Furthermore, the two bonding techniques, which are based on stamping process or on non-adhesive layer allow the bottom substrates to be re-used many times. It thus opened some new tendencies in packaging PDMS microfluidic chip with the aim of decreasing cost and time consumption in

fabrication. It is also able to solve some problems of PMDS channel and non-specific adsorption when it is difficult to clean well the channel.

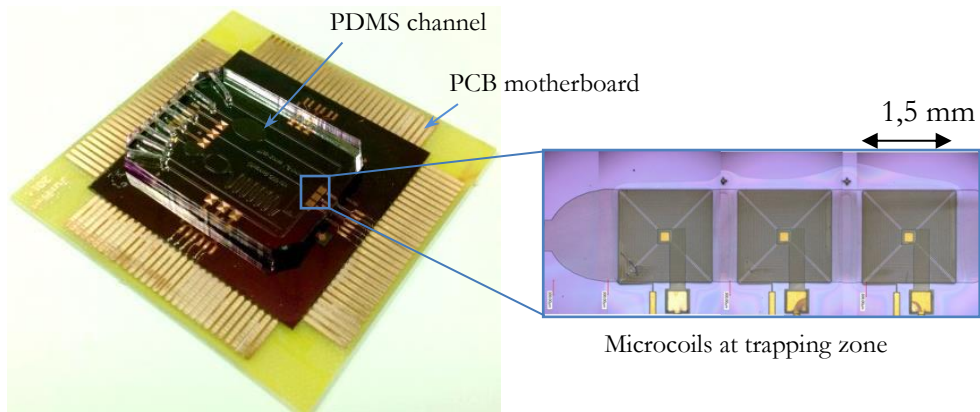


Figure 4.18. Final microfluidic chip

4.3. First trapping experiments with microfluidic chip

4.3.1. Study on the temperature of the microchip

We want to determine the highest current that can be injected in the coil without leading to a temperature increase incompatible with the biological species used in immunoassay.

a. Experiment description

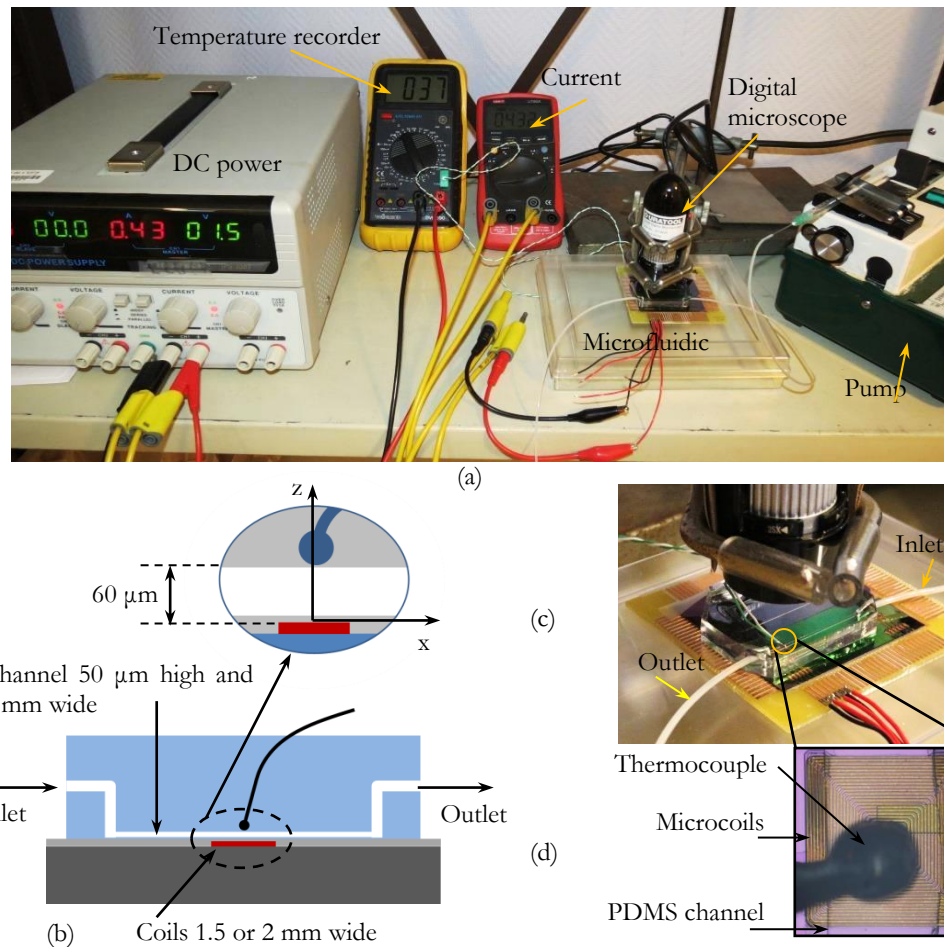


Figure 4.17. (a) setup of temperature measurement; (b) Cut view of the microfluidic channel; (c) One of microfluidic chips for temperature measurement; (d) integrated thermocouple on top of PDMS channel

For temperature measurement purposes, a specific microfluidic chip is fabricated with a K-type thermocouple fixed on the top of the channel, Figure 4.17 (b-d). The thermocouple is positioned as close as possible to the SU-8 channel master mold before pouring the master with PDMS. The rest of the process is exactly the same than those for a classical microfluidic chip. The thermocouple position very close to surface coil ($z \approx 60 \mu\text{m}$, including $10 \mu\text{m}$ thick of protect layer and $50 \mu\text{m}$ high of PDMS channel) allows a precise measurement of the channel's temperature.

The temperature measurement setup is shown in Figure 4.17 (a). When the flow injected inside the channel by pumping (6.6 μ L/min) or without any flow inside, a direct current DC is injected into the coil. The temperature is recorded as a function of the current intensity in stationary conditions (we wait 10 minutes to stabilize the system).

We measure the temperature with two types of coils (Figure 4.18). These coils have the same geometrical parameters, except the outer diameter, which affect the number of turns.

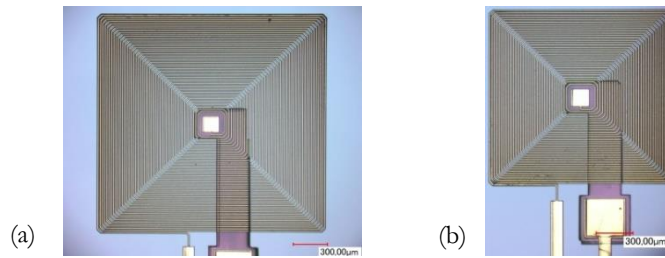


Figure 4.18. Coils used in the experiment of temperature measurement : $w = 10 \mu\text{m}$; $s = 10 \mu\text{m}$; $h \approx 10 \mu\text{m}$,
(a) Coil 1 with 2 mm of size $N = 46$ turns, (b) Coil 2 with 1.5 mm of size $N = 33$ turns

b. Results and discussion

The Figure 4.19 shows that the liquid flowing through the channel has a negligible effect on the temperature inside the channel: the volume of fluid flowing through the channel is very small compared to the overall volume.

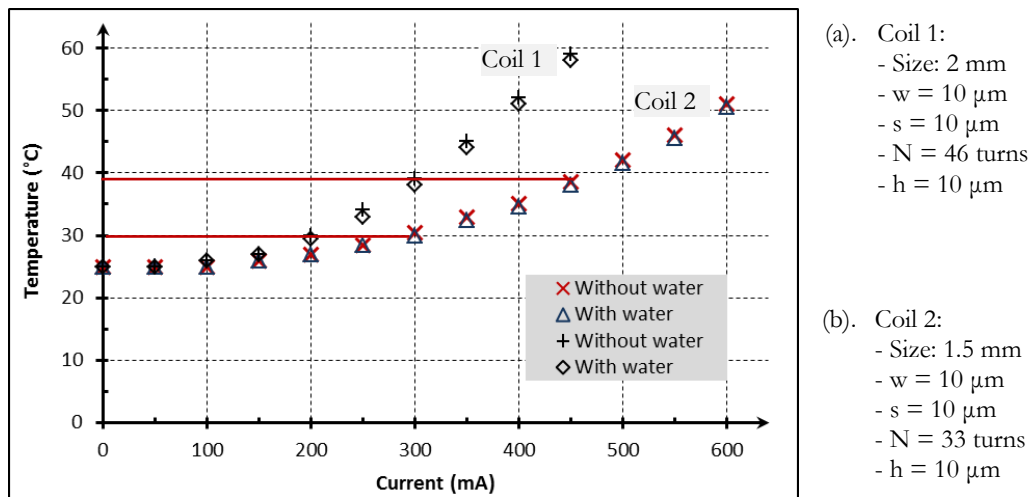


Figure 4.19. The influence of applied current on temperature inside channel of two chips with different coils

A parabolic temperature elevation as a function of the current (The power dissipated in a resistance is $P = R.I^2$) is observed for both coils. For coil 1, an

elevation of temperature of approximately 40°C is obtained with a current of 330 mA. For coil 2, this temperature elevation is obtained with a higher current (470 mA).

Table 4-1 compares the calculated and measured power consumption of the coil and temperatures for different values of the current. A ratio of 4/3 for the resistance values can roughly be observed between the two coils.

Table 4-1. The difference between simulation and experiment values of coil parameters

	Simulation value			Experimental value				
	I (mA)	Resistance (Ω)	P (W)	T(°C)	I (mA)	U (V)	Resistance (Ω)	P(W)
Coil 1	200	27.31	1.04	30	200	6.12	30.60	1.22
Coil 2	300	15.12	1.35		300	3.02	10.07	0.91
Coil 1	310	27.31	2;6	40	310	10.34	33.35	3.21
Coil 2	470	15.12	3.31		470	6.05	12.87	2.84

The copper temperature coefficient of $3.9 \cdot 10^{-3}$ suggests a resistance increment of 4% for a 10°C temperature rise. The observed resistance change is approximately 10% for coil 1 and 25% for coil 2. The difference between calculations and experiments suggests that either the temperature of the coil is higher than the chip temperature although the thermocouple is placed as close to the coil as possible. Another possible explanation resides in the coil fabrication technology: connecting the center point of the coil to the bonding pads is done by a thin copper track while the windings are thick (electroplated). Higher power dissipation in the bottom track can explain both the higher resistance value as well as the higher temperature coefficient.

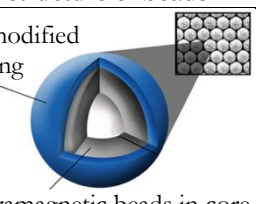
4.3.2. Magnetic nanobeads trapping experiments

a. Magnetic beads

In these experiments, as in the immunoassay ones, commercial carboxyl-300 nm magnetic beads (Adembeads, purchased from AdemTech) are used. Carboxyl-Adembeads⁽¹⁾ are mono-dispersed and super-paramagnetic beads composed of magnetic core encapsulated by a highly cross-linked hydrophilic polymer shell. The surface is activated with carboxylic acid functionality. The hydrophilic surface ensures low non-specific binding, excellent dispersion abilities and easy handling of the beads in a wide range of buffers. The properties of beads are present in Table 4-2.

⁽¹⁾ Product information, <http://www.ademtech.com/images/carboxyl-adembeads%200213%20v%202.5.pdf>

Table 4-2. Some basic properties of beads

Physical characteristics	Core-shell structure of beads
Diameter: 300 nm (CV max 20%) Density: $\sim 2.0 \text{ g/cm}^3$ Magnetization at saturation: $\sim 40 \text{ emu/g}$ Specific surface area: $15 \text{ m}^2/\text{g}$ Iron oxide content: $\sim 70\%$ COOH density: $> 350 \mu\text{mol/g}$ Solid content: 30 mg/ml (3%)	<div style="display: flex; align-items: center;"> <div style="margin-right: 10px;"> Carboxylate-modified Polymer coating </div>  </div>

<http://www.ademtech.com>

b. Microfluidic chip

Two types of microfluidic channels were designed (Figure 4.20 and Figure 4.21): a narrow channel of $100 \mu\text{m}$ wide, and a 1.5 mm wide channel. Trapping in narrow channel corresponds to experimental conditions very close to the FE simulations configuration. The trapping force was calculated to be proportional to the product of the magnetic field magnitude by its gradient (equation 3-17 in chapter 3). Wide channel presents zones (corners of coils) where the gradient should be high with low change in magnitude.

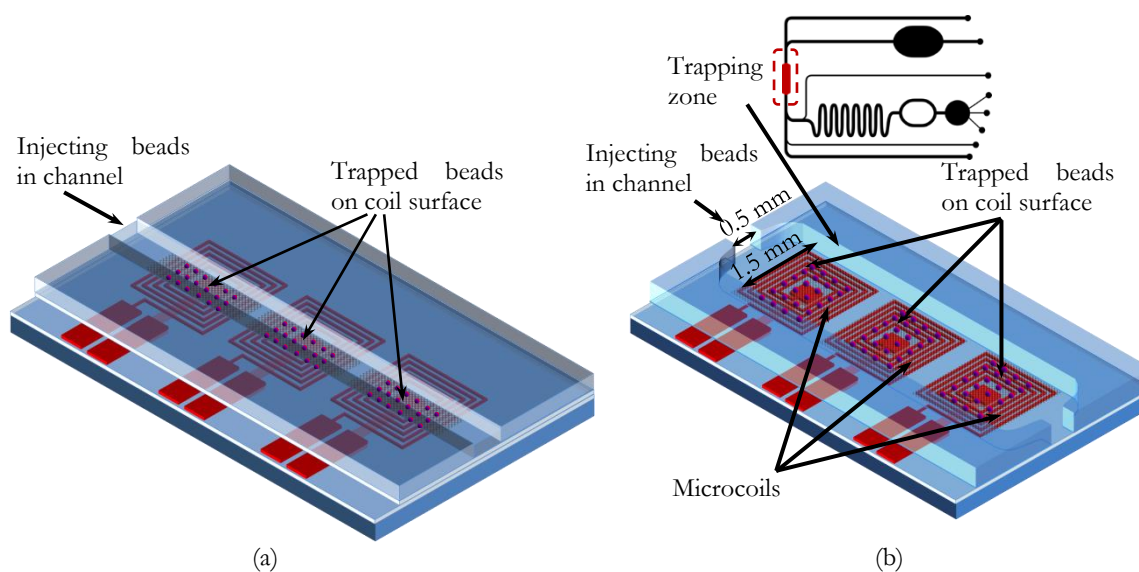


Figure 4.20. Schematic description of the trapping beads in narrow channel (a) and in large channel (b)

Figure 4.21 show example of realization of the two types of microfluidic chips used in this experiments.

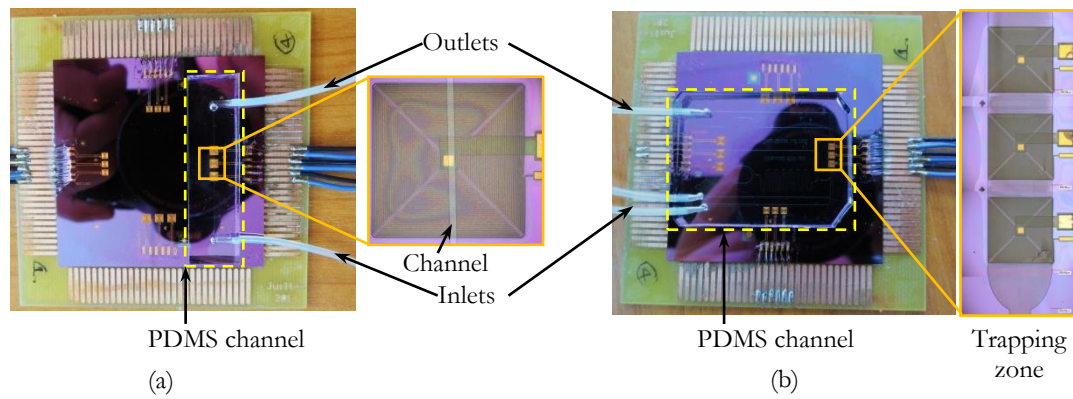


Figure 4.21. Microfluidic chips are used in experiments of trapping magnetic beads. Chip using for the trapping test (a) with narrow channel (100 μm wide), (b) with wide channel (1.5 mm wide)

▪ **For the chip with narrow channel,**

- Coils parameters are: 2 mm wide, Cu-wire width $w = 10\ \mu\text{m}$, space between two Cu wires $s = 10\ \mu\text{m}$, number of turn $N = 46$ turns, Cu-wire height $h = 10\ \mu\text{m}$.
- Channel parameters are: straight channel with 100 μm wide, 3 cm long, and 50 μm high.

▪ **For the chip with wide channel:**

- Coils parameters are: 1.5 mm wide, Cu-wire width $w = 10\ \mu\text{m}$, space between two Cu wires $s = 10\ \mu\text{m}$, number of turn $N = 33$ turns, Cu-wire height $h = 10\ \mu\text{m}$.
- Channel with multi inlets and outlet (as described in Figure 4.1): The width of all lines in this channel is 500 μm , and only the width of the trapping zone is 1.5 mm.

c. Experiment description

The experimental setup is shown in Figure 4.22. Two pumps supply nanobeads suspended in PBS 1 \times and only PBS 1 \times (pH=7.4) as cleaning. First, the pump 1 injects PBS buffer solution into the microchannel for 1 minute in order to wet the channel's surface. This step is required to limit the adhesion of beads on the channel surface and to eliminate the bubble appearance during the experiments. Then, pump 2 injects magnetic nanobeads suspended in PBS solution with 5 μL of original concentration in 100 μL of PBS. This high concentration of beads is injected into the channel in order to easily observe trapped beads. In the immunoassay experiments, the beads concentration will be much lower. The flow rate of both pumps is kept constant at 0.59 $\mu\text{L}/\text{min}$.

The two injected liquids are controlled by multi-valve switch, which allows to change/turn off gently each liquid during experiment. The two pumps work

alternately during the trapping experiment. For example, in the first step – wetting – the pump 1 is injecting PBS into the channel while the pump 2 is stopped; in the trapping process, the pump 2 works with beads solution while the pump 1 is stopped. The trapped beads are tracked by digital microscopy (KEYENCE digital microscopy VHX – 1000 with zoom lens VH-Z100R).

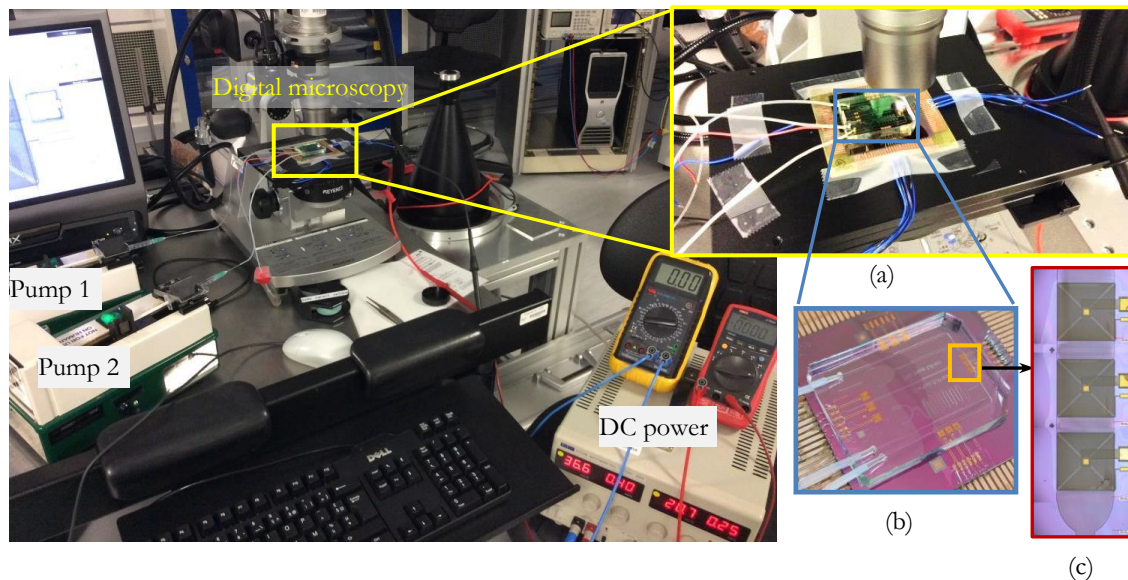


Figure 4.22. The schematic setup of trapping experiments, (a) View of pumps and DC power connect to chip, (b) Chip view, (c) View of trapping zone with coils

In case of narrow channel, only one pump is used for injecting magnetic beads dispersed in PBS solution. When magnetic beads are injected into the channel, a current is applied in microcoils by a DC power supply.

▪ ***Two experiments are carried out:***

- For the narrow channel experiment, a constant current is injected in the microcoils for around 1 minute leading to a stable amount of beads trapped on the coils' surface;
- For the wide channel, a set of current values in the range 150 – 500 mA is applied. The distribution and the amount of beads trapped as a function of the current is observed.

The information of the two experiments is summarized in Table 4-3.

Table 4-3. Summary information of the two experiment of trapping magnetic beads

Trapping experiments	Channels	Coils	Beads concentration	Current applying to coils (mA)	Time of current application
<i>Experiment in chip with narrow channel</i>	Straight channel: 100 μm wide 3 cm long 50 μm high	2mm wide $w = 10 \mu\text{m}$ $s = 10 \mu\text{m}$ $N=46$ turns $h = 10 \mu\text{m}$	5 $\mu\text{L}/100 \mu\text{L}$ PBS	250	1 minute
<i>Experiment in chip with large channel</i>	Multi inlets and outlets channel: 500 μm wide 3 cm long 50 μm high 1.5 mm wide of trap zone	1.5mm wide $w = 10 \mu\text{m}$ $s = 10 \mu\text{m}$ $N=33$ turns $h = 10 \mu\text{m}$	5 $\mu\text{L}/100 \mu\text{L}$ PBS	150 - 500 mA	10 – 120 seconds

4.3.3. Results and discussion

a. Trapping magnetic beads in a narrow channel

The PDMS coil protection layer is here 10 μm thick. The trapping results presented on Figure 4.23, show an image of the magnetic flux density performing at $z = 10 \mu\text{m}$ above the coil's surface. In this experiment, a current of 250 mA is applied. According to the simulations, the magnetic flux density has high slopes at the center and outer edges of the microcoil. In the middle zone of the microcoil the magnetic flux density tends to decrease slightly. The temperature inside the channel (at the trapping zone) is then approximately 35°C, which is suitable for the immunoassay experiment. The magnetic field value can be estimated to 0.014 T.

Figure 4.23 (d) show first that trapping is realizable with such microfluidic chips and that the trapping distribution follows exactly the simulation.

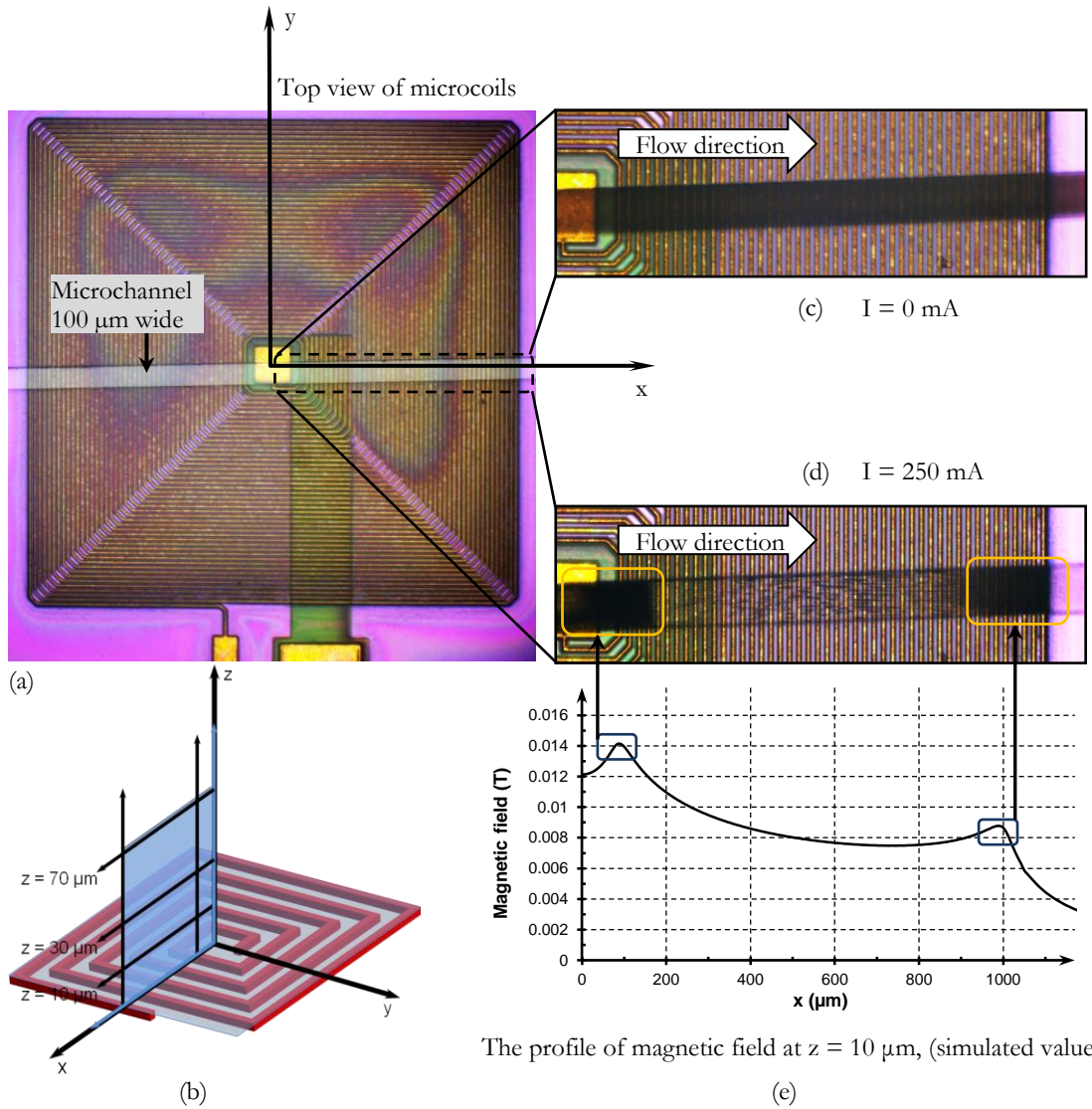


Figure 4.23. Results of trapping beads by coils: (a) Top view of bonded channel on top of coil, (b) The model of coil and area for magnetic calculation, (c) and (d) Views of trapping beads process, (e) Reminder of the simulation results of the magnetic field intensity.

b. Trapping magnetic beads in a wide channel: current value effect

The goal of this experiment is to find out how beads are trapped on these coils in dynamic mode, continuous flow. Figure 4.24 shows a full view of the test chip as well as a zoom of the trapping zone. In this zone, the coils are placed to trap the beads, and the zone's width is fitted to the coil size. With wide channels, the trapping experiment is not realized in the same conditions as for narrow channels. Here, the main microchannel is 500 μm wide and the trapping chamber is 1.5 mm wide: the speed of the liquid decreases when the microchannel widens. This fluid velocity reduction significantly improves the trapping efficiency.

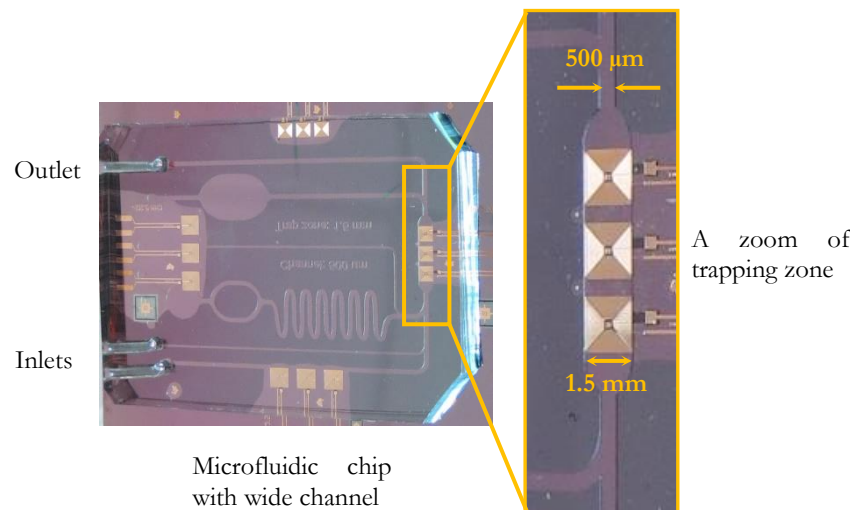


Figure 4.24. Microfluidic chip with wide channel and trapping zone for trapping magnetic beads.

Trapping capability of the coils have been simulated and experimentally checked under specific conditions. Bead trapping occurs if the magnetic force is higher than the hydrodynamic forces exerted on the bead.

The trapping process is carried out in the same conditions than the previous experiment. Current in the 100 to 500 mA range is applied for one minute. Figure 4.25 shows the result of the effect of current on the efficiency of trapping beads. As naturally expected, the density of trapped beads increases when the current increases.

An asymmetric distribution of the beads can be observed because of the liquid flow. The trapping occurs for current values as low as 100 mA. At 400 mA, corresponding to a temperature of 36°C, the trapped beads almost hide the coil.

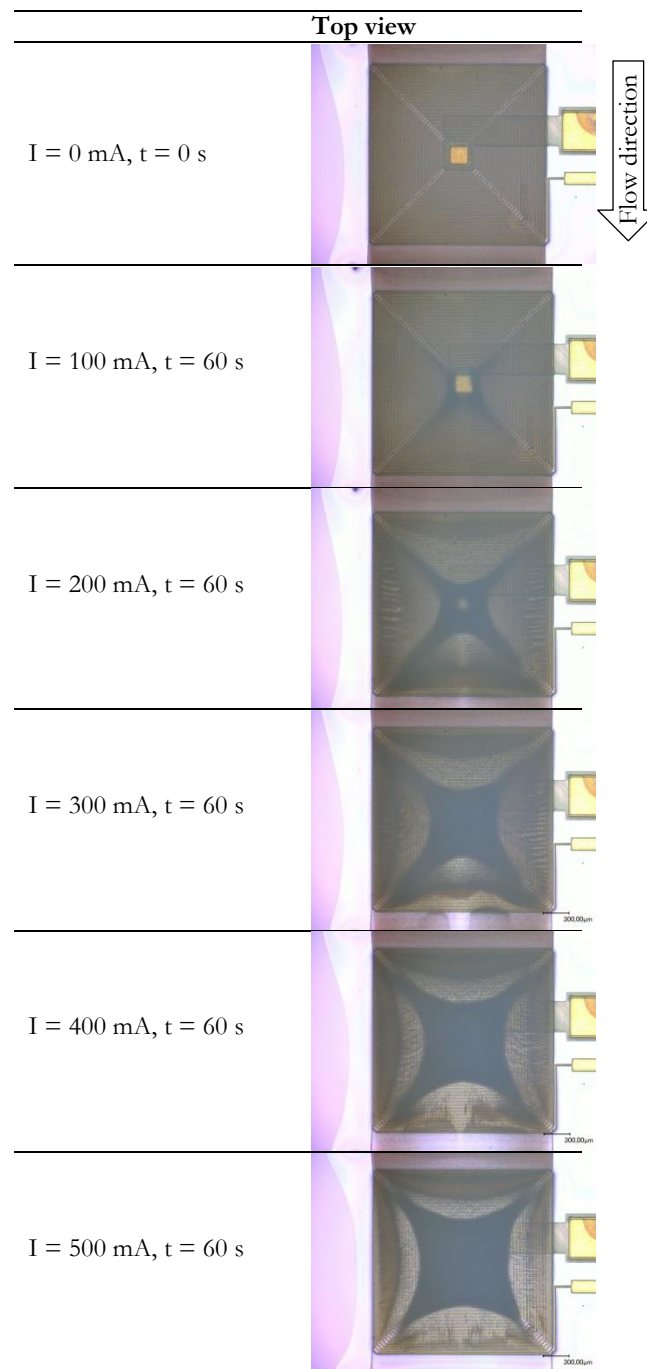


Figure 4.25. Results of trapping beads at different current, after 60 s of applying current, flow rate: $0.59 \mu\text{L}/\text{min}$

c. Trapping magnetic beads in a wide channel: time cumulative experiment

After injecting beads in channel (with $0.59 \mu\text{L}/\text{min}$ of flow rate) and injecting a current (400 mA) in the coil, the beads get trapped immediately. The number of trapped beads increases with time, as shown in Figure 4.28.

After 120 seconds, the current is cut off ($I = 0 \text{ mA}$) in order to release the beads from the surface of coil. As shown in Figure 4.28, at 123 seconds, of the beads remove from coil and follow the liquid stream.

As shown in Figure 4.28, beads are trapped at the center, outer edges, and corner of each turn (the diagonal of rectangle coil). The density of trapped beads at the corner of each turn of the coil is also much higher than at the straight part of conductors.

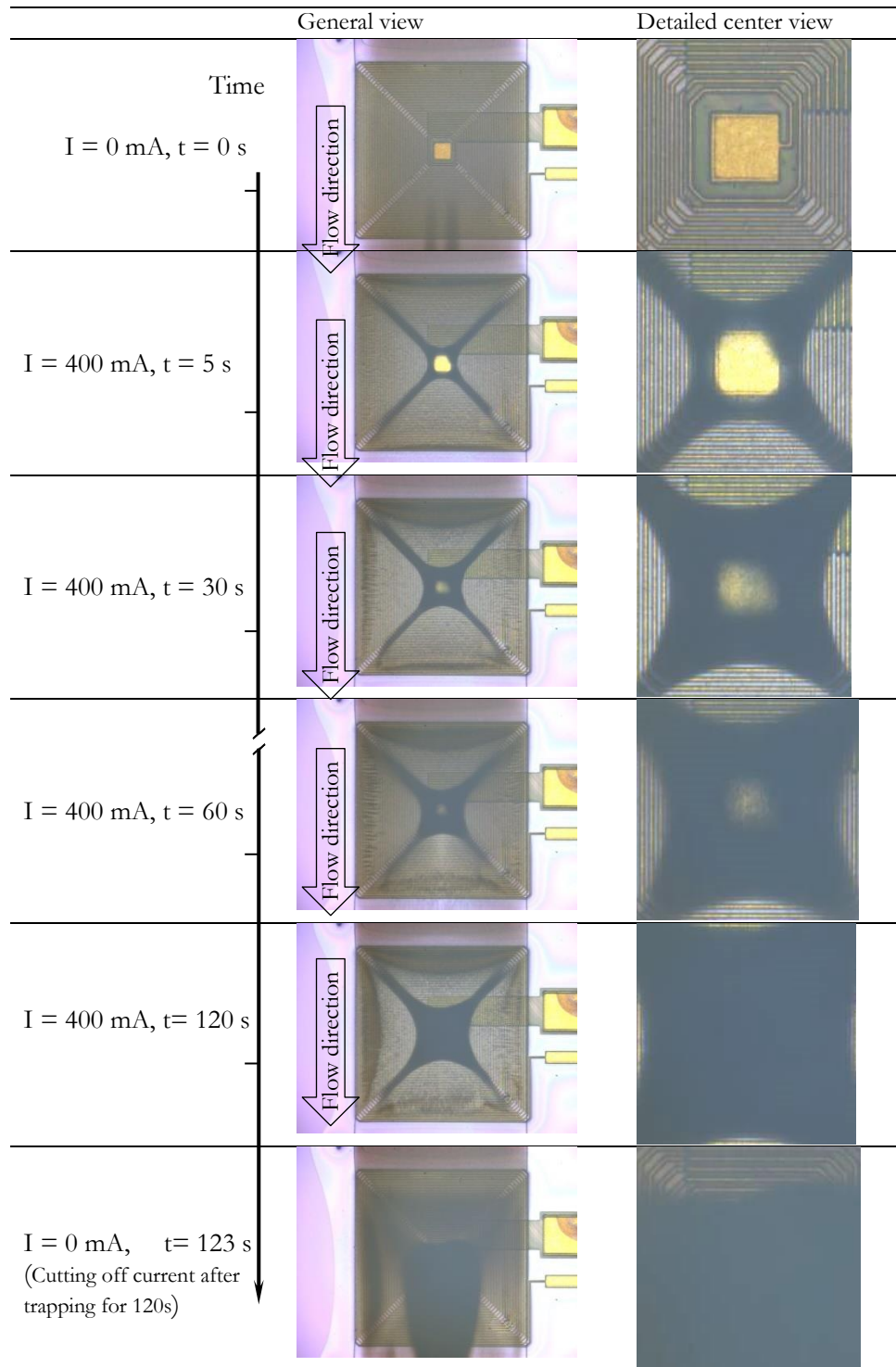


Figure 4.26. Results of trapping beads by microcoil 1.5 mm-size depend on time, current (I) = 400 mA; flow rate of liquid: 0.59 $\mu\text{L}/\text{min}$

This can be explained by the fact that the current direction changes at these positions. The change in direction of the magnetic field, i.e. the gradient of the magnetic field, becomes high and allows a strong trapping even with a moderate field modulus. An oblique path was designed in order to ease the electroplating process (avoid bubbles trapping in sharp corners). Figure 4.27 shows the detail of the coil's corners and a detail of the trapped beads in the corners.

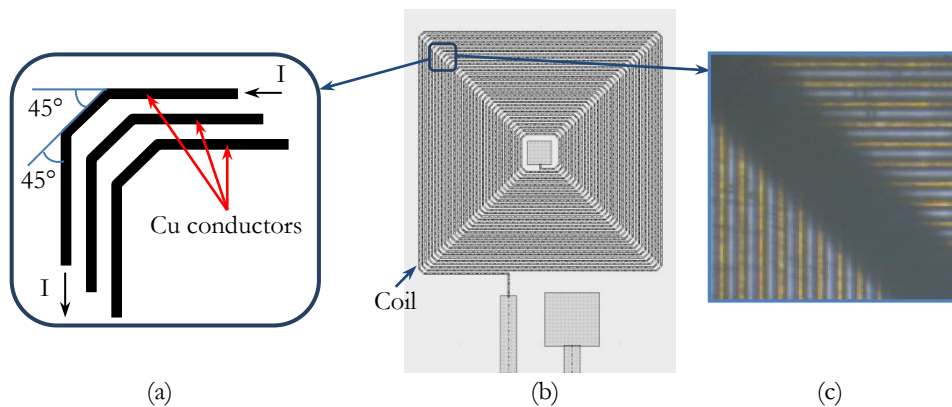


Figure 4.27. Detail of the coil's design: (a) Detail of the corner design; (b) General view of the coil; (c) Trapped beads at the corner of Cu conductors.

4.3.4. Conclusion of trapping experiment

A set of designed coils has been manufactured and two experiments were carried out in order to experimentally check the usability of the device for the application:

- A trapping experiment in a narrow channel showed that the distribution of trapped beads corresponds to the profile of the simulated magnetic flux density generated by coils, and thus validates the simulation results.
- In a wider channel, the experiment allowed to show the shape effect of the coil.

Both experiments showed the ability of coils to efficiently trap magnetic nanobeads at temperatures in the 30 to 37°C range. The designed microfluidic chip can then be used for bead-based immunoassay inside channel.

4.4. Microfluidic chip for on-chip magnetic beads-based immunoassay

We have chosen to develop a magnetic bead-based immunoassays based on the sandwich-like immunoassays protocol. Specific antibodies are coated on beads, which enabled the specific isolation and collection of target antigens by using a magnetic force. Furthermore, magnetic nanoparticles have advantages including multiplexing, reduced analysis time and selectivity control.

The fabricated microfluidic chips will be a prototype devices used for the first immunoassay in which the sandwich {magnetic beads – primary antibody – labeled second antibody} is performed inside microchannel. The trapping step plays a role in pre-concentrating and mixing of the biomarkers with magnetic beads.

Protocol inside channel of activating carboxyl-beads (e.g. Adembeads®, 300nm) and immobilizing the first antibodies (e.g. IgG) on the bead surface will be built. The antibodies layer is evaluated by using the second labelled antibodies (e.g. IgG-FITC-conjugated) coupling with the immobilized antibodies on beads. To avoid any unspecific adsorption of antibodies (or antibodies-FITC) on the PDMS, the inner surface of the channels has to be chemically functionalized. This study is presented first in the next part before developing the biochemical grafting of nanobeads in the following parts.

4.4.1. Modification of PDMS surface

Because of the highly hydrophobic surface of PDMS, the non-specific adsorption is a major problem for immunoassay experiment with PDMS material as its surface easily adsorbs many bio-substances or fluorescent substance (i.e. protein, cell, antibody, fluorescent conjugation, etc.). Thus, treatment of PDMS channel surface is needed [2, 9].

In this study, the modification of PDMS surface is performed by using two substances: poly(ethylene oxide) – PEO and bovine serum albumin – BSA. In this modification process, PDMS surface is coated by PEO in order to stabilize the hydrophilicity of activated PDMS surface and BSA is used as a blocking surface agent which can limit the adsorption of protein. The surface modification step are briefly described in Figure 4.28, each step is performed following the description in Figure 4.30.

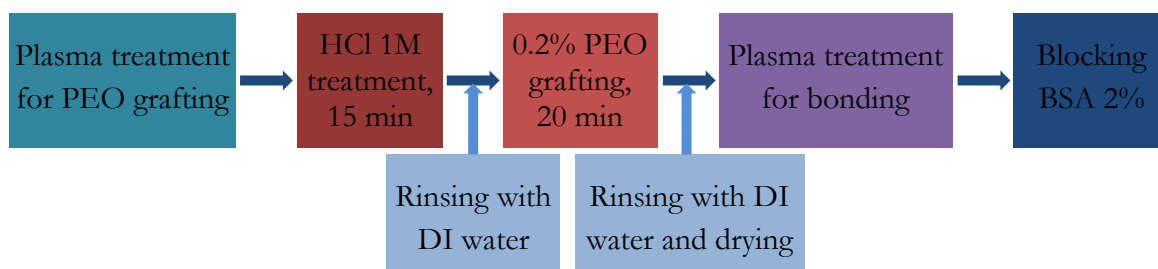


Figure 4.28. Surface modification steps of PDMS channel surface with PEO, BSA

4.4.1.1. Materials and surface modification protocol

a. Materials:

PEO 0.2% solution [10]:

Polymer chain: $(-\text{CH}_2\text{CH}_2\text{O}-)_n$.

Molecular structure in solution: $\text{H}-\left[\text{O}-\text{CH}_2-\text{CH}_2\right]_n-\text{OH}$

PEO is also known as Polyethylene glycol (PEG) or Poly(oxyethylene) (POE⁽¹⁾) [11].

A stock solution of PEO is prepared by gradual addition (in less than 1min) of 0.1 g of the PEO polymer powder ($M_v \sim 400,000$; purchased from Sigma Aldrich) to 45 mL of water in an Erlenmeyer flask. The water is vigorously mixed by stirring and heated to 40-50 °C. After the addition of PEO, the flask is sealed and heated at ~80 °C for at least 15 min (this solution can be used for up to 2 weeks). Neutral or acidified 0.2% PEO solutions are prepared by the addition of 0.5 mL of water or 1M HCl to 4.5 mL of PEO stock solution. The acidified gel is used for at most 2 days after the addition of acid. It is better if this solution is used in few ten minutes or few hours after adding acid. Although no change in analytical performance was observed within 2 weeks, the acidified gel became less viscous over that period. This is probably a result of formation of shorter chain polymers due to the acid hydrolysis of PEO [10].

BSA 2% solution: The Bovine serum albumin – BSA is a single polypeptide chain (molecular weight: approximately 66 kDa) consisting of about 583 amino acid residues and no carbohydrates [12].

⁽¹⁾ The two names polyethylene glycol and polyethylene oxide are chemically synonymous, but historically polyethylene glycol – PEG has tended to refer to shorter polymers with molecular weight $M_w < 20000$, polyethylene oxide – PEO to high-molecular adducts.

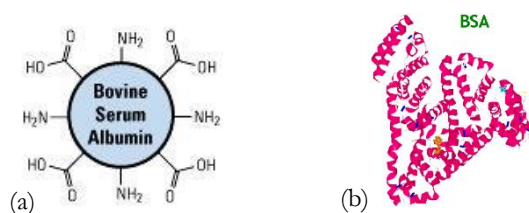


Figure 4.29. Molecule structure of BAS (a). Main chemical groups in protein BSA molecule (b). The BSA protein structure

BSA stock solution 2% is prepared by dissolving 2 g of BSA powder (BioExtra, purchased from Sigma Aldrich) in 98 mL DI water or PBS solution 1x (pH 7.4). Because generally BSA causes foam, BSA has to be wet properly before to be actually dissolves with gentle stirring (no more than one rotation of the stirring bar per second – using magnetic stirrer). The stock BSA/PBS solution can be stored maximum of 6 months in refrigerator at 4°C, but will better in 1 or 2 months.

b. Protocol of surface modification and bonding process

- Firstly, both surfaces of channel cap and bottom substrate are cleaned with acetone and dried under nitrogen gas (or simple way, by using scotch tape to remove dusts) and then treated with plasma for 3 minutes (160W of power, 0.4 mbar of oxygen pressure), as shown in the first step of Figure 4.28 and Figure 4.30.a. After taking plasma treatment, the PDMS channel is soaked immediately in HCl 1M solution. The bottom substrate is also treated with HCl 1M solution on specific area defined thanks to a PDMS frame : a high edges rectangle of PDMS with a free inner area fitting to area of channel, as shown in the second step of Figure 4.28 and Figure 4.30.b. This rectangle frame will prevent HCl solution from contacting other parts of bottom substrate (*i.e.* electrical connecting pad of coils, PCB motherboard). The soaking time in HCl solution is 15 minutes. In acidic solution, the PDMS activated surfaces are acidized, leading to a longer hydrophilicity of PDMS surface and an easy PEO grafting.
- After 15 minutes soaking in HCl, both PDMS channel and bottom substrate are rinsing with DI water about 1 or 2 minutes to clean all free acid, as shown in rising step of Figure 4.28. Then, the PEO grafting is performed by using the prepared PEO 0.2% solution following the same step which is done with HCl solution and with a grafting time of 20 minutes. In this step, both PDMS channel and bottom substrate are placed in closed box during PEO grafting to prevent the solution from evaporating, as shown in Figure 4.30.b and Figure 4.30.d.

- Both grafted polymer surfaces (channel and bottom substrate) are rinsed gently with DI water for about 2 minutes to remove all un-grafted PEO. After that, they are dried slowly in nitrogen flow, and then put in oven at 50°C for few minutes leading water evaporation. The microfluidic chip bonding is performed by plasma treatment on channel and bottom substrate (160 W of power, 0.4 mbar of oxygen pressure for 1 minute). Then, channel is put immediately in contact with bottom substrate, as shown in Figure 4.30 and Figure 4.30.c. Finally, a thermal treatment in oven at 75°C for 1 hour is carried out.

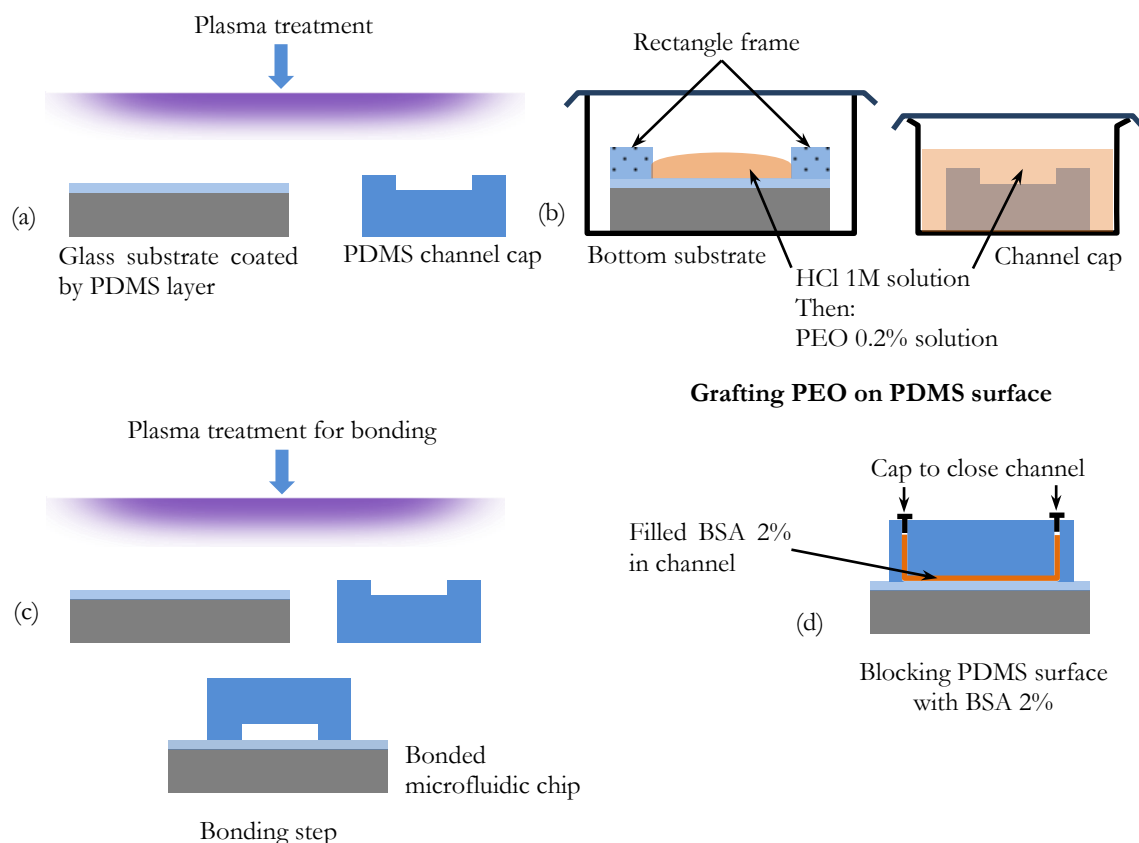


Figure 4.30. Protocol of PDMS surface modification, (a) Pre-plasma treatment step, (b) Incubating HCl and PEO 0.2% steps, (c) Bonding step, (d) Blocking PDMS surface by BSA

- Finally, the inside surface of PDMS channel is coated by a molecular layer of BSA by adsorbing BSA on polymer grafted surface from BSA 2% solution in stop-flow mode for 20 minutes. The BSA solution is injected in channel, and then inlet and outlet of channel are closed by two caps in order to prevent evaporation of the solution, as shown in Figure 4.30 and Figure 4.30.d. After 20 minutes of incubating with BSA solution, inlet and outlet are opened, BSA solution is released out of channel by injecting DI water for 2 minutes and PBS 1x solution

for 5 min at low flow rate (proposed flow rate is less than 1 $\mu\text{L}/\text{min}$ in channel with 500 μm wide and 50 μm high).

4.4.1.2. Results and discussions

a. The effect of PEO treatment on PDMS surface

After activating PDMS surface by plasma, this unstable surface is stabilized by a layer of PEO molecule. This PEO layer makes also the surface becomes hydrophilic. Before incubating with PEO, the oxidized surface of PDMS is pre-treated with HCl 1M in order to protonating silanol groups on PDMS surface. Because the PEO chains contain negative charges, which come from the oxygen atoms of ether oxygen groups – they work as a hydrogen acceptor [13], the polymer chains adsorb easily on surface, which are rich in hydroxyl groups – which normally act as hydrogen donors, by hydrogen bonds, as shown in Figure 4.31 (c) and Figure 4.31 (d).

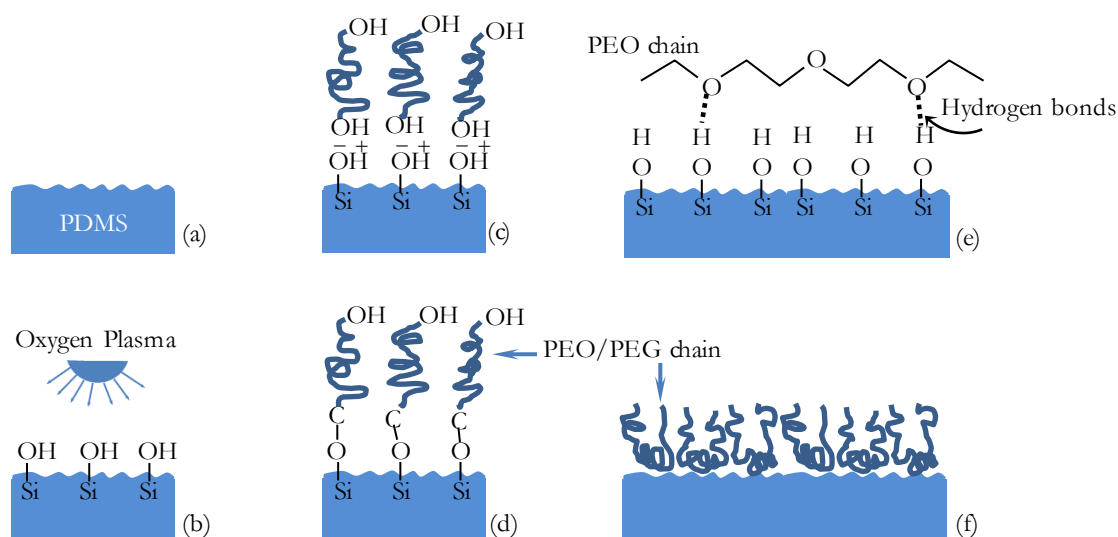


Figure 4.31. Schema of covalent attachment and adsorptive attachment of PEO: (a). Native surface of PDMS. (b). High density of silanol groups on the surface are produced by plasma treatment; (c) and (d). The silanol groups on the silica surface react with the end group of the PEO/PEG to form a Si–O–C linkage; (e) and (f). Physical and chemical adsorption of PEO/PEG chain generates a polymer layer on PDMS surface.

There are two attachment types of PEO on PDMS surface: Covalent attachment and adsorptive attachment of PEO. For the covalent attachment of PEO on PDMS, the PEO chains with hydrophilic end groups are coupled to the oxidized PDMS surface containing silanol groups [14-17], the PDMS surface required a plasma treatment in this case. After the first covalent attached layer of PEO, the oligomer/monomer molecules of PEO can be adsorbed on this surface and polymerize, leading to a thin layer. By covalent attaching, the polymerized PEO layer

bonds strongly enough on surfaces and can be stable several cycles of channel using. For adsorptive attachment, the PEO chain can be adsorbed directly on native PDMS (without activating surface by plasma). It is suggested that, the adsorption includes physical and chemical adsorption by hydrogen bonds because of the oxidized surface PDMS. The contact angle characterization of PDMS surface before and after coating PEO is shown in Table 4-4.

Table 4-4. Contact angle measurement of surfaces PDMS and treated PDMS surface

	Native PDMS (control)	Oxidized PDMS (O ₂ plasma)	PDMS – PEO	PDMS – PEO – BSA
Contact angle, θ (°)	113 ^(*)	39.8 ^(*) , ^(†)	46.2 ^(*) /111 ^(†)	78.1 ^(*)

(*) The contact angle is measured (using water) after 30 minutes of treating with plasma, PEO coating or BSA blocking step and rising with water in 3 minutes. (†) The plasma condition is 160 W of power, 0.4 mbar of oxygen pressure and 3 minutes of exposure. (‡) PDMS is coated by PEO without plasma treatment

The contact angle of plasma treated PDMS surface ($\theta = 39.8^\circ$) is lower than the one treated by PEO ($\theta = 46.2^\circ$). It can be explained by the structure of coated PEO molecule on PDMS surface or hydrophilic silica surfaces. The adsorption mechanism of PEO or other surfactant polymers on hydrophobic/hydrophilic surface is described in literatures [18, 19]. On hydrophilic surfaces, the polymer adsorbs in a flat conformation resulting from an interaction of PEO units with the hydrophilic surface. This is mainly due to H-bonding with oxygen atoms on the surface and acid base interaction [20]. On the contrary, on hydrophobic surfaces of native PDMS, the PEO unit long tail reaches into solution, and forms a thick layer of polymerized PEO. After this first layer, the surface becomes hydrophilic because the hydrophobic PEO parts adsorb strongly to the hydrophobic of PMDS, and then the hydrophilic PEO tails invert into solution. In fact, these adsorption processes cannot be controlled enough to control the thickness of the adsorbed layer. In addition, the molecular structure of PEO chains contains balance of hydrophobicity and hydrophilicity. Thus, the adsorbed PEO layers will have both hydrophobic and hydrophilic properties.

b. The effect of BSA and PEO treatment on PDMS surface

To enhance the preventability of PDMS surface from nonspecific adsorption, the PEO grafted PDMS surface required to be blocked by surface blocking agents. For immunoassay, BSA is the common one [12]. BSA is adsorbed on surface (which was grafted by PEO) to block channel surfaces. Because the BSA molecules have hydrophilic parts, they adsorb only easily on the hydrophilic surface. Generally, the

BSA adsorption is usually restricted to a monolayer for less than 2 hours of incubation time at low concentration about 10 mg/mL [21]. There is a trade-off between the incubating time and solution concentration. As the BSA solution concentration is increased, many BSA molecules absorb on the surface, layer by layer, leading to a thick BSA layer on attached PEO layer. A desorption process of BSA can occur after some cycles of washing channel. Therefore, a new BSA adsorption step can be performed after performing each experiment.

As shown in Table 4-4, the contact angle after coating PEO and BSA adsorbing is 78.1° , this value is higher than PDMS – PEO surface ($\theta = 46.2^\circ$) because of the hydrophilic part of BSA. It can be explained by the hydrophilic parts of BSA molecule adsorbed on hydrophilic surface (attached PEO surface), decreasing the hydrophilic property of channel surface. However, there were not all hydrophilic groups of albumin molecules adsorbed by on PEO surface. Some of them are still free on surface, it leads to the hydrophilicity of surface is still lower than native PDMS surface and higher than PDMS treated by only PEO. In addition, because the molecule of BSA is smaller than its PEO, BSA molecules covered easily onto entire channel surface as a coating block layer.

c. Roughness study by AFM

AFM investigations are carried out in order to evaluate the topography change and the coating homogeneity of PEO on the PDMS surface. Figure 4.32 (a) and Figure 4.32 (b) demonstrate a series of AFM images of treatment processes (these images are obtained by tapping mode in air). In the case of the only PEO coating on oxidized PDMS surface, the topography after PEO attachment has been changed significantly. The RMS roughness decreased from 1.09 nm for native PDMS to 0.74 nm for the PDMS – PEO surface, a decrease which could be attributed to the filling of topographical structuring with the PEO chain leading to a smoother surface. It may be predicted that, longer PEO coating time will change the topography of the surface at increased roughness values compared to PDMS. The thick polymerized PEO layer above the first attached layer to PDMS surface could become more porous than thin polymerized layer.

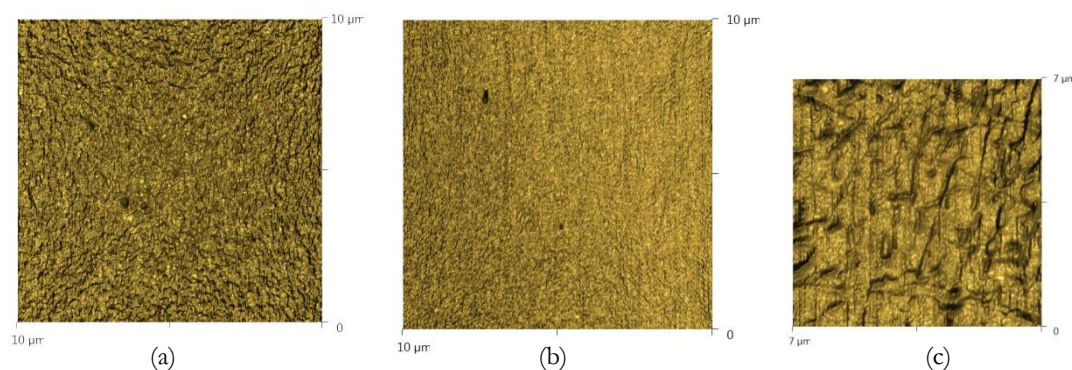


Figure 4.32. AFM images of (a) Native PDMS surface – control sample, (b) PDMS – PEO surface, and (c) PDMS – PEO – BSA surface. Measurement mode: Tapping mode with frequency of Si cantilever $f \sim 290$ kHz. The roughness of the three samples (RMS) is 1.09 nm; 0.74 nm; and 4.78 nm respectively.

The changing of PEO/PDMS surface by blocking process with BSA is shown in AFM image, Figure 4.32 (c). The higher roughness of BSA/PEO/PDMS surface (RMS = 4.78 nm) compare to native PDMS surface (RMS = 1.09 nm) indicated that the attachment of PEO and adsorption of BSA induced the foaming structure of these two layers, that probably had not high density.

d. Adsorption of fluorescent dye on modified PDMS surface

In order to confirm the ability of anti-adsorption of fluorescent dye on modified PDMS surface, three simple PDMS chips are prepared with single channel (500 μm wide, 50 μm high and 3.5 cm long) and bottom substrate coated by 100 μm -thick of cured PDMS, Figure 4.33.

- The first chip is a control sample: the bonding step is done without any PDMS surface treatment (neither with PEO or BSA).
- For the other two chips, the presented PDMS surface modification process is performed with different BSA incubating time: 10 and 20 minutes (but the same PEO grafting conditions).

A fluorescent labeled antibody, FITC – conjugated ⁽¹⁾, solution of 1 μL /100 μL PBS (pH = 7.4) concentration is injected in these chips and incubated in channel for 2 hours at room temperature. The incubating process is taken place in darken space in order to prevent the FITC from interacting with light. After 2 hours of incubating, the three PDMS chips are washed by injecting gently a PBS 1 \times solution at 0.5 $\mu\text{L}/\text{min}$ of flow rate for 10 minutes. The washing process is also taken place in dark

⁽¹⁾ Fluorescein isothiocyanate, <http://www.sigmaaldrich.com/content/dam/sigma-aldrich/docs/Sigma/Datasheet/7/f5262dat.pdf>

space. Fluorescent images of the channels of the three PDMS chips are taken before and after washing by Olympus fluorescence microscope IX71 (inverted type). The setup parameters of microscope for taking images: Excitation (Ex): 438 nm; Emission (Em): 578 nm; and Dichroic Filters (Di): 495 nm.

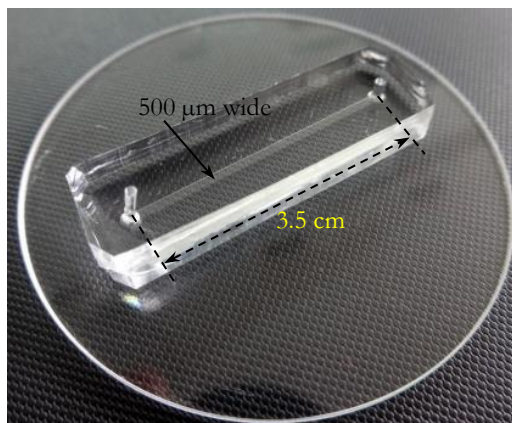


Figure 4.33. Microfluidic chip for experiment of modifying PDMS surface

Results of the interaction of IgG-FITC-conjugated (FITC) with and without surface treatment are shown in Figure 4.34. In the control sample, Figure 4.34.a, the FITC adsorbs strongly on all surface and especially at edges of channel wall. The cleaning process removes a part of FITC on surface of PDMS channel. The FITC still adsorbs quite strongly at the edge inside channel, which are usually dead zones of flow inside rectangle microchannel. At these positions, there is a high potential site of non-specific interaction and cleaning step is hardly efficient. The PEO and BSA treatment overcomes the trouble as they easily attach on surface and fill into these positions. It implies also that PEO coating and BSA adsorbing not only limit protein adsorption, but they decrease also the dead zones inside channel. The significant anti-adsorption of FITC on PDMS surface thanks to PEO and BSA treatment is shown in Figure 4.34 (b), (c). As shown in these images, the binding of FITC decreases stronger than control sample with non-treated surface. Moreover, there is no adsorption of FITC at edges of channel walls. It confirms more about the significant anti-protein-adsorption. In addition, there is a comparison of the incubating time of BSA in two experiments (b) and (c). The ability of anti-protein-adsorption in experiment with 20 minutes of BSA incubating time is better than the other one with 10 minutes. Some other experiments with longer incubating time showed that results were quite as same as sample with 20 minutes of incubating time. Therefore, 20 minutes of incubating time is chosen for all following experiments. Results of the modification step will help optimizing the ratio signal: noise ratio in immunoassay.

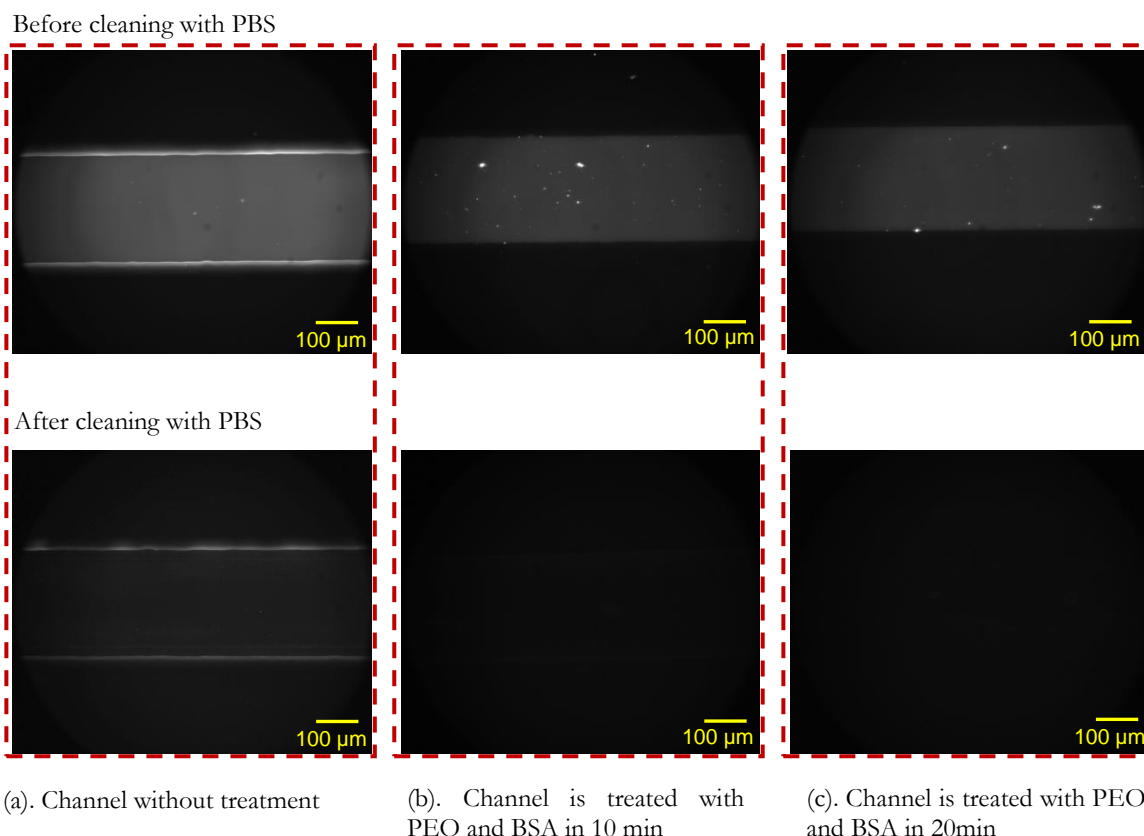


Figure 4.34. Fluorescent images of channels after incubating with IgG-FITC-conjugated for 2 hours (before and after cleaning with PBS for 10 minutes at flow rate 1.4 $\mu\text{L}/\text{min}$); channel: 500 μm wide, 50 μm high, 3.5 cm long; FITC concentration: 1 μL (original concentration) in 100 μL PBS.

From these results of the modification of PDMS surface, the define protocol is validated and can be applied to the microfluidic chips used for immunoassay. Some complementary tests have to be done to validate the necessary of BSA treatment.

4.4.2. First steps in bead-based immunoassay inside microfluidic chip

After modification of PDMS channel surface, the microfluidic chip is ready for the on-chip bead-based immunoassay. The principal aim of this section is to demonstrate the possibility to do an immunoassay inside a microchannel starting from carboxyl-beads (not functionalized beads) and using magnetic field generated by microcoil to trap and mix beads during a immunoassay.

We choose to do this demonstration by building a sandwich structure {bead - primary IgG antibody – FITC labeled second antibody}, Figure 4.35).

Carboxyl bead – primary antibody (IgG type) – second labeled antibody (FITC)

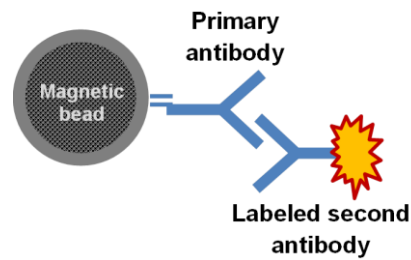


Figure 4.35. Description of ELISA sandwich structure

As this sandwich structure is commonly used to evaluate the primary antibody grafting thanks to the detection of the second labeled antibody, the whole protocol is named IgG grafting.

After presenting the IgG grafting experimental protocol, experiments in two conditions will be related. First experiments performed in micro test tube will validate the experimental protocol. Then, experiments in microfluidic chip will be performed using in two types of chip: one with permanent magnets and the other one with integrated microcoils for trapping magnetic beads.

4.4.2.1. General IgG grafting protocol

The aimed sandwich structure {bead - primary antibody - labeled second antibody} will be built in several steps:

- Surface carboxyl beads (e.g. Adembeads®, 300nm) activation, which will be based on the process of activating beads' surface from Ademtech's products
- Primary antibody grafting (IgG type)
- Second labeled antibodies (e.g. IgG-FITC-conjugated) coupling. These antibodies of detection are labeled with fluorescence dye – FITC

The control of the primary antibody grafting (IgG type) on the activated surface of beads is of paramount importance in the immune-assay recognition.

a. The preparation of materials

- Magnetic beads: carboxyl-Adembeads: 300 nm, purchased from Ademtech.
- Activation substances of beads' surface:
- N-(3-Dimethylaminopropyl)-N'-ethylcarbodiimide hydrochloride - powder (synonyms: EDC or EDAC), purchased from Sigma Aldrich, Code: E7750.

- N-Hydroxysulfosuccinimide sodium salt – powder (synonyms: S-NHS), purchased from Sigma Aldrich, Code: 56485.
- Primary antibody and labeled conjugation antibody:
- Primary antibody: antibody from mouse serum, IgG type – lyophilize powder (synonym: IgG), purchased from Sigma Aldrich, Code: I5381
- Labeled conjugation antibody, second antibody: Anti-Mouse IgG (Fab specific)-FITC (synonym: FITC), purchased from Sigma Aldrich, Code: F5262
- Other basic materials:
- Phosphate buffered saline – PBS 1× (pH: 7.4) diluted from stock solution 10x, purchased from Sigma Aldrich.
- Bovine serum albumin – BSA 2%, as prepared in section 4.4.1

Table 4-5. Summarized information of the substances' concentrations in experiments

		Beads	EDC	S-NHS	IgG	FITC	BSA	PBS
Original concentrations		30 mg/mL	10 mg/mL (DI water)	15 mg/mL (DI water)	0.1 mg/mL (PBS)	3-6.5 mg/mL	20 mg/mL (DI water)	10x
Stock concentrations		30 mg/mL	1 mg/mL (DI water)	1.5 mg/mL (DI water)	0.1 mg/mL (PBS)	0.5 mg/mL	2 mg/mL (DI water)	
Working condition. Volume or weight of subs. in exp. ($V_{\Sigma} = 500 \mu\text{L}$)	Vol.	10 μL	20 μL	20 $\mu\text{L}^{(*)}$	15 μL	5 $\mu\text{L}^{(**)}$	25 μL	1x
	wt.	300 μg	10 μg	15 μg	1.5 μg	3.5 μg	50 μg	
Recommended Concentration (from Ademtech protocol and literatures)								
Stock concentrations		30 mg/mL	4 mg/mL (DI water)	4 mg/mL (DI water)	10 mg/mL (PBS)	3-6.5 mg/mL ^(**)	0.5 mg/mL (DI water)	10x
Working condition. Volume or weight of subs. in exp. ($V_{\Sigma} = 500 \mu\text{L}$)	Vol.	16.7 μL	40 μL	60 μL	1-5 μL	0.5 μL	100 μL	1x
	wt.	500 μg	160 μg	230 μg	10-50 μg	3.5 μg	50 μg	

^(*) In literature, the concentration ratio of NHS and EDC is recommended 1.43, which is suitable ratio for activating effectively carboxyl-groups and protein immobilization, [22]-*supporting information*).

^(**) F/P Molar Ratio: 2.5-6.5, Data sheet of product Anti-Mouse IgG (Fab specific)-FITC ⁽¹⁾

⁽¹⁾ Antibody is labeled by fluorescein isothiocyanate:

<http://www.sigmaaldrich.com/content/dam/sigma-aldrich/docs/Sigma/Datasheet/7/f5262dat.pdf>

b. IgG grafting protocol

Figure 4.36 presents the protocol in general, which can be divided in two main parts before the detection step:

- Steps for chemical activation: Washing and activation of the beads.
- Steps for biological grafting: Grafting and labeling beads

The detailed information about the protocol is presented in **Appendix 4**.

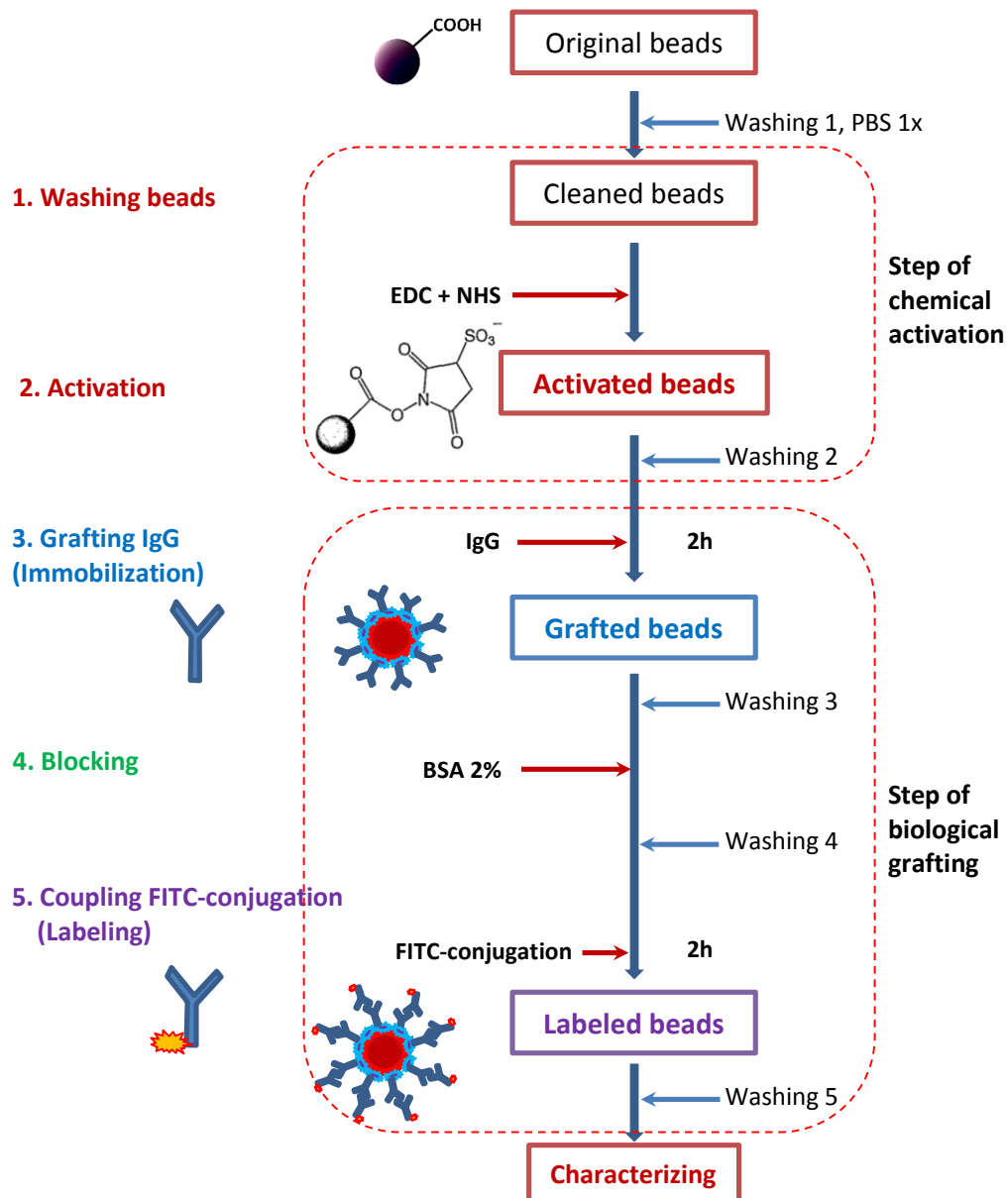


Figure 4.36. Protocol overview of IgG grafting on beads surface and then detecting by the second labeled antibody – Anti-mouse IgG (Fab specific) FITC-conjugated

4.4.2.2. Experiment and results in micro test tube (control experiment)

a. Protocol description

Figure 4.37 shows the process of the grafting IgGs on the surface of carboxyl-magnetic beads in micro test tube, *i.e.* process outside microfluidic chip.

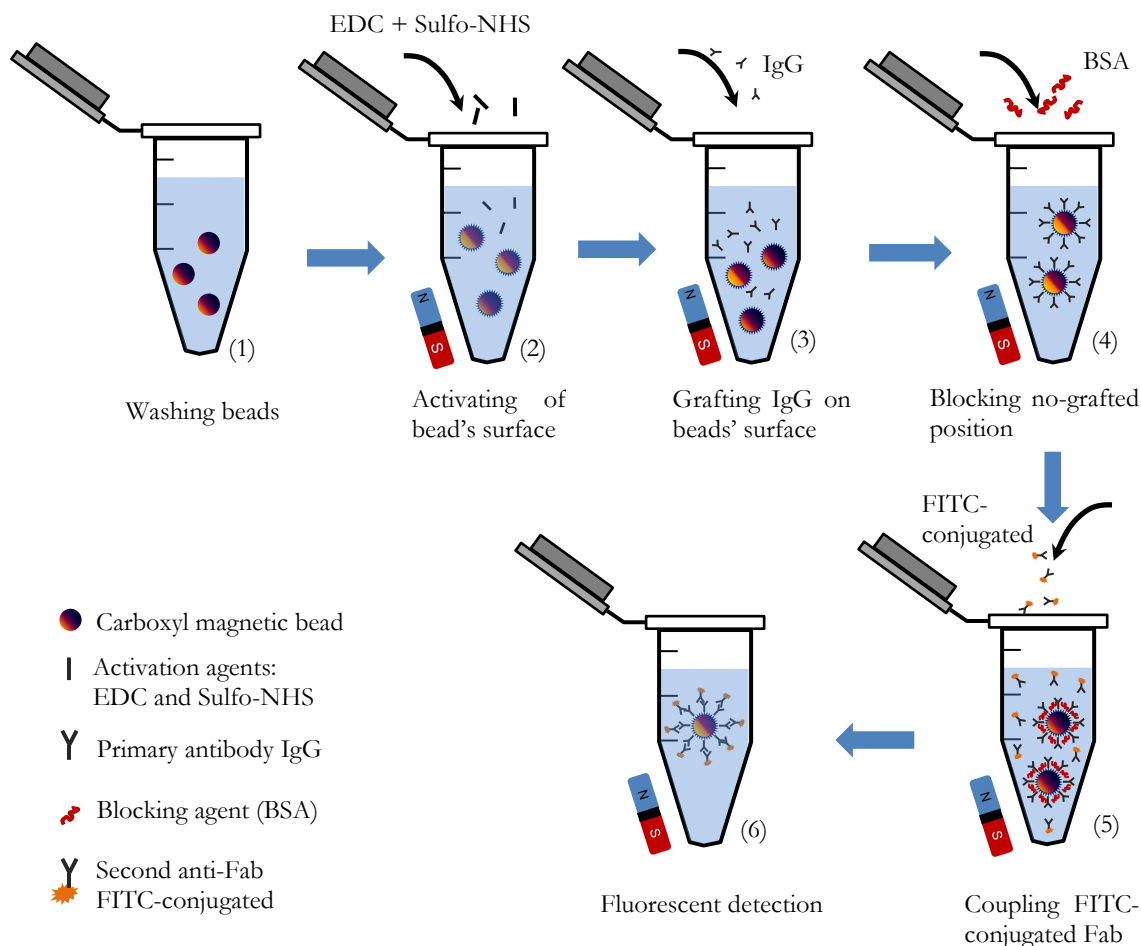


Figure 4.37. Process flows of IgG grafting on beads and coupling IgG-FITC-conjugated in micro test tube

All steps are detailed bellow. In each step, the beads are separated of the solution thanks to a magnet bar:

(1). *Bead washing*: 10 μL beads (original concentration) in 100 μL PBS 1x are washed 3 times with 500 μL PBS 1x each time, in plastic micro-test tube.

(2). *Beads' surface activation*: 20 μL of EDC and 20 μL of Sulfo-NHS solution are added together in beads. PBS 1x is added to obtain 500 μL of total volume. The activation is performed in 20 minutes under shaking. A washing step is carried out with 500 μL PBS 1x (3 time) as the activation is finished.

(3). *Grafting of the first antibody on activated beads*: 15 μL of IgG is added activated beads, and PBS 1x is added to obtain 500 μL of total volume. The grafting procedure

is taken in 2 hours at 25°C under shaking. As the grafting process is finished, a washing step is carried out with 500 μ L PBS 1x (3 time).

(4). *Blocking*: 25 μ L of blocking agent, BAS 0.2%, is added in the grafted beads for blocking free-grafted bead's surface. The blocking step is performed in 20 minutes at 25°C under gentle shaking. A washing step is carried out with 500 μ L PBS 1x (3 time) when blocking step finishes.

(5). *Labeling*: The grafted antibodies will be detected by coupling with second labelled antibodies (IgG-FITC-conjugated, called FITC). 5 μ L of FITC is added into grafted beads and incubated for 2 hours at 25°C under shaking, and PBS 1x is added to obtain 500 μ L of total volume. This process is protected from light by covering with dark box. When the coupling procedure finishes, a washing step is carried out with 500 μ L PBS 1x (3 time).

(6). *Fluorescent detection*: Magnetic beads are characterized by taking fluorescent images.

b. Results and discussion

Figure 4.38 shows the fluorescent images resulting from three experiments:

- Experiment 1: step of beads' surface activating by EDC and Sulfo-NHS has been skipped from the proposed protocol, Figure 4.37. The result shows that the signal of FITC is very limited in the fluorescent images. It proves that IgGs could not be grafted on un-activated surface of beads.
- Experiment 2: step of IgGs grafting on activated beads' surface has been skipped. The result shows that the signal of FITC is also limited, like in previous experiment. It also proves that the second antibody labeled by FITC could not be immobilized on activated surface of beads without the primary antibody.
- Experiment 3: all steps (beads' surface activating, IgGs grafting, and coupling FITC) of the proposed protocol are performed. The result shows that there are significant signals of FITC. It demonstrates that, when the beads' surface is activated, the primary IgG antibody can be grafted on this surface, and the second antibodies labeled by FITC can be coupled with these primary antibodies




	Beads activating	IgGs Grafting	FITC coupling	Results
Experiment 1	-	+	+	
Experiment 2	+	-	+	
Experiment 3	+	+	+	

Figure 4.38. Fluorescent images of samples resulting from the process of immobilizing IgGs on beads and detecting by FITC; Experiment 1: the process skip the step of beads' surface activating; Experiment 2: the process skip the step of IgG grafting on beads' surface; Experiment 3: all steps are performed.

Figure 4.39 shows results of immobilizing IgG on beads' surface, and then coupling with IgG-FITC-conjugated. The comparison of fluorescent images to optical images shows that there is a relative similarity of the beads quantity in the bright field image to the fluorescent signal in the UV-field image. It proves that most of beads in solution are grafted by IgG and then coupled by FITC.

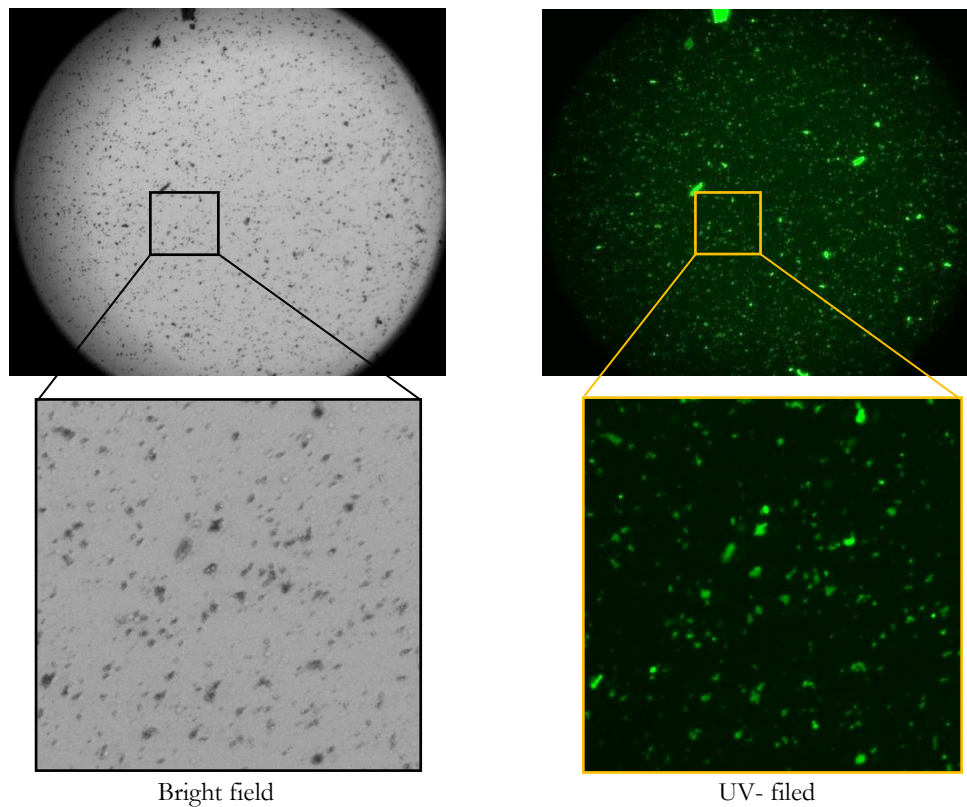
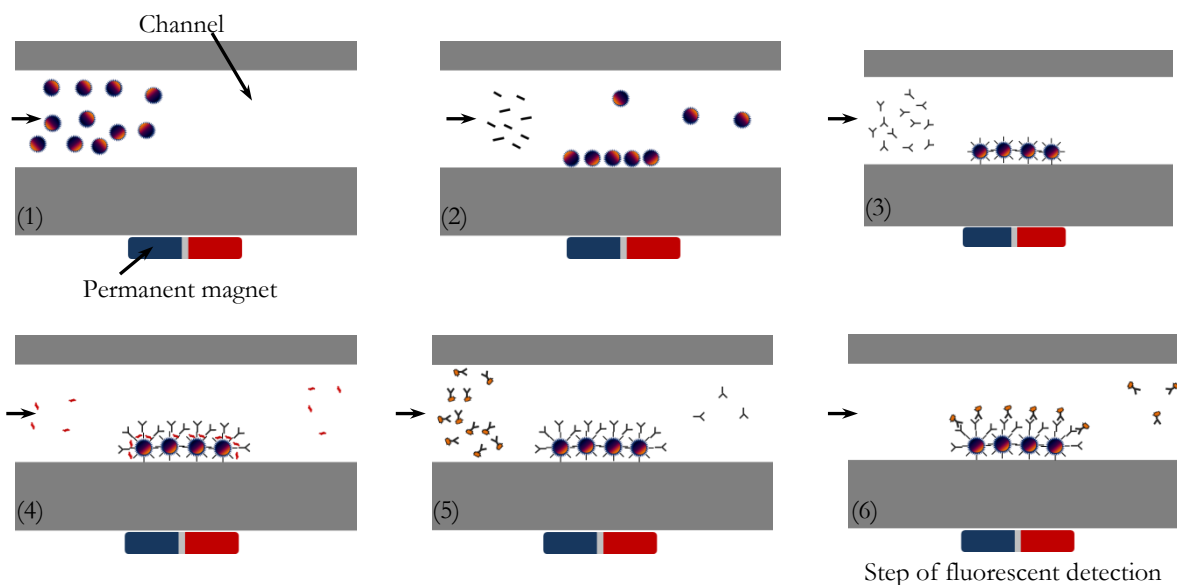


Figure 4.39. Fluorescent images (full view (magnification 20x) and zoom view by fluorescence microscopy using bright field and UV-filed) of primary IgG grafted on beads' surface recognized by secondary anti-Fab FITC-conjugated in micro test tubes

4.4.2.3. Experiments in microfluidic chip

Figure 4.40 show the two configurations of IgGs grafting on beads' surface experiments in microfluidic chips (processes inside microchannel) using magnet bar (A) or microcoils (B) to trap the magnetic beads.

(A)



(B)

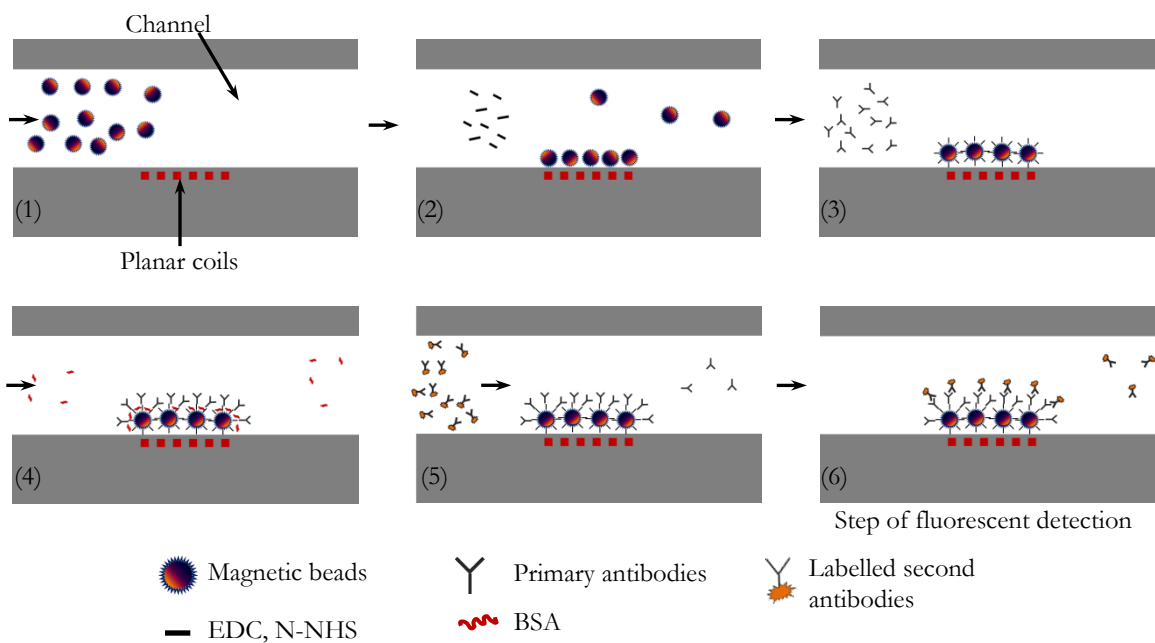


Figure 4.40. Process flows of IgG grafting on beads surface and coupling IgG-FITC-conjugated in microfluidic chips using permanent magnet (A) or electromagnet for trapping magnetic beads (B)

The step of magnetic beads trapping in chip using permanent magnet is different from the one of the chip using microcoils. In the latter one, turning on/off of the applied current into to the coil controls the magnetic field generating/stopping in

channel. In the former one, the use of permanent magnet involves a manually controlled of the magnetic field in channel.

a. Setup of microfluidic chip for grafting IgGs:

Figure 4.41 shows the diagram description of the setting up microfluidic chips (including a chip using permanent magnet, and chip using microcoils for trapping magnetic beads) with all supporting modules (pumps, valve switch, DC power supply, and microscope) in experiment.

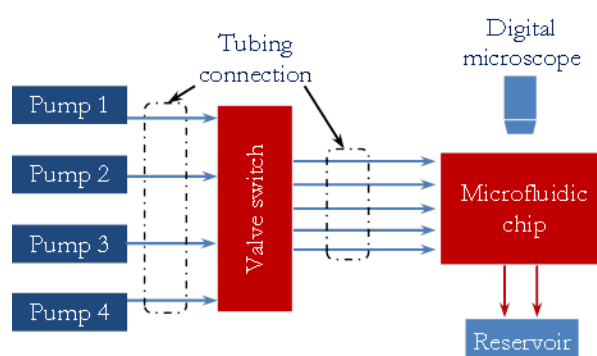


Figure 4.41. Schematic setup of microfluidic system for on chip immunoassay

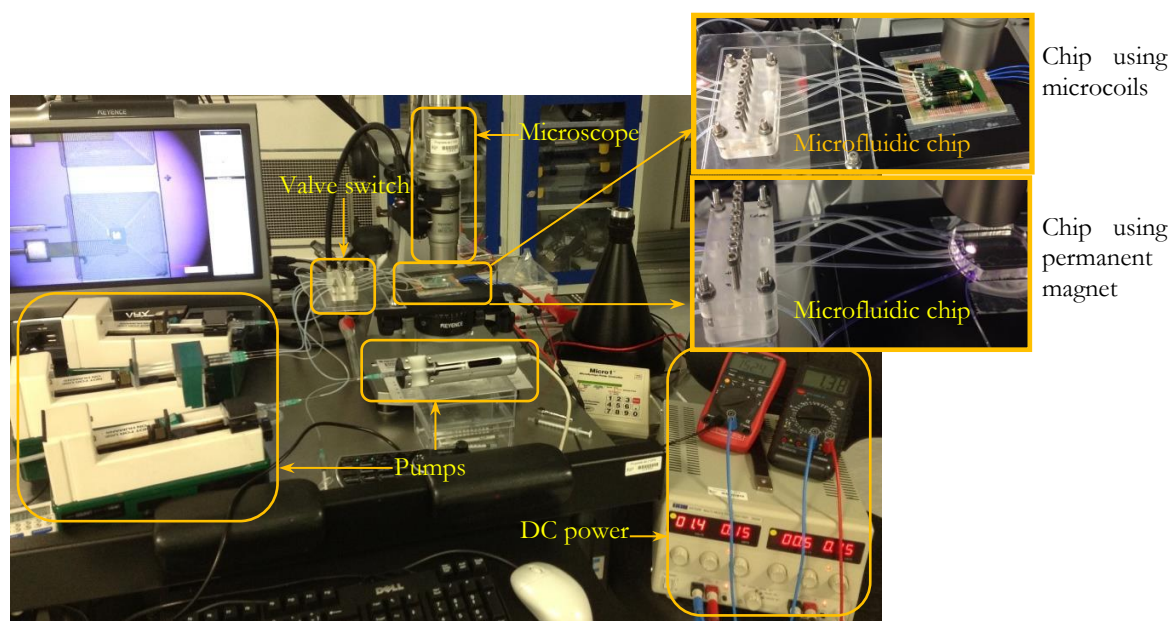


Figure 4.42. Photograph of the experiment setup.

As shown in Figure 4.41 and Figure 4.42, series of micro-pumps (from pump #1 to #4) will supply and control flows of different liquids (including buffer – PBS for all cleaning steps; beads; activating beads solutions – EDC and S-NHS; blocking beads surface solution – BSA; antibody solution – IgG and labeled antibody – FITC). Then,

all liquids go through the tubing connection, and enter the valve switch in order to operate following by stop-flow or continue-flow mode of each liquid. Thanks to the valve switch, all liquids are controlled to be injected sequentially into channel network corresponding to substance requirements in each step of the total process of on-chip immunoassay. The waste liquids from the process inside channel are led out through two outlets to reservoir.

Figure 4.43 shows the two microfluidic chips: chip using permanent magnet and other using microcoils, which are used for experiment of immobilizing IgGs.

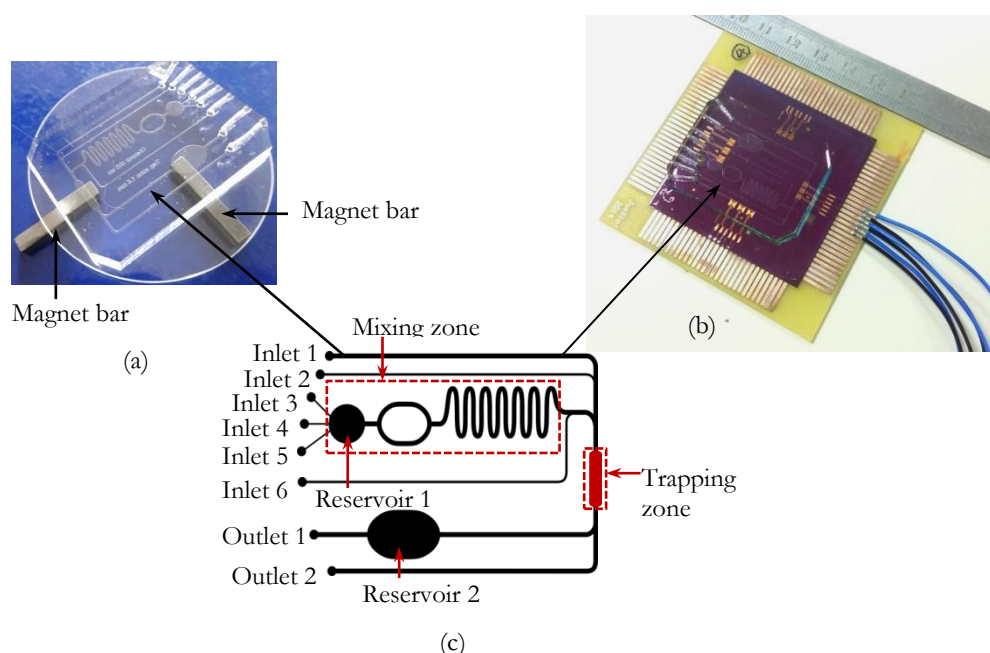


Figure 4.43. Microfluidic chips used in the experiment of immobilizing IgGs on beads' surface. (a). Chip with PDMS channel network and using permanent magnet for trapping beads. (b). Chip with PDMS channel network using microcoils for trapping beads. (c). PDMS channel parameters: 500 μm wide with 1.5 mm wide of trapping zone, microcoils' parameters: size: 1.5 mm; $w = 10 \mu\text{m}$; $s = 10 \mu\text{m}$; $N = 33$ turns; $h = 10 \mu\text{m}$.

b. IgG grafting protocol

Procedures of grafting in the two microfluidic chip are performed in the same conditions of experiments than in micro tubes. Based on the experimental setup of microfluidic chip, the following protocols is applied for chip using embedded microcoils:

Preliminary step: Channel is pre-cleaned by injecting PBS 1x in channel for 10 minutes in order to wet all channel's surface and limit air bubbles. This step is a very important step, and can sometime take longer time than 10 minutes. The flow rate of PBS is kept constant at 0.59 $\mu\text{L}/\text{min}$.

(1). Beads washing: beads and PBS are injected in channel (inlet 4 and inlet 1 respectively, Figure 4.43 (a)) at 0.3 $\mu\text{L}/\text{min}$ of flow rate for each solution (it is noted that the total flow rate is kept at $\sim 0.6 \mu\text{L}/\text{min}$). As beads move through reservoir 1, mixing zone, and reach the coil position/trapping zone, a 400 mA of current is applied immediately to the coils for generating magnetic field to trap magnetic beads. While beads continue reaching to coils and being trapped at these positions, the PBS goes through trapped beads and the beads washing step is performed. Beads are washed in 10 minutes. The washing procedure will clean all surfactants and solution for stabilizing beads in stock solution.

After washing procedure finishes, pumps supplying beads and PBS are stopped and these inlets are locked by closing valve switch.

(2). Beads' surface activation: The solutions of EDC and Sulfo-NHS are injected together in inlet 3 and 5, Figure 4.43 (a), with 0.3 $\mu\text{L}/\text{min}$ of flow rate of each solution. The activation procedure is done in 10 minutes (total volume 3.0 μL of each EDC and Sulfo-NHS). Then, the two lines 3 and 5 of valve switch are closed, and PBS is injected for 15 minutes in inlet 1 with 0.59 $\mu\text{L}/\text{min}$ of flow rate in order to take the second washing step. It is noted that, EDC/Sulfo-NHS are released as much as possible out of trapping zone in order to limit the conjugation of EDC with carboxyl or amine groups of biomolecules leading these molecules to self-polymerize. As the washing step finishes, the inlet 1 is closed. It is noted that a current of 400 mA is applied in to the coils during the entire experiment.

(3). Grafting the first antibody on activated beads: while nanobeads are still trapped in the trapping zone, IgG is injected into channel through the inlet 6, while all other inlets are closed. The grafting procedure is taken in 2 hours at 36°C with a flow rate keeping constant at 0.3 $\mu\text{L}/\text{min}$, at half of normal flow rate (Total volume = 36 μL). Then a washing step of 20 minutes is carried out in order to remove all non-grafted IgG. In the washing step, the inlet 6 is closed and the inlet 1 is opened for PBS injection.

It is noted that, when beads are under magnetic force they aggregated into cluster of beads. Thus, the interacting surface of beads is decreased. To enhance the efficiency of IgG grafting on beads surface, mixing of beads and IgGs in channel is required. Thus, the nanoparticles are regularly released and re-trapped from the coil surface. This is done by turning off syringe pump and cutting off the injected current

in the coil (1 minute every 30 minutes). This turns off the magnetic field, and then nanoparticles are subject to *Brown movement*. As the nanoparticles have to stay in the trapping zone, no fluid movement is insured by stopping the supplying IgG pump and closing inlet 6 (4 minutes before cutting off the current).

In addition, after each step (activating, grafting), beads can be moved respectively from the first coil to third coil in order to make some mixing (because three coils are arranged in line along to flow direction, Figure 4.47)

(4). Blocking step: BSA 2%, blocking agent, is injected in channel from inlet 2 in order to be adsorbed on free surface of beads, limit interaction of beads, and prevent undesired adsorption on un-grafted bead surface of the fluorescent dye (FITC) in next step. The blocking step is performed for 20 minutes, and the flow rate is kept at 0.59 $\mu\text{L}/\text{min}$. After blocking step finishes, a washing step is performed to clean beads from BSA. The BSA inlet 2 is closed and inlet 1 is opened for 20 minutes for PBS injection with a flow rate of 0.59 $\mu\text{L}/\text{min}$.

(5). Fluorescence conjugation: Finally, to evaluate the primary grafted antibodies on beads surface, these antibodies are labelled by coupling with other labelled antibodies (IgG-FITC-conjugated) for characterization by fluorescent imaging. The IgG-FITC-conjugated is injected for 2 hours through inlet 2, after removing BSA pump supplier. The flow rate is 0.3 $\mu\text{L}/\text{min}$. The total volume of FITC is 36 μL . It is noted that, IgG-FITC-conjugated interacts easily with light, thus, in this step all the microfluidic chip, tubing connection and pump are protected from light by covering with dark box or placing in dark room. The bead self-mixing in channel at trapping zone – bt cutting off current for a while- is applied in this step. When the coupling procedure finishes, channel is cleaned carefully by injecting PBS through inlet 1, while all other inlets are closed. The flow rate for the 20 minutes washing step is 0.59 $\mu\text{L}/\text{min}$.

IgG grafted and FITC labeled magnetic beads are then characterized by taking fluorescent images.

For chip using permanent magnet to trap nanobeads, the protocol is very similar except the step of the mixing nanobead with liquid component in order to increase chemical reaction efficiency. **Two permanent magnets** are used to trap magnetic beads in that kind of chip: one is placed at the trapping zone; and other is placed at reservoir 2 of channel, as shown in Figure 4.44. The activation process (chemical process) of beads surface takes a short time (20 minutes), it usually happens

immediately after injecting beads, EDC and Sulfo-NHS into channel. Therefore, most of the carboxyl groups on beads' surface react with activation substances when they move to the trapping zone and are trapped by the first magnet, Figure 4.45 (a). To enhanced the IgG grafting, after haft time of the step (1 hour), beads are transited from trapping zone (using magnet (a)) to reservoir 2 (using magnet (b)). Finally, all the remaining steps of process are performed at the reservoir 2, which is used the second magnet for trapping beads. The fluorescence images are taken at this area.

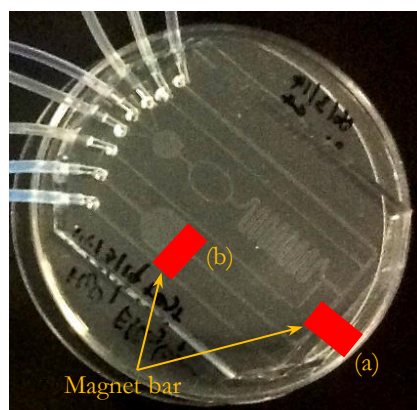


Figure 4.44. Microfluidic chip using permanent magnet for trapping beads. (a) The first trapping area; (b) The second trapping area at reservoir 2.

c. Results and discussion

▪ *The results of experiment in microfluidic chip using permanent magnet:*

Figure 4.45 shows microscopy images of magnetic beads which are trapped at the trapping zone during the step of IgGs grafting. The pictures (a) and (b) of Figure 4.45 show that big mount of beads are trapped. In addition, these beads are aggregated into big clusters (the size of these clusters is much bigger than the free bead's size).

Fluorescent images are taken at position of reservoir 2 after the step of FITC coupling. Figure 4.46 shows the comparison of image in bright-field (a) and image in UV-field (b). The population of beads in image (a) corresponds to the fluorescent signals in image (b). It proves that, during the protocol, most of beads bound IgGs and then are labeled by FITC.

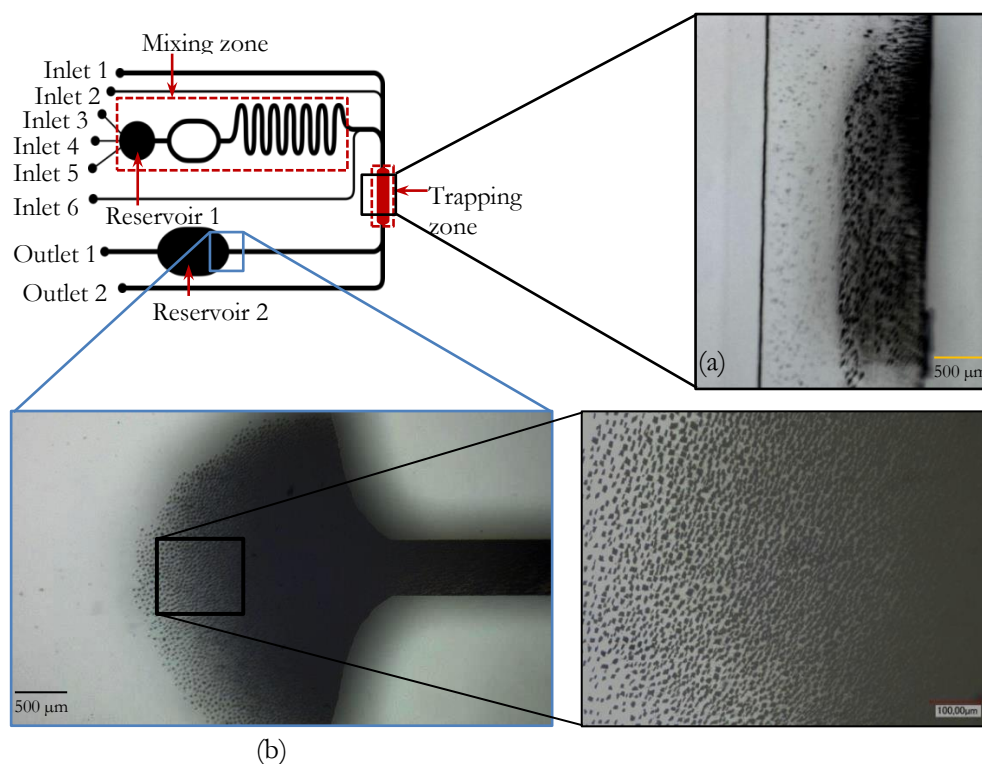


Figure 4.45. Microscope images of magnetic beads at the trapping positions in channel network during the step of IgGs grafting; (a) Beads trapped at trapping zone of channel. (b) Beads trapped at reservoir 2.

The mount of fluorescent labeled beads in the image (b) - Figure 4.46 is limited due to the lower bead's concentration in fluidic conditions.

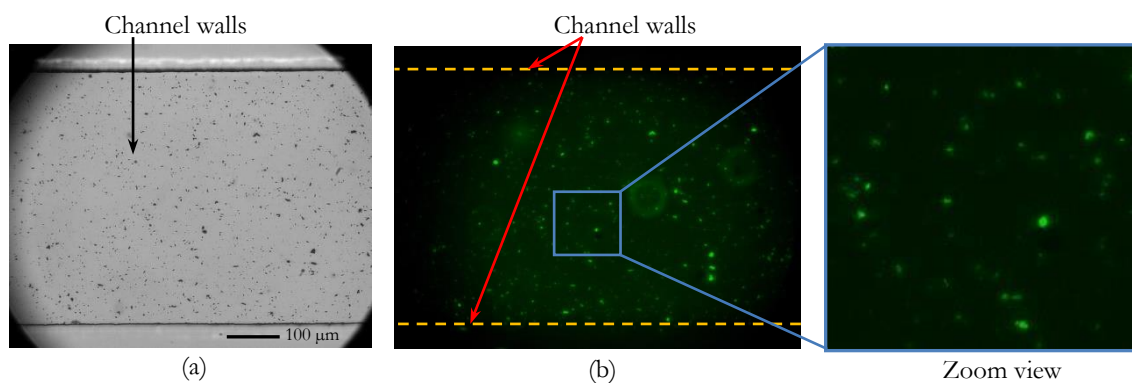


Figure 4.46. Microscope image (a) and fluorescent image (b) of beads after immobilizing IgGs on surface and labeling with IgG-FITC-conjugated

Qualitatively, we can conclude that, the process of immobilizing IgGs on beads surface can be performed inside microfluidic chip under the same conditions as it is performed in micro test tubes.

▪ ***The results of experiment in microfluidic chip using microcoils:***

As describe in the protocol, in this experiment magnetic beads are manipulated in channel network by microcoils at only trapping zone. Three microcoils are used for

the aim of separating and mixing beads during this experiment, as described in Figure 4.47.

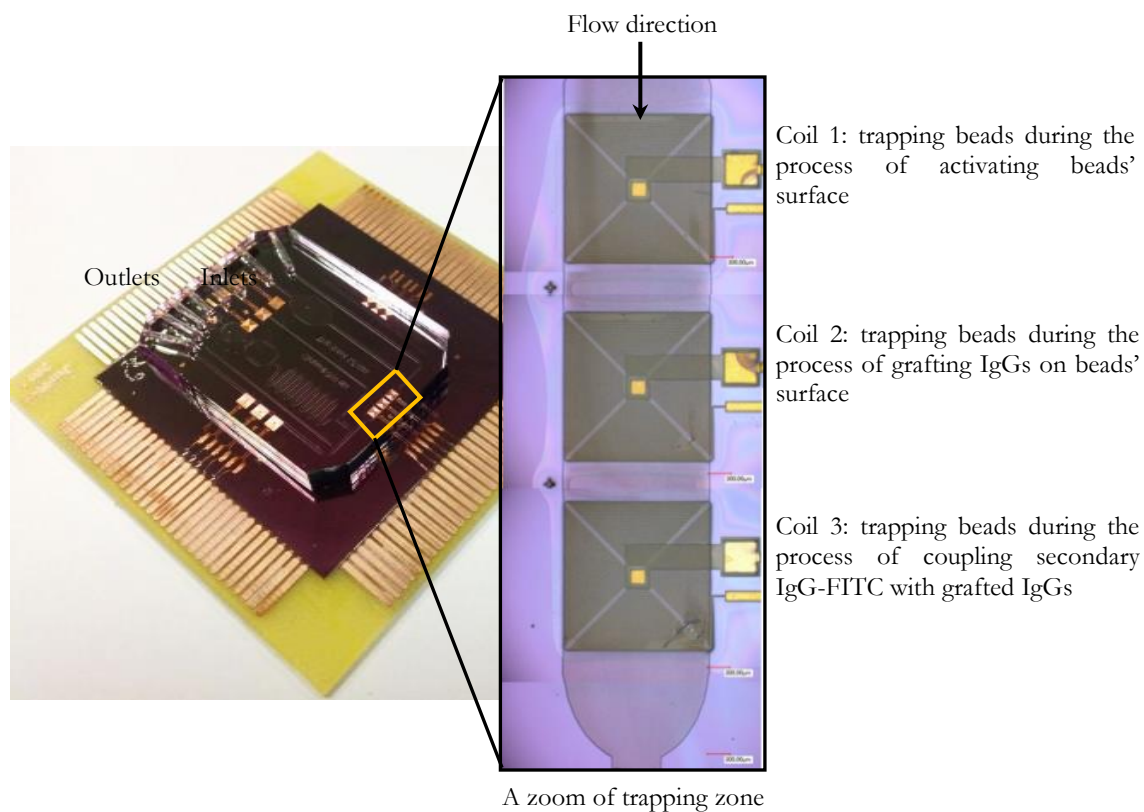
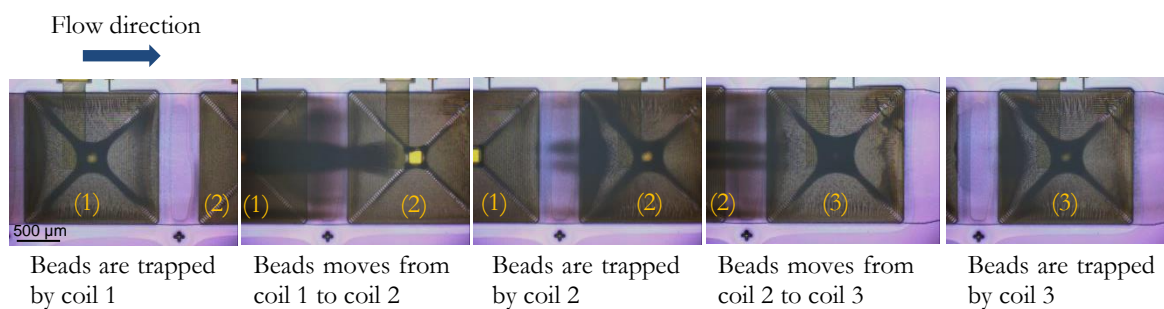


Figure 4.47. Description of microcoils' position and the role of each microcoil at the trapping zone; parameters of coils 1-3: 1.5 mm wide, $w = 10\ \mu\text{m}$; $s = 10\ \mu\text{m}$; $h = 10\ \mu\text{m}$ and $N = 33$ turns

Figure 4.48 shows the results of the process of trapping and moving beads during the experiment of immobilizing IgGs on beads' surface. Beads do not aggregate when they are released off microcoils by stopping magnetic field. The free moving of beads in flow makes the mixing of beads with other substances effective and efficient.

In fact, by using serial microcoils at trapping zone of channel network, the trapping and mixing processes lead to enhance the control of the immobilization of IgGs on beads' surface.



The injection of current (*I*) during the experiment

	Trapping step 1	Moving step 1	Trapping step 2	Moving step 2	Trapping step 3
Coil 1	On	Off	Off	Off	Off
Coil 2	Off	Off	On	Off	Off
Coil 3	Off	Off	Off	Off	On

Current = on $\rightarrow I = 400$ mA; Current = off $\rightarrow I = 0$

Figure 4.48. Description of the mixing and trapping process during immunoassay in microfluidic chip with embedded coils. Current $I = 400$ mA, flow rate: $0.59 \mu\text{L}/\text{min}$

To characterize the immobilization of IgGs on beads' surface, fluorescent images after FITC coupling with grafted IgGs are taken. Because the characterization is performed by using an inverted fluorescence microscope, the images cannot be taken through silicon substrates (non-transparent substrates). In fact, we used specific set-up where all beads after experiment are released from microfluidic chip to another transparent chip (glass substrate), as described in Figure 4.49. This chip can work under inverted fluorescence microscope and contains a single channel.

Figure 4.50 shows the fluorescent images of coupled FITC to grafted IgGs on beads' surface inside the channel of characterization chip. Compare to the image in bright field, the population of beads labeled by FITC in the fluorescent image is lower. It can be explained that, in the grafting IgG, whereas beads were being trapped on coils' surface the mixture of beads with substances (EDC, Sulfo-NHS, IgG, BSA and IgG-FITC-conjugated) was not carried out very well. Therefore, some parts of beads' surface or beads were covered or hidden and then IgG- FITC could not be grafted or coupled efficiently on these parts of beads' surface. Thus the bead mixing with liquid component has to be enhanced, but these results show the possibility of performing a bead-based immunoassay inside a microfluidic chip with bead trapping steps insured by integrated microcoil.

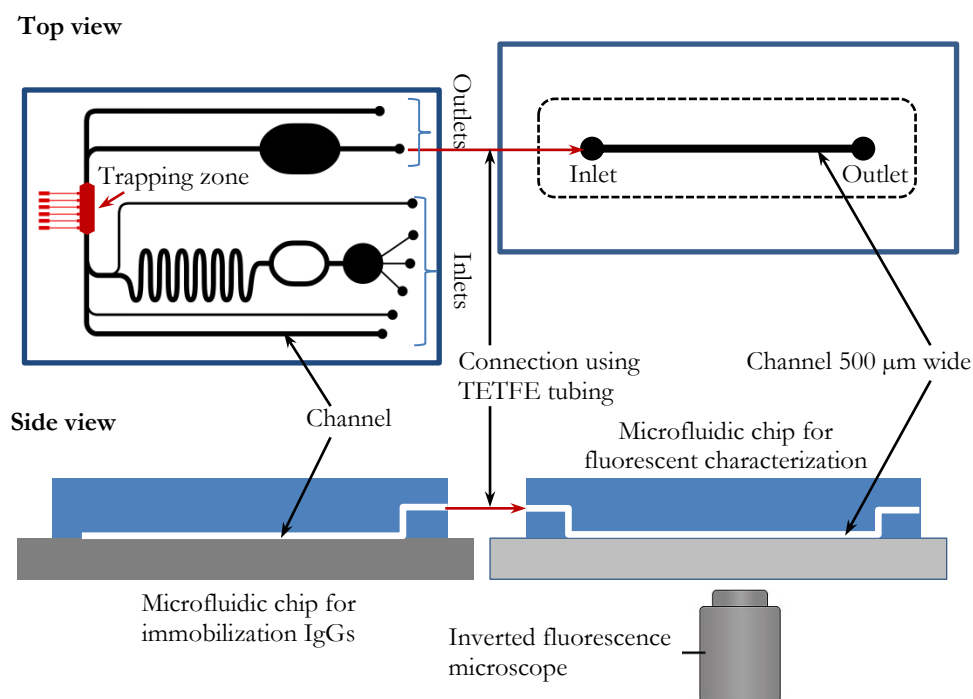


Figure 4.49. Scheme of releasing beads from the main microfluidic chip to minor microfluidic chip for supporting the fluorescent characterization

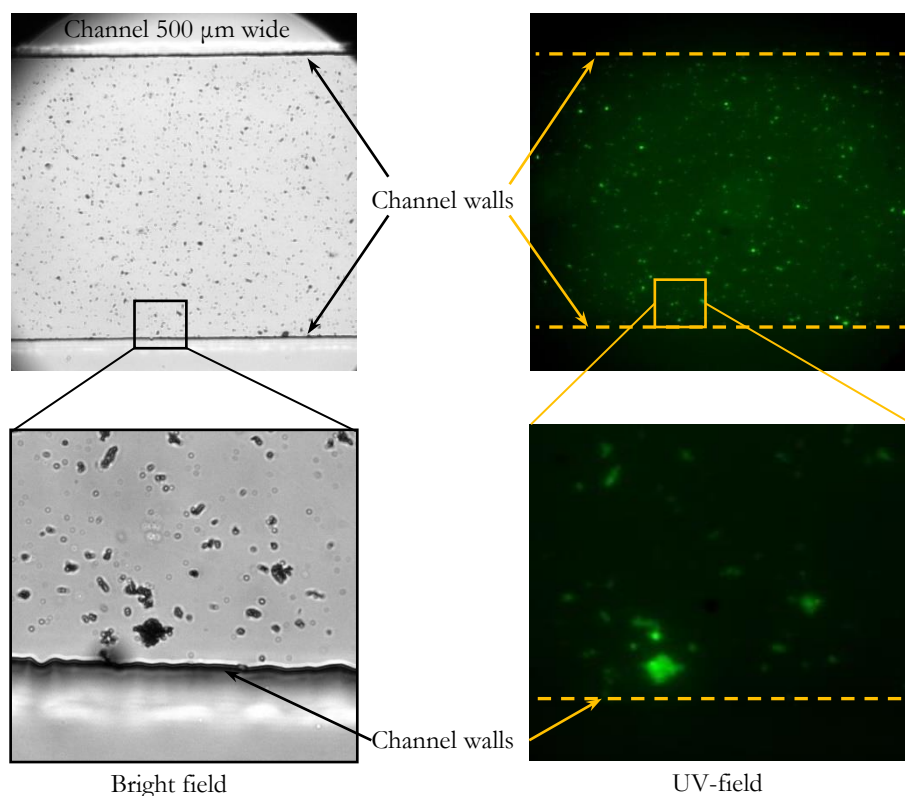


Figure 4.50. Fluorescent images (full view (magnification 20x) and zoom view (magnification 60x) by fluorescence microscopy using bright field and UV-filied) of the detection of primary grafted IgG on beads' surface by second anti-Fab IgG-FITC-conjugated

4.4.3. Conclusions from applying microfluidic chip with embedded microcoil in immunoassay

A modification of PDMS surface is carried out successfully by using PEO to coat PDMS and BSA to block all surfaces and reduce the non-specific adsorption of fluorescent dyes (FTTC). The IgG immobilization inside microfluidic chips, which use permanent magnet or embedded microcoils, showed that IgGs could be grafted on bead's surface in similar conditions to the process performed outside channel (in micro-test tube) which is a very good result. The IgGs immobilization process should be optimized in future studies to obtain optimal immune-assay response of biomarkers with quantitative results.

4.5. General conclusion of chapter 4

In this chapter, a microfluidic chip with embedded coils is fabricated and characterized. First the microchannels are designed and the process of packaging is carried out with a flexible micro-valve. We verified that the trapping is compatible with the use of temperature inferior to 37°C. The trapping of functionalized beads is then performed. For each step, we propose a specific development concerning packaging and biological functionalization of nanobeads for which the grafting is performed inside the channel. Concerning the packaging, we developed several techniques using the non-adhesive layer (Teflon-like thin layer – CYTOP product) and a stamping process. It allows us to re-use the bottom substrates several times. In addition, PDMS surface was modified fast (about 1 hour) by coating PEO 0.2% and blocking surface thanks to BSA 2%. This treatment avoids the non-specific adsorption on PDMS surface.

Concerning the trapping, successful trapping beads (Adembeads 300 nm) experiments in biocompatible environment (temperature around 37°C) have been performed by integrated microcoils. The distribution of trapped beads on coil's surface corroborates the profile of magnetic field that was calculated by simulation.

The IgG immobilization has been performed inside microfluidic chip, and results showed that all steps of this process, validated in micro-tube conditions, could be carried out on chip: beads' surface activation, IgGs immobilization, surface blocking, and IgG-FTTC conjugated coupling.

REFERENCES

- [1] W. Hellmich, J. Regtmeier, T.T. Duong, R. Ros, D. Anselmetti, A. Ros, Poly(oxyethylene) Based Surface Coatings for Poly(dimethylsiloxane) Microchannels, *Langmuir*, 21 (2005) 7551-7557.
- [2] K. Boxshall, M.-H. Wu, Z. Cui, Z. Cui, J.F. Watts, M.A. Baker, Simple surface treatments to modify protein adsorption and cell attachment properties within a poly(dimethylsiloxane) micro-bioreactor, *Surface and Interface Analysis*, 38 (2006) 198-201.
- [3] S. Brault, O. Garel, G. Schelcher, N. Isac, F. Parrain, A. Bosseboeuf, F. Verjus, M. Desgeorges, E. Dufour-Gergam, MEMS packaging process by film transfer using an anti-adhesive layer, *Microsystem Technologies*, 16 (2010) 1277-1284.
- [4] G. Schelcher, S. Brault, F. Parrain, E. Lefeuvre, E. Dufour-Gergam, M. Tatoulian, D. Bouville, M. Desgeorges, F. Verjus, A. Bosseboeuf, MEMS Process by Film Transfer Using Fluorocarbon Anti-Adhesive Layer, *ECS Transactions*, 33 (2010) 287-296.
- [5] D.C. Duffy, J.C. McDonald, O.J.A. Schueller, G.M. Whitesides, Rapid Prototyping of Microfluidic Systems in Poly(dimethylsiloxane), *Analytical Chemistry*, 70 (1998) 4974-4984.
- [6] G.M.W. J. Cooper McDonald, Poly(dimethylsiloxane) as a material for fabricating, *Accounts of Chemical Research*, (2002) 491-499.
- [7] S. Li, P.N. Floriano, N. Christodoulides, D.Y. Fozdar, D. Shao, M.F. Ali, P. Dharshan, S. Mohanty, D. Neikirk, J.T. McDevitt, S. Chen, Disposable polydimethylsiloxane/silicon hybrid chips for protein detection, *Biosensors and Bioelectronics*, 21 (2005) 574-580.
- [8] M.A. Eddings, M.A. Johnson, B.K. Gale, Determining the optimal PDMS–PDMS bonding technique for microfluidic devices, *Journal of Micromechanics and Microengineering*, 18 (2008) 067001.
- [9] I. Nikcevic, A. Bange, E.T.K. Peterson, I. Papautsky, W.R. Heineman, H.B. Halsall, C.J. Seliskar, Adsorption of fluorescently labeled microbeads on PDMS surfaces, in, 2005, pp. 159-167.
- [10] J. Preisler, E.S. Yeung, Characterization of Nonbonded Poly(ethylene oxide) Coating for Capillary Electrophoresis via Continuous Monitoring of Electroosmotic Flow, *Analytical Chemistry*, 68 (1996) 2885-2889.
- [11] N.A. Alcantar, E.S. Aydil, J.N. Israelachvili, Polyethylene glycol-coated biocompatible surfaces, *Journal of Biomedical Materials Research*, 51 (2000) 343-351.
- [12] S. Sugio, A. Kashima, S. Mochizuki, M. Noda, K. Kobayashi, Crystal structure of human serum albumin at 2.5 Å resolution, *Protein Engineering*, 12 (1999) 439-446.
- [13] N. Iki, E.S. Yeung, Non-bonded poly(ethylene oxide) polymer-coated column for protein separation by capillary electrophoresis, *Journal of Chromatography A*, 731 (1996) 273-282.
- [14] E. Delamarche, A. Bernard, H. Schmid, A. Bietsch, B. Michel, H. Biebuyck, Microfluidic Networks for Chemical Patterning of Substrates: Design and Application to Bioassays, *Journal of the American Chemical Society*, 120 (1998) 500-508.
- [15] E. Delamarche, A. Bernard, H. Schmid, B. Michel, H. Biebuyck, Patterned Delivery of Immunoglobulins to Surfaces Using Microfluidic Networks, *Science*, 276 (1997) 779-781.
- [16] H. Lee, R.M. Venable, A.D. MacKerell Jr, R.W. Pastor, Molecular Dynamics Studies of Polyethylene Oxide and Polyethylene Glycol: Hydrodynamic Radius and Shape Anisotropy, *Biophysical Journal*, 95 (2008) 1590-1599.
- [17] H. Chen, Z. Zhang, Y. Chen, M.A. Brook, H. Sheardown, Protein repellent silicone surfaces by covalent immobilization of poly(ethylene oxide), *Biomaterials*, 26 (2005) 2391-2399.

- [18] T.J. Barnes, C.A. Prestidge, PEO–PPO–PEO Block Copolymers at the Emulsion Droplet–Water Interface, *Langmuir*, 16 (2000) 4116-4121.
- [19] N.E. Esipova, S.V. Itskov, N.V. Churaev, Stability of Wetting Films of F108 Triblock Copolymer Aqueous Solutions on Quartz, *Colloid Journal*, 64 (2002) 699-705.
- [20] B.M. Moudgil, T.S. Prakash, Competitive adsorption of polymer and surfactants on solid substrates, *Colloids and Surfaces A: Physicochemical and Engineering Aspects*, 133 (1998) 93-97.
- [21] R. Ishiguro, Y. Yokoyama, H. Maeda, A. Shimamura, K. Kameyama, K. Hiramatsu, Modes of conformational changes of proteins adsorbed on a planar hydrophobic polymer surface reflecting their adsorption behaviors, *Journal of Colloid and Interface Science*, 290 (2005) 91-101.
- [22] S. Puertas, P. Batalla, M. Moros, E. Polo, P. del Pino, J.M. Guisán, V. Grazú, J.M. de la Fuente, Taking Advantage of Unspecific Interactions to Produce Highly Active Magnetic Nanoparticle–Antibody Conjugates, *ACS Nano*, 5 (2011) 4521-4528.

5. CONCLUSION AND PROSPECTS

In this study, a new type on-chip bead-based immunoassay platform with embedded planar microcoils was designed and fabricated for the aim of trapping effectively functionalized magnetic nano/micro beads, and the immobilization of capture antibodies inside microchannel. The microcoils as electromagnets are proposed to integrate in microfluidic chip instead of permanent magnets in order to control well the magnetic force in the trapping and mixing magnetic beads inside microchannel. It allows to control the magnetic field without displacement of any part of the device which is obligatory in the case of permanent magnet. The originality is to couple the very high sensitivity and specificity totally integrated and which even allows to functionalize the nanoparticles within the micro-device.

In *chapter 2*, a review of integrated microfluidic system and the using of this system in immunoassay are presented specifically for bead-based microfluidics immunoassay. Some of them integrate microcoils inside but we never identify some teams which develop the sandwich grafting and the functionalization of the device with microcoils. The design of these microcoils was carried out basing on the calculation and simulation of magnetic field on surface of microcoils, *in chapter 3*. Thanks to the FE method and ANSYS® v12.1 software, the simulation results showed the criteria for designing planar microcoils: optimal magnetic field obtained with low power consumption, *i.e.* high power efficiency should be chosen in order to decrease coil heating in the microfluidic chips and stay compatible with biological applications. Merit factors such as the magnetic field generated for a given power loss were defined. These factors gave very important parameters to fabricate the planar microcoils as a heart of microfluidic chip for trapping effectively magnetic beads at low rising temperature in the procedure of bead-based immunoassay inside microfluidic chip. The microcoils were fabricated by microfabrication technique, and they were characterized by temperature measurement on surface of microcoils and trapping magnetic test. These experimental results (*in chapter 4*) validated those microcoils were able to trap well magnetic beads at bio-compatible temperature (without any module of temperature controller).

The microfluidic chip was fabricated basing on the embedded microcoils on the bottom substrate and microchannel network in PDMS materials. The PDMS channels were designed with multi-inlets/outlets and functionalized zones such as mixing zone,

trapping zone. These designs were suitable for the aim of the manipulation of multi-components (e.g. magnetic beads; chemicals; biological materials, etc.) of immobilization antibody IgG on carboxyl beads' surface inside microfluidic chip. The microfluidic chip assembling was performed by bonding the PDMS channel to bottom substrate with embedded microcoils. This packaging process was carried out by the techniques of reversible bonding which allows to reuse the bottom substrate in many times. This bottom substrate contains planar microcoils and was requires a complex fabrication process. In this study, the development of reversible bonding for general PDMS microfluidic chips contributed simple and useful techniques in packing chip.

The fabricated microfluidic chips were applied to the immobilization (on chip) of the antibody IgG-type on carboxyl magnetic beads. In this immobilization process, the efficiently trapping 300 nm magnetic beads at low temperature ($< 37^{\circ}\text{C}$) was an important step to perform successfully the immobilization of antibody on beads' surface basing on the standard protocol which is performed in micro test tube. These immobilization results inside the two microfluidic chips: using embedded microcoils and using permanent magnets were compared to the results which were performed in micro test tube. In addition, a process of the PDMS surface modification (using a process of coating PEO 0.2% and blocking surface thanks to BSA 2%) was required to anti-the non-specific adsorption biological substances.

▪ ***Study's prospects:***

We have seen during the experiments that the magnetic beads in external magnetic field are often aggregated leading to decreasing reaction surface. Therefore, a mixing step of the trapped magnetic beads at trapping zone needs really to be developed in order to increase the reaction area of the beads surface with activation surface agents, antibodies, etc. This problem can be solved by arranging microcoils at trapping zone (like a microcoils array) or controlling the characterization of magnetic field. The ability of trapping beads of the microcoils may be enhanced by using magnetic materials with coils (such as Permalloy core).

The process of immobilizing IgGs on beads' surface need to be optimized varying the concentrations of the antibodies IgGs and FITC-conjugation beads solutions.

Based on the results from the immobilization IgGs on beads' surface inside microfluidic chip, the ELISA sandwich structure of Bead – Capture antibody – Antigen – Second antibody/detection antibody (such as Fab-FITC conjugation) will be performed on chip in order to detect bio-markers (antigens) such as (β -*amyloid*(1–42) – Alzheimer disease; *HER-2/neu* – Breast cancer disease).

APPENDICES

PUBLICATIONS:

1. T.H.N. Dinh, H.H. Cao, F.S. Hamdi, M. Couty, E. Martincic, M. Woytasik, E. Dufour-Gergam, *Development of reversible bonding for microfluidic applications*, Microfluidics and Nanofluidics, (2015) 1-6.
2. H.H. Cao, T.H.N. Dinh, F.S. Hamdi, M. Couty, E. Martincic, M. Woytasik, E. Dufour-Gergam, *Reversible bonding by dimethyl-methylphenylmethoxy siloxane – based stamping technique for reusable poly(dimethylsiloxane) microfluidic chip*, Micro & Nano Letters, 10 (2015) 229-232.
3. M. Araya-Farias, M. Taverna, M. Woytasik, F. Bayle, M. Guerrouache, I. Ayed, H.H. Cao, B. Carbonnier, N.T. Tran, *A new strategy for simultaneous synthesis and efficient anchorage of polymer monoliths in native PDMS microchips*, Polymer, 66 (2015) 249-258.

APPENDIX 1. Chapter 3 – Microcoils design and fabrication

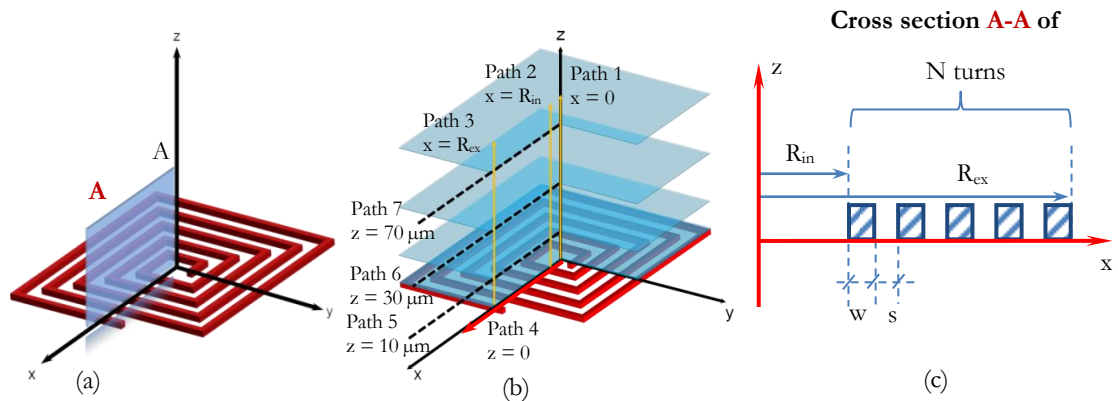


Figure 1. Simulation model: (a). Coil model; (b). The magnetic calculation at the positions that will be shown in simulation results; (c). The detail parameters of coil model at cross section A-A. w = the width of Cu wire; s = the space between two Cu wires; R_{in} : inner radius of coil; R_{ex} : outer radius of coil.

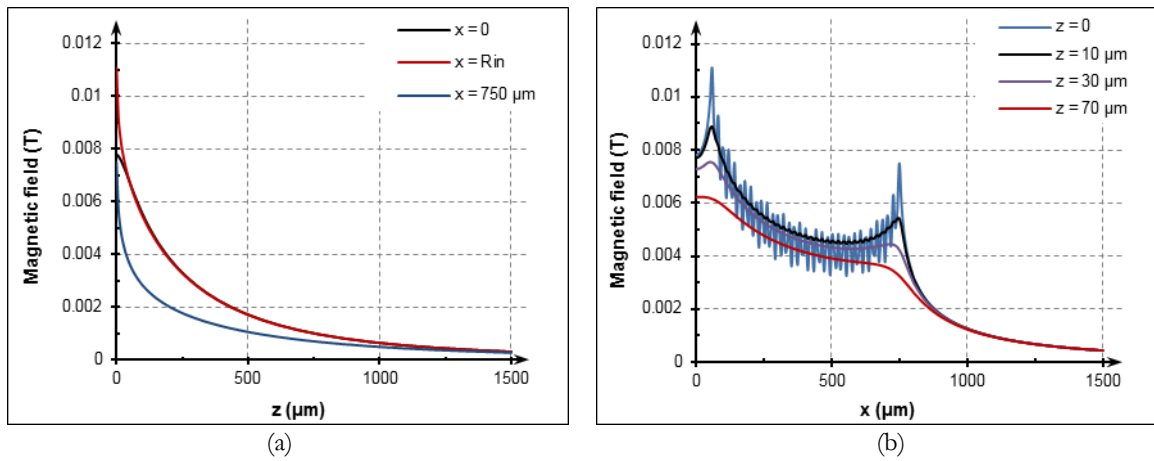


Figure 2. The profile of magnetic flux (B) of coils at path 1, 2, 3 (a) and 4, 5, 6, 7 (b); Coil's parameters: $R_{ex} = 750 \mu\text{m}$; $w = 10 \mu\text{m}$; $s = 10 \mu\text{m}$; $h = 15 \mu\text{m}$; $N = 35$ turns (maximum value)

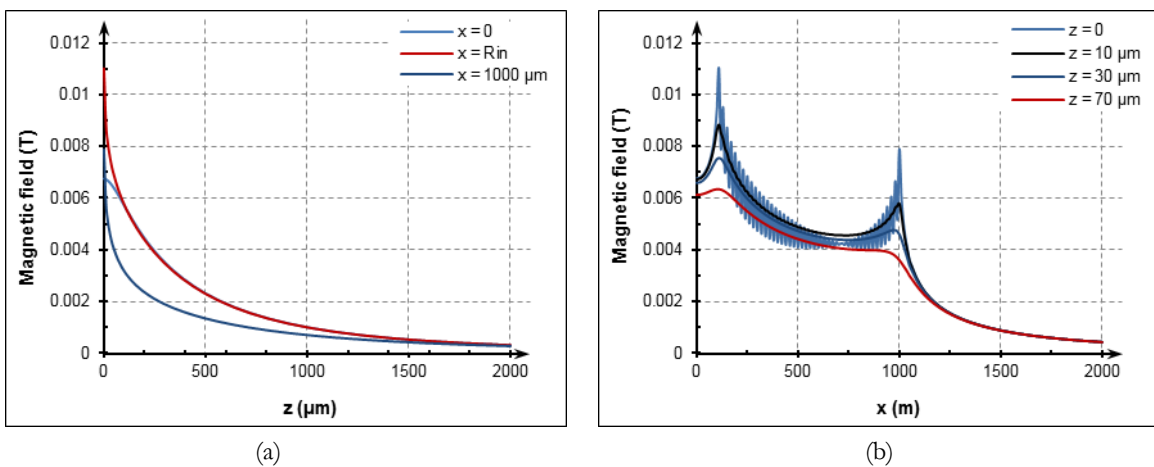


Figure 3. The profile of magnetic flux (B) of coils at path 1, 2, 3 (a) and 4, 5, 6, 7 (b); Coil's parameters: $R_{ex} = 1000 \mu\text{m}$; $w = 10 \mu\text{m}$; $s = 10 \mu\text{m}$; $h = 15 \mu\text{m}$; $N = 45$ turns (maximum value)

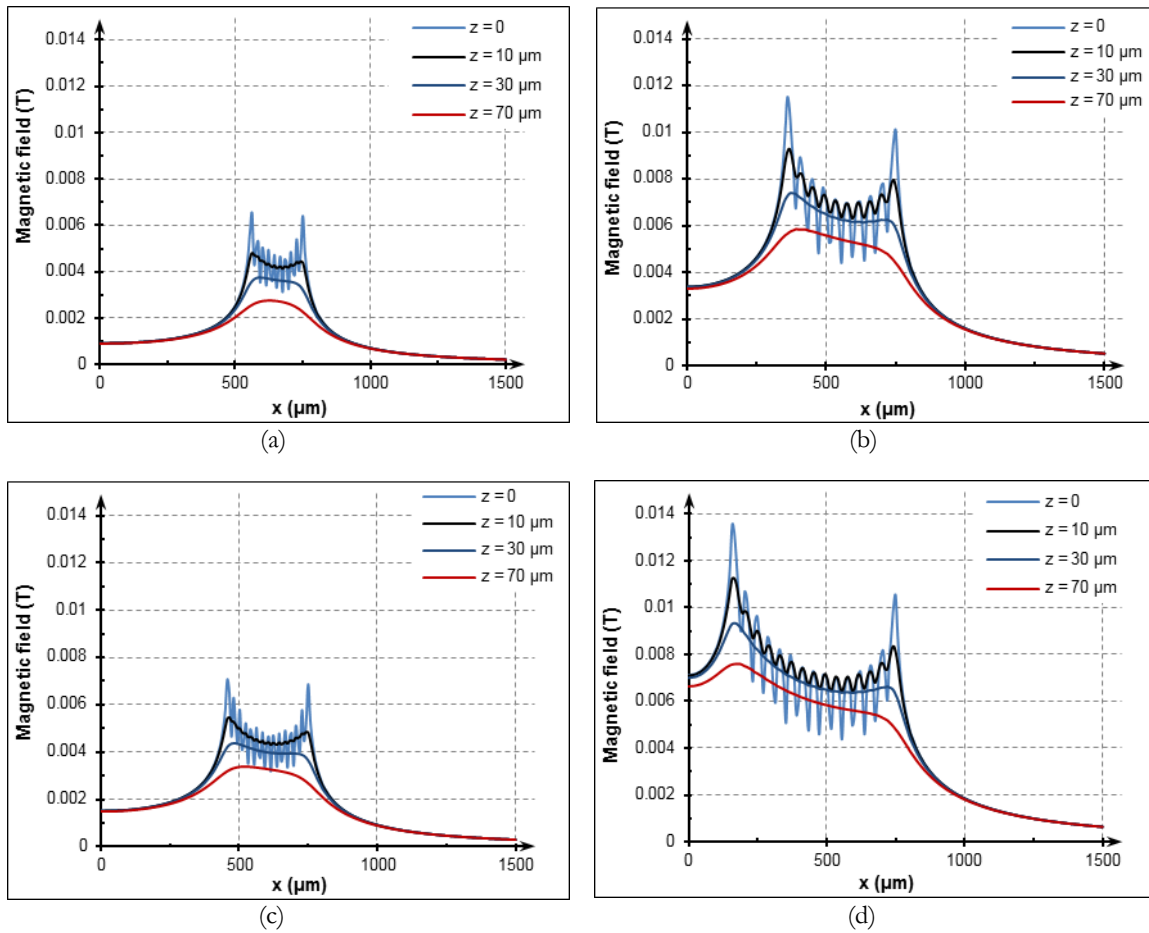


Figure 4. The profile of magnetic flux (B) of coils at paths 4, 5, 6, 7; Coils with $R_{ex} = 750 \mu\text{m}$. A pair of graphs (a) and (b) or (c) and (d): show the changing of magnetic field when the width of Cu wires is changed from 10 to 30 μm ; A pair of graphs (a) and (c) or (b) and (d) shown also the changing of magnetic field when number of turn is changed from 10 to 15 turns.

- (a). Coils with $R_{ex} = 750 \mu\text{m}$; $w = 10 \mu\text{m}$; $s = 10 \mu\text{m}$; $N = 10$ turns, $h = 15 \mu\text{m}$
- (b). Coils with $R_{ex} = 750 \mu\text{m}$; $w = 30 \mu\text{m}$; $s = 10 \mu\text{m}$; $N = 10$ turns, $h = 15 \mu\text{m}$
- (c). Coils with $R_{ex} = 750 \mu\text{m}$; $w = 10 \mu\text{m}$; $s = 10 \mu\text{m}$; $N = 15$ turns, $h = 15 \mu\text{m}$
- (d). Coils with $R_{ex} = 750 \mu\text{m}$; $w = 30 \mu\text{m}$; $s = 10 \mu\text{m}$; $N = 15$ turns, $h = 15 \mu\text{m}$

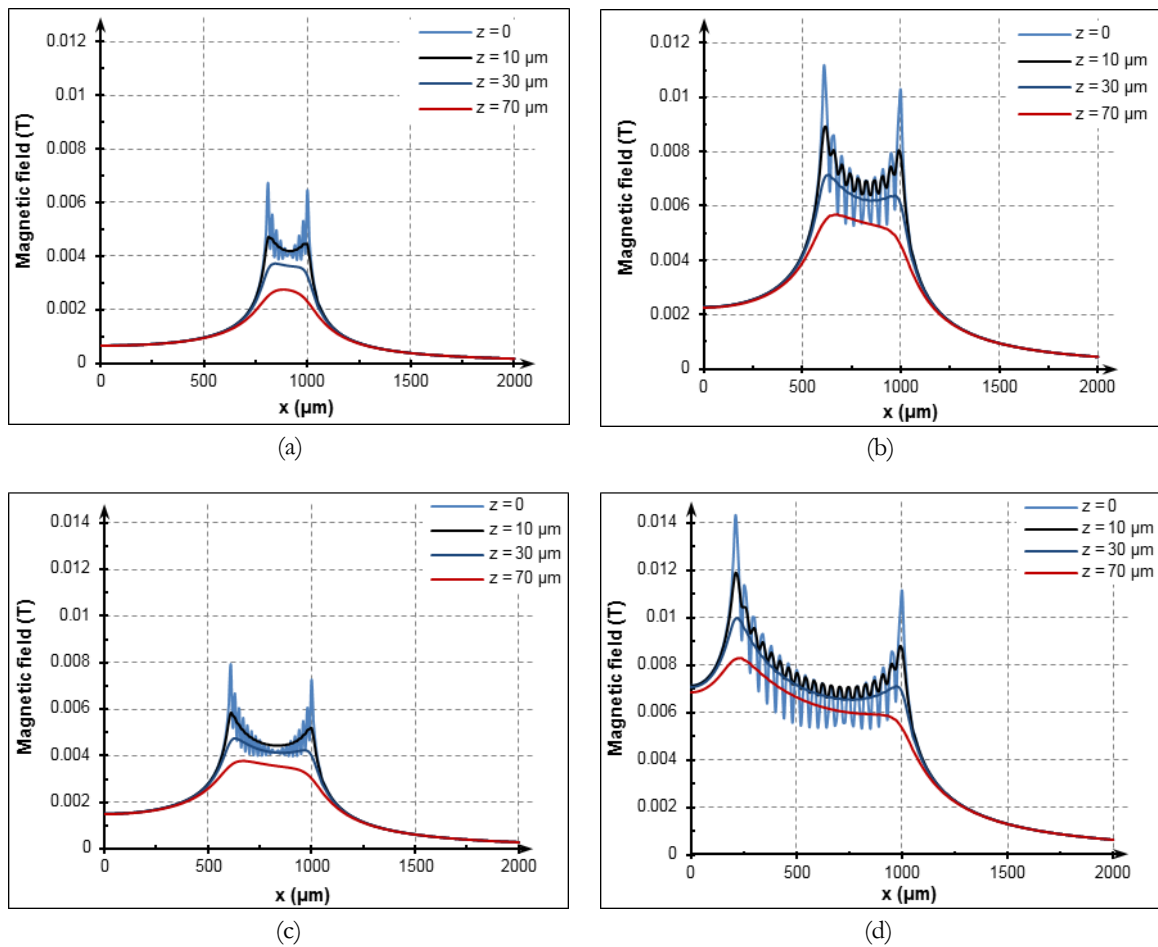


Figure 5. The profile of magnetic flux (B) of coils at paths 4, 5, 6, 7; Coils with $R_{ex} = 1000 \mu\text{m}$. A pair of graphs (a) and (b) or (c) and (d): show the changing of magnetic field when the width of Cu wires is changed from 10 to $30 \mu\text{m}$; A pair of graphs (a) and (c) or (b) and (d) shown also the changing of magnetic field when number of turn is changed from 10 to 20 turns.

- (a). Coils with $R_{ex} = 1000 \mu\text{m}$; $w = 10 \mu\text{m}$; $s = 10 \mu\text{m}$; $N = 10$ turns, $h = 15 \mu\text{m}$
- (b). Coils with $R_{ex} = 1000 \mu\text{m}$; $w = 30 \mu\text{m}$; $s = 10 \mu\text{m}$; $N = 10$ turns, $h = 15 \mu\text{m}$
- (c). Coils with $R_{ex} = 1000 \mu\text{m}$; $w = 10 \mu\text{m}$; $s = 10 \mu\text{m}$; $N = 20$ turns, $h = 15 \mu\text{m}$
- (d). Coils with $R_{ex} = 1000 \mu\text{m}$; $w = 30 \mu\text{m}$; $s = 10 \mu\text{m}$; $N = 20$ turns, $h = 15 \mu\text{m}$

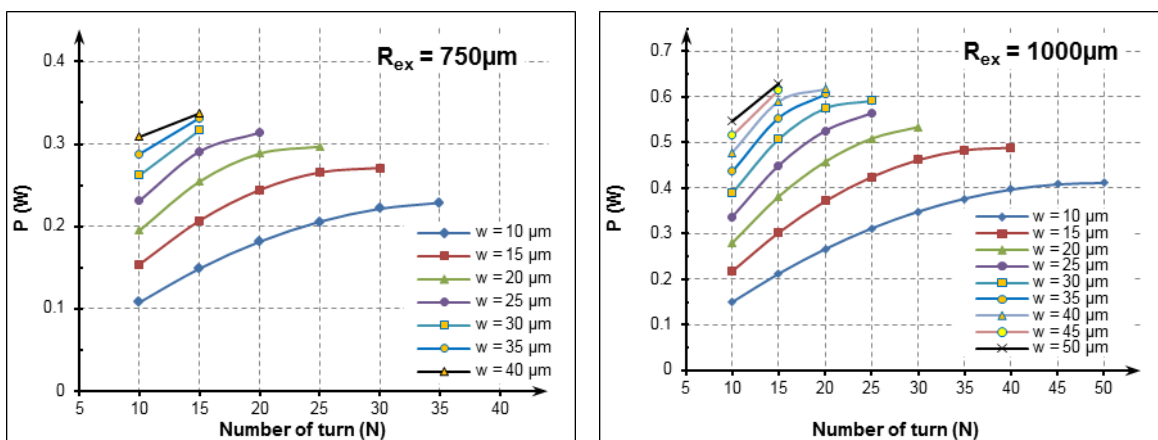


Figure 6. The power consumptions (P) in coil with different turn number (N) and width of copper wire (w) ($R_{ex} = 750 \mu\text{m}$ and $1000 \mu\text{m}$).

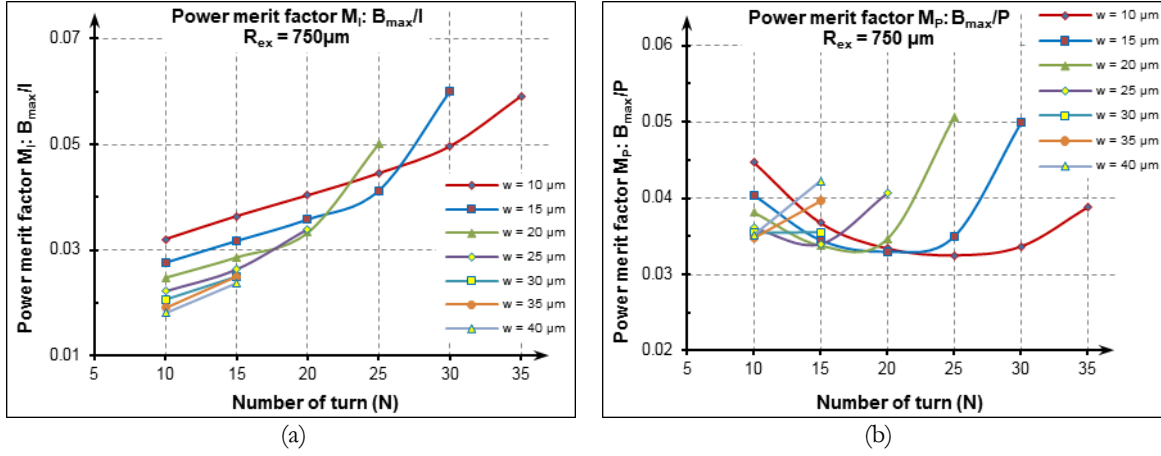


Figure 7. Power merit factors M_i and M_p of coils with $R_{ex} = 750 \mu m$; $s = 10 \mu m$; $h = 15 \mu m$ and different turn numbers and wire widths. (a). Power merit factor M_i is calculated by the maximum generated magnetic field on each unit of injected current (I) in coils. (b). Power merit factor M_p is calculated by the maximum generated magnetic field on each unit of energy consumption;

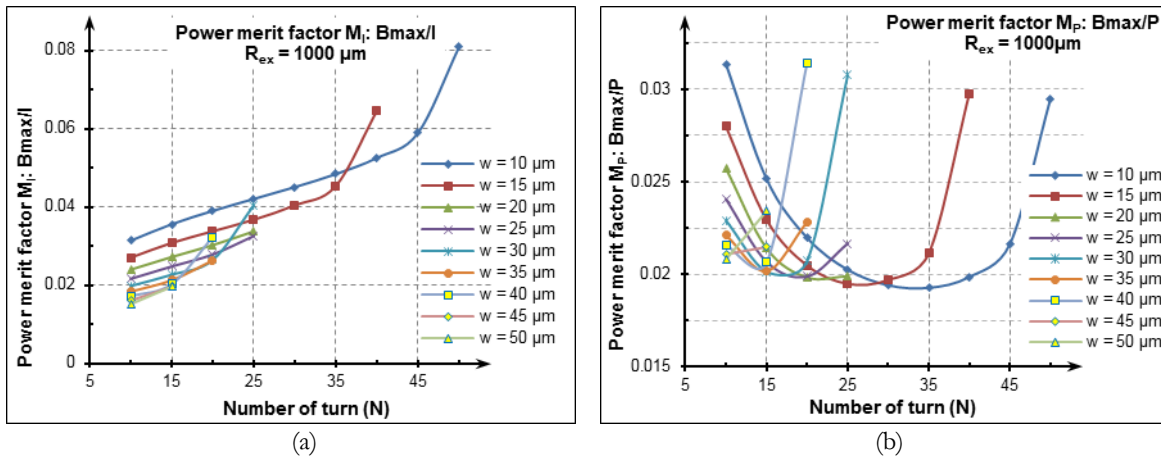
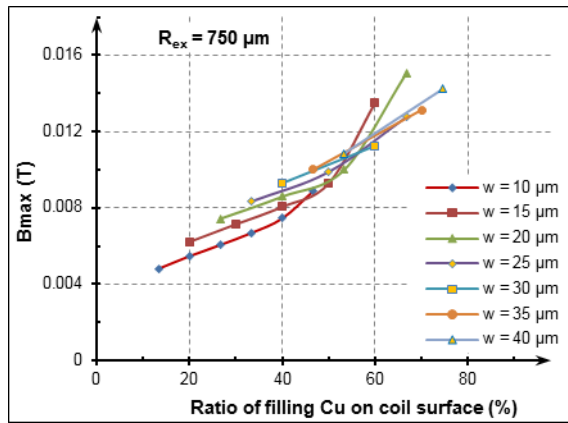
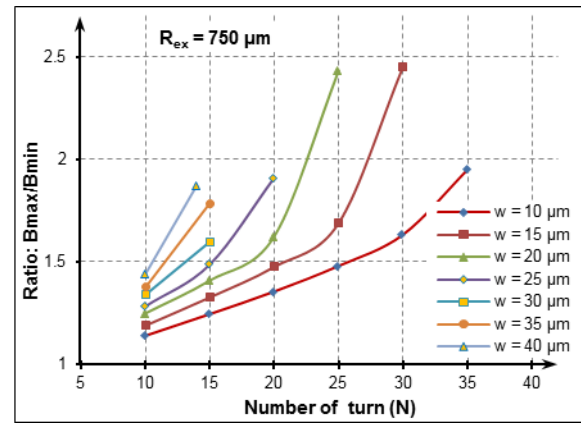


Figure 8. Power merit factors M_i and M_p of coils with $R_{ex} = 1000 \mu m$; $s = 10 \mu m$; $h = 15 \mu m$ and different turn numbers and wire widths. (a). Power merit factor M_i is calculated by the maximum generated magnetic field on each unit of injected current (I) in coils. (b). Power merit factor M_p is calculated by the maximum generated magnetic field on each unit of energy consumption;

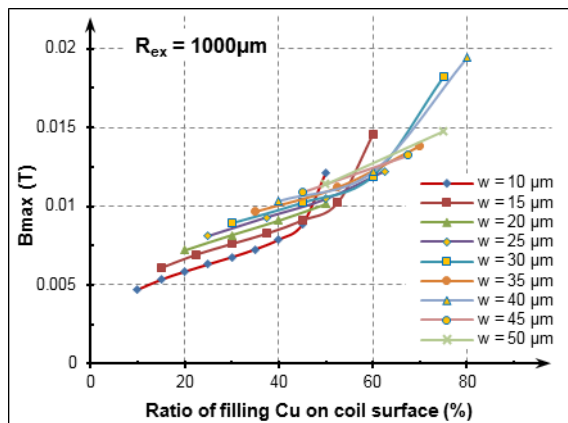


(a)

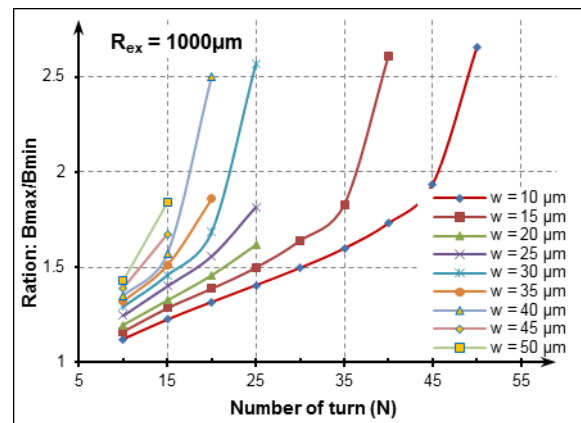


(b)

Figure 9. (a). Effect of filling ratio on B_{\max} value; (b) Homogeneity of the magnetic induction: B_{\max}/B_{\min} , coil with $R_{\text{ex}} = 750 \mu\text{m}$



(a)



(b)

Figure 10. (a). Effect of filling ratio on B_{\max} value; (b) Homogeneity of the magnetic induction: B_{\max}/B_{\min} , coil with $R_{\text{ex}} = 1000 \mu\text{m}$

APPENDIX 2. Paper

“Reversible bonding by dimethyl-methylphenylmethoxy siloxane – based stamping technique for reusable poly(dimethylsiloxane) microfluidic chip”

Reversible bonding by dimethyl-methylphenylmethoxy siloxane – based stamping technique for reusable poly(dimethylsiloxane) microfluidic chip

Hong Ha Cao¹, Thi Hong Nhung Dinh¹, Ferial S. Hamdi^{1,2}, Magdalène Couty¹, Emile Martincic¹, Marion Woytasik¹, Elisabeth Dufour-Gergam¹

¹Institut d'Electronique Fondamentale, Université Paris-Sud, CNRS, F91400 Orsay, France

²SATIE, Ecole Normale Supérieure de Cachan, CNRS, F94230 Cachan, France

E-mail: hong-ha.cao@u-psud.fr

Published in Micro & Nano Letters; Received on 14th October 2014; Revised on 28th January 2015; Accepted on 5th February 2015

Reversible packaging is very desirable for microfluidic chips: it allows changing the chip upper cap when it is damaged, cleaning and reusing the chip bottom substrate. This latter case becomes even more attractive when integrated components are present on the substrate and have required a complex and expensive microfabrication process. The feasibility of poly(dimethylsiloxane) (PDMS)/PDMS and PDMS/glass reversible bonding is demonstrated using the stamping technique. Dimethyl-methylphenylmethoxy siloxane (DMPMS), a type of silicone conformal coating, is used as an adhesive layer between the PDMS channel and the substrate (PDMS or glass). This technique is easy to perform as it only needs spin-coating and thermal curing steps. The bond strength is suitable for high working flow rate/pressure of liquid in the channel (up to 500 $\mu\text{l}/\text{min}$ and 200 kPa). The cycle 'peeling/bonding' of the cap can be repeated up to five times. In addition, an MTT cell proliferation assay has been performed and suggests the non-cytotoxicity of DMPMS. Thus, the DMPMS-stamping bonding technique opens new perspectives for PDMS biochips where plasma treatment is not possible such as functionalised surfaces.

1. Introduction: Poly(dimethylsiloxane) (PDMS) is the most commonly used silicone polymer in the fabrication of microfluidic systems and is applied in many biological analysis processes, such as protein, DNA analysis [1–5], cells analysis, immunoassays [6, 7] and so on. This is due to its physical and chemical properties (e.g. permeability, transparency, flexibility and bio-compatibility) in addition to its easy, flexible, low-cost and quick fabrication process [8]. Moreover, the replica moulding process on SU-8 masters makes the channel network's design simple [2].

The package is an essential part of a device as it ensures its protection. For PDMS microfluidic devices, it also generally contains the channel network. In specific applications, the development of reversible packaging, which enables reuse of the microfluidic chip several times, is very attractive, especially when integrated components (e.g. electrodes for electrochemical detection, micro-coils for magnetic trapping or analysis etc.) have been required for a complex and expensive microfabrication process. Indeed, the reversible packaging allows the PDMS cap removal for better cleaning and/or channel replacement. Thanks to the PDMS adhesive properties and the easy activation of its surface, PDMS cap bonding on various materials (e.g. glass, silicon etc.) is common. Even if the accurate alignment of cap and bottom substrate is still an issue, the bonding can be done quickly by using oxygen plasma, UV/ozon, corona discharge or even by self-adhesion [9–11]. With this latter technique, the bonding is reversible, but only very low fluidic pressures can be applied in the channel in order to avoid any leakage. Other techniques allow the use of high pressure conditions: above 30 kPa and up to 200 kPa or from a few tens to few hundreds of $\mu\text{l}/\text{min}$ of liquid flow rate, but they are generally irreversible [12, 13].

A few reversible packaging methods allowing PDMS microfluidic chips to work at quite high pressure have been already published. The simplest method is to fasten the contact between the cap and the device wafer with a mechanical strength thanks to two clamps (Plexiglas[®]) tightened with screws [14, 15]. In addition to the specific design of the mechanical clamps, channel deformation can appear when a hard press is applied onto the cap. Packaging by aspiration through a dedicated crossing channel

network patterned in the cap suffers from the same drawback [16]. In addition, using a vacuum system implies that the applied pressure needs to be well regulated. Magnetic field strength can be used to clamp both parts of the microfluidic chip thanks to magnets or embedded iron powder in PDMS. Rafat *et al.* [17] reported a working pressure of up to 145 kPa, but this technique is not compatible with microfluidic chips using magnetic beads inside the channel. Another way is to seal the PDMS microfluidic chip with an adhesive layer or special double-sided tape. Chong *et al.* [18] used a bio/chemical compatible tape to bond the channel cap to the bottom substrate. The tape enhances the bonding strength (the pressure inside the channel is up to 100 kPa) and the cap is easily removed from the substrate. The PDMS bonding on different substrates combining a plasma and an adhesive layer (dimethyl-methylphenylmethoxy siloxane (DMPMS)) between the channel cap and the bottom substrate has previously been performed by Vézy *et al.* [19]. This technique allows chips to be reused and to work in high pressures (100 kPa) with no leakage. However, in both cases, the surface of the bottom substrate is covered with the tape or the adhesive layer, making it impossible to perform specific surface treatment or to access electrodes on the bottom substrate before channel sealing.

DMPMS is a suitable material for microfluidic chip, as it is a popular silicone conformal coating like parylene, acrylic resin, epoxy and polyurethane. In addition, there are similarities in some common properties with PDMS (Table 1). These properties make the material easy to use. As a translucent liquid, it is easy to spray or spin-coat, flexible, easy to cure (in the oven or at room temperature), highly adhesive to most common substrates and materials and containing a safe solvent base. It is particularly useful for low- and high-temperature applications. Like PDMS, it provides high humidity and corrosion resistance with high coefficient of thermal expansion. In common usage of making a thin film of spin coating, DMPMS is even more suitable than PDMS because of its lower viscosity. These properties make DMPMS suitable for use as an adhesive layer in bonding and protecting printed circuit boards (PCBs) or other electronic substrates [20, 21].

In this Letter, we propose to combine the use of DMPMS as an adhesive layer and the stamping method, also known as

Table 1 Common properties of PDMS and DMPMS

Material properties	PDMS	DMPMS
mixture	two parts	one part
optical	transparent	translucent ^d
mechanical	750 kPa (Young's modulus) [1]	105 kPa ^a
permeability	impermeable to liquid water; permeable to gases and non-polar organic solvents [1]	impermeable to liquid water; permeable to gases and non-polar organic solvents ^d
reactivity	non-reaction with common chemicals and solvent [1]	non-reaction with common chemicals and solvent ^d
toxicity	non-toxic [1]	non-toxic ^d
contact angle	around 110° ^b	103° ^b
viscosity (cP)	3900 ^c	350 ^d
useful	−45–200°C ^c	−45–200°C ^d
temperature ranges		

^aTensile strength – ISO 527-2. <http://www.iq.ul.com/ul/cert.aspx?ULID=231517>.

^bThe experimental average values are measured in this Letter.

^cSilicone elastomer with ratio base: curing agent 10:1, Sylgard® 184 Silicone Elastomer.

^dDOW CORNING, Material Safety Data Sheet.

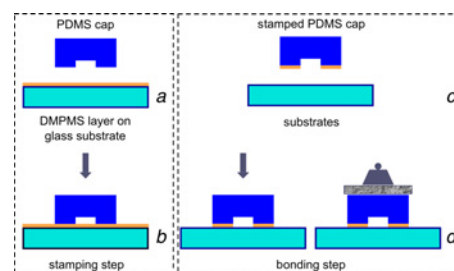
'stamp-and-stick' process [22], for its structuration. In this technique, a thin adhesive layer (e.g. acrylic resin, epoxy, polyurethane or silicone) is transferred to the cap from a spin-coated layer on a wafer by manual or automatic stamping system. Then, the cap is put in contact with the device wafer. The bonding process is performed easily at room temperature or with a soft thermal treatment (below 100°C). As the adhesive layer is not spin coated on the bottom substrate and is only present at the substrate and cap interface, structuration and/or functionalisation of the bottom surface are possible before the bonding step. In addition, no plasma activation is required, preserving plasma-sensitive surfaces.

2. Materials and experiments

2.1. Materials: PDMS (Sylgard 184 Silicone Elastomer Kit, purchased from Dow Corning Corp.), DMPMS-based silicone resin solution (Dow-Corning 1-2620 Low VOC Conformal Coating, purchased from Dow Corning), glass wafers (2 inches, optical wafer BK-7 type), silicon wafers (2 inches), and SU-8 3050 photoresist (purchased from MicroChem Corp.).

2.2. Experiments

2.2.1 PDMS microfluidic chip fabrication: Microfluidic chips are obtained by bonding a PDMS channel cap to a flat surface (the bottom substrate). Two different types of bottom substrates are used: glass and thick PDMS layers of glass. The glass substrate is cleaned with solvents and dried using nitrogen gas. In the case of the PDMS bottom, a layer of 100 µm thickness is spin coated over a previously cleaned glass substrate. For that purpose, pre-polymer PDMS is prepared by mixing two components, base and curing agent, with a weight ratio of 10:1. After blending, the mixture is degassed in a vacuum desiccator. Then, the PDMS is spin coated at 500 rpm for 60 s and cured in an oven at 75°C for 1 h. For the channel cap preparation, it is necessary to fabricate an SU-8 mould first. A 50-µm high, 500-µm wide and 3-cm long mould in SU-8 3050 photoresist is moulded on a silicon wafer [1]: an SU-8 layer of up to 50 µm is spin coated on a silicon wafer and then soft-baked on a hot plate at 95°C for 15 min. Subsequently, the SU-8 layer is exposed to UV light by using an optical lithography system at 250 mJ/cm², post-baked at 65°C for

**Figure 1** Bonding process by stamping technique

a Glass substrate with spin-coated DMPMS of 7 µm-thick layer and cured PDMS cap

b PDMS cap is stamped onto DMPMS layer

c Stamped PDMS cap is put in contact with the bottom substrate: glass or cured PDMS/glass

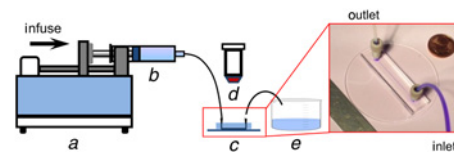
d Oven thermal curing: sample with and without a load on top

1 min after that and then at 95°C for 4 min. Finally, the SU-8 layer is developed in SU-8 developer solution for 5 min., then rinsed with isopropyl alcohol and dried using nitrogen gas. In the next step, the pre-polymer PDMS is poured onto the SU-8 mould and cured in an oven at 75°C for 2 h. Finally, the cured PDMS cap is released from the master mould and cut into a suitable shape. The channel inlet and outlet are drilled using a PDMS tool kit.

2.2.2 Bonding process: Fig. 1 shows the bonding process using the stamping technique. A DMPMS layer of 7 µm-thick is spin coated at 5000 rpm for 90 s over a glass substrate. Then, the cured PDMS cap is stamped on this fresh DMPMS layer (Figs. 1*a* and *b*), peeled off and placed on top of one of the two bottom substrates previously prepared (either glass or PDMS/glass) (Fig. 1*c*) and the position is fixed. Finally, the microfluidic chip is placed in an oven at 70°C for 4 h to let the DMPMS cure (Fig. 1*d*). The bonding is performed with and without a load of 0.7 kg on top of the microchannel to enhance the adhesion of both parts, leading to an applied pressure of around 7 N related to the cap size.

2.2.3 Leakage test: This test is performed after the bonding to evaluate the reliability of the microchannel. As shown in Fig. 2, coloured water (for easy observation) is injected into the channel at several flow rates ranging from 20 to 500 µl/min using a glass syringe controlled by a syringe pump (RaZEL™ R99-FMZ). The flow rate is increased by intervals of 30–80 µl/min. For each flow rate, the coloured water is kept flowing inside the channel for 10 min. The maximum tested flow rate has been fixed at 500 µl/min, which is high compared with the working flow in the common microfluidic experiments.

2.2.4 Peeling/bonding test: After the chip has passed the leakage test, the channel cap is carefully, manually peeled. The peeling process is considered to be successful when the channel is entirely removed from the substrate without any tearing of the channel

**Figure 2** Set-up for leakage tests

a Flow rate controller, syringe pump

b Syringe containing the coloured water to inject into the channel

c Microfluidic chip

d Digital camera microscope focused on the channel

e Liquid reservoir

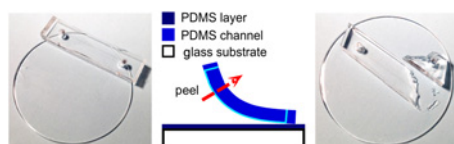


Figure 3 Process of peeling off channel
a Channel cap peeled successfully from the substrate
b Channel cap peeled unsuccessfully from the substrate

surface or the PDMS substrate layer (Fig. 3a). On the contrary, if the cap is cracked, the process has failed (Fig. 3b). Once the channel cap is successfully removed without any tear, the bonding process is performed again as shown in Fig. 1. The number of peeling/bonding repetitions reveals the process robustness. Tests are performed until five successful peeling/bonding cycles are achieved. The channel cap can be either reused or replaced by a new one in each cycle.

3. Results and discussion: First, it has been necessary to adjust the couple ‘baking temperature’ and ‘curing time’ to ensure DMPMS curing. As reported in the product data sheet of DMPMS [20], the typical curing time recommended for a 75- μm coating layer in contact with air is 10 min at room temperature followed by a soft bake at 60°C for 10 min in an oven. In our case, even if the DMPMS layer is thinner, at this process step, it is sandwiched between the PDMS cap and the substrate, limiting its solvent evaporation. Several conditions with times ranging from 1 to 4 h and temperatures ranging from 60 to 70°C have been tested for the bonding process. The optimum conditions are 4 h at 70°C. Such bonded channels pass the leakage test until a flow rate of 330 $\mu\text{l}/\text{min}$ is reached (Table 2). Reversible bonding is then a success for both types of substrates, glass and PDMS/glass, as the cycle of peeling/bonding can be performed up to five times and the cap is easily peeled off from the substrates.

Then, the effect of pressure applied on the top of the microchannels during the bonding step was investigated. When the bonding is performed by the load, the maximum value of flow rate that can be injected into the channel with no leakage is 500 $\mu\text{l}/\text{min}$, instead of 330 $\mu\text{l}/\text{min}$ without the load (Table 2). Therefore, adding a load to apply pressure during the process increases the adhesion of the two surfaces. It maximises the contact of the two surfaces (channel cap and bottom), and enhances the cross-linking of DMPMS with both surfaces. However, a flow rate of 330 $\mu\text{l}/\text{min}$ is high enough to be used in any microfluidic applications related to biological assays, as it is higher than the reported values (from ten to a few tens psi of pressure or <10 $\mu\text{l}/\text{min}$) [14–19].

It is noted that a few tests have been done with the same conditions on non-patterned SU-8/silicon substrate, but the results were not reproducible and the quality of bonding was poor.

When performing the peeling process, the PDMS cap may be destroyed, leading to the use of a new cap. This may be caused by different factors. The major factor can be the strong cross-

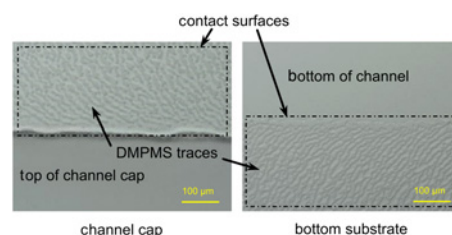


Figure 4 Optical microscope images of contact surfaces of PDMS channel cap and bottom substrate after peeling off channel cap

linking that occurs between DMPMS and PDMS or glass at both bonding interfaces, leading to partially irreversible bonding. Another factor is the handled peeling, which can induce a cohesive break in the cap.

As the fracture takes place in the DMPMS inter-layer, a roughness appears on both contact surfaces (channel cap and bottom substrate) after peeling, as shown in Fig. 4. The trace aspect can come from the tearing of the cross-linked DMPMS, which sticks partly to both surfaces. After each peeling/bonding cycle, the roughness increases, decreasing the bonding reversibility. This sometimes results in bonding failure after four cycles. As the roughness on the bottom surface cannot be controlled, replacing with new channel cap, in each cycle or after several cycles, is proposed to trade off between the bond strength and the reversible ability.

In the stamping technique, DMPMS plays the role of adhesive interlayer. If this adhesion layer is too thick, the fresh uncured DMPMS may overflow inside the channel during the stamping process when the channel cap is put in contact with the bottom substrate and pressed onto it, as shown in Fig. 5. It means that the excess of DMPMS, after its curing, could hinder and retain substances inside the channel and thus disturb the laminar flow by changing the Reynolds number. In this case, it would make the chip use and the cleaning of the channel difficult. A thick adhesion layer can also significantly affect the height of channels.

In our case, the chosen DMPMS thickness is 7 μm , which reaches a good compromise that limits the above mentioned problems and ensures an optimal strength for reversible bonding.

4. DMPMS cytotoxicity: Although DMPMS is commonly used as a coating layer in civil and industrial applications, to our knowledge, no tests of toxicity and/or biocompatibility have already been reported. To evaluate whether this material can be used in microfluidic chips for biological applications, an MTT cell proliferation assay has been performed with suspended human T-lymphoblastoid cells (CEM) [23]. This colorimetric test

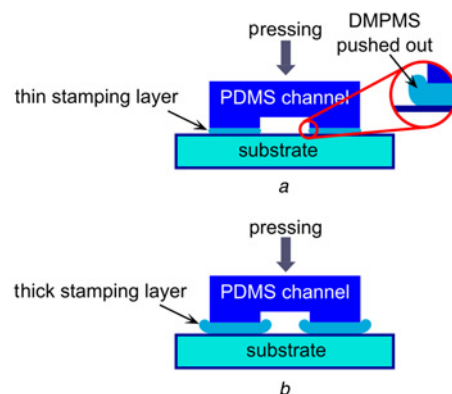


Figure 5 Schematic representation of stamped microchannel
a Thin stamping layer
b Thick stamping layer: DMPMS overflow changing the geometry of channel and possibly causing the blocking of substances in flow

Table 2 Bonding results using DMPMS stamping

Bonded surface	Additional conditions (entire thermal curing step)	Passed leakage test (flow rate, $\mu\text{l}/\text{min}$)	Number of peeling/re-bonding cycles
glass	without load	330	5
	with load	500	5
PDMS layer on glass substrate	without load	330	5
	with load	500	5

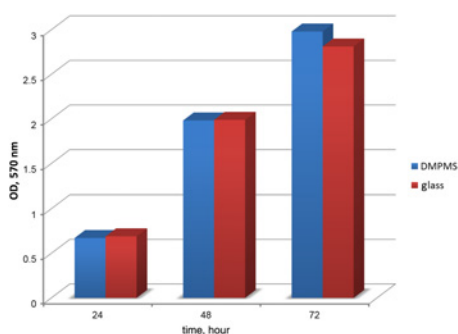


Figure 6 Culture cell test MTT on sterilised DMPMS and glass surface

is frequently used to assess cell viability. For that purpose, the yellow tetrazolium MTT solution is added to the cell suspension. Metabolically active cells reduce tetrazolium molecules to purple formazan crystals. The resulting intracellular crystals are then solubilised and their absorbance quantified at 570 nm using a UV spectrophotometer.

The proliferation of active cells, proportional to the measured optical density, is used to evaluate the toxicity of the DMPMS while a glass surface represents the positive control. Prior to the experiments, cured DMPMS and glass surfaces are dipped in ethanol before performing a 1 h UV light sterilisation. After that, CEM cells are plated on both surfaces. Cell samples are harvested every 24 h to realise an MTT assay. The toxicity results, shown in Fig. 6, indicate that the cell proliferation on the DMPMS surface is equivalent to the positive control surface, suggesting its non-toxicity. Therefore, the use of DMPMS as an adhesive layer in microfluidic chips is compatible with biological applications.

5. Conclusion: The reversible packaging of PDMS microfluidic chips using the stamping technique and DMPMS as an adhesive layer has been demonstrated on common substrates such as glass and PDMS. Such bonded channels can sustain high injection rates (up to 500 $\mu\text{l}/\text{min}$) and are suitable for most microfluidic applications. The use of a load during the bonding process increases the bond strength but also the risk of misalignment. The cycles of peeling/bonding can be performed up to five times, which can reduce the cost and fabrication time. Moreover, plasma activation is not required, allowing the use of surface treatment (functionalisation, grafting etc.) of the channel before the closing step. The experiments on DMPMS demonstrated that this material is not toxic, so is compatible with biological applications. In future work, the process will be extended to the other materials commonly used in microfluidics, such as SU-8, PMMA and COC.

6. Acknowledgments: This work was partly supported by the French RENATECH network and the Vietnamese Overseas Scholarship Program (Project – 322) of the Vietnamese government for the financial support of H. H. Cao during the study period at IEF, University of Paris-Sud, France.

7 References

- [1] McDonald J.C., Whitesides G.M.: 'Poly(dimethylsiloxane) as a material for fabricating microfluidic devices'. *Accounts of Chemical Research*, 2002, pp. 491–499
- [2] McDonald J.C., Duffy D.C., Anderson J.R., Chiu D.T., Wu H., Schueller O.J., Whitesides G.M.: 'Fabrication of microfluidic systems in poly(dimethylsiloxane)', *Electrophoresis*, 2000, **21**, pp. 27–40
- [3] Lee J., Kim J., Kim H., Bae Y.M., Lee K.H., Cho H.J.: 'Effect of thermal treatment on the chemical resistance of polydimethylsiloxane for microfluidic devices', *J. Micromech. Microeng.*, 2013, **23**, (3), p. 035007
- [4] Lien K.-Y., Liu C.-J., Lin Y.-C., Kuo P.-L., Lee G.-B.: 'Extraction of genomic DNA and detection of single nucleotide polymorphism genotyping utilizing an integrated magnetic bead-based microfluidic platform', *Microfluidics Nanofluidics*, 2009, **6**, (4), pp. 539–555
- [5] Diercks A.H., Ozinsky A., Hansen C.L., Spotts J.M., Rodriguez D.J., Aderem A.: 'A microfluidic device for multiplexed protein detection in nano-liter volumes', *Anal. Biochem.*, 2009, **386**, (1), pp. 30–35
- [6] Liu Y., Singh A.K.: 'Microfluidic platforms for single-cell protein analysis', *J. Lab. Autom.*, 2013, **18**, (6), pp. 446–454
- [7] Pla-Roca M., Juncker D.: 'Pdms microfluidic capillary systems for patterning proteins on surfaces and performing miniaturized immunoassays', *Methods Mol. Biol.*, 2011, **671**, pp. 177–194
- [8] Neethirajan S., Kobayashi I., Nakajima M., Wu D., Nandagopal S., Lin F.: 'Microfluidics for food, agriculture and biosystems industries', *Lab Chip*, 2011, **11**, (9), pp. 1574–1586
- [9] Fu Y.-J., Qui H.-z., Liao K.-S., ET AL.: 'Effect of UV-ozone treatment on poly(dimethylsiloxane) membranes: surface characterization and gas separation performance', *Langmuir*, 2009, **26**, (6), pp. 4392–4399
- [10] Haubert K., Drier T., Beebe D.: 'Pdms bonding by means of a portable, low-cost corona system', *Lab Chip*, 2006, **6**, (12), pp. 1548–1549
- [11] McDonald J.C., Chabinyc M.L., Metallo S.J., Anderson J.R., Stroock A.D., Whitesides G.M.: 'Prototyping of microfluidic devices in poly (dimethylsiloxane) using solid-object printing', *Anal. Chem.*, 2002, **74**, (7), pp. 1537–1545
- [12] Eddings M.A., Johnson M.A., Gale B.K.: 'Determining the optimal Pdms–Pdms bonding technique for microfluidic devices', *J. Micromech. Microeng.*, 2008, **18**, (6), p. 067001
- [13] Wang L., Zhang M., Yang M., ET AL.: 'Polydimethylsiloxane-integratable micropressure sensor for microfluidic chips', *Biomicrofluidics*, 2009, **3**, (3), p. 034105
- [14] Khademhosseini A., Yeh J., Eng G., ET AL.: 'Cell docking inside microwells within reversibly sealed microfluidic channels for fabricating multiphenotype cell arrays', *Lab Chip*, 2005, **5**, (12), pp. 1380–1386
- [15] Wittig J.H.Jr., Ryan A.F., Asbeck P.M.: 'A reusable microfluidic plate with alternate-choice architecture for assessing growth preference in tissue culture', *J. Neurosci. Methods*, 2005, **144**, (1), pp. 79–89
- [16] Le Berre M., Crozatier C., Velve Casquillas G., Chen Y.: 'Reversible assembling of microfluidic devices by aspiration', *Microelectron. Eng.*, 2006, **83**, (4–9), pp. 1284–1287
- [17] Rafat M., Raad D.R., Rowat A.C., Auguste D.T.: 'Fabrication of reversibly adhesive fluidic devices using magnetism', *Lab Chip*, 2009, **9**, (20), pp. 3016–3019
- [18] Chong S.C., Xie L., Levent Y., Ji H.M., ET AL.: 'Disposable polydimethylsiloxane package for 'bio-microfluidic system''. *Electronic Components and Technology Conf.*, 2005
- [19] Vézy C., Haddour N., Dempsey N.M., Dumas-Bouchiat F., Frénéa-Robin M.: 'Simple method for reversible bonding of a polydimethylsiloxane microchannel to a variety of substrates', *Micro Nano Lett.*, 2011, **6**, (10), p. 871
- [20] Dowcorning: 'Dow Corning® 1-2620 Low Voc Conformal Coating, Product Information, Electronics', 2013
- [21] Dowcorning: 'Information About Dow Corning® Brand Conformal Coatings', 2013
- [22] Srinath Satyanarayana R.N.K., Majumdar A.: 'Stamp-and-stick room-temperature bonding technique for microdevices', *J. Microelectromech. Syst.*, 2005, **14**, (2), pp. 392–399
- [23] Mosmann T.: 'Rapid colorimetric assay for cellular growth and survival: application to proliferation and cytotoxicity assays', *J. Immunol. Methods*, 1983, **65**, (1–2), pp. 55–63

APPENDIX 3. Chapter 4

Leakage test and peeling off channel

After bonding, a leakage test is required in order to evaluate the reliability of the microchannel. Figure shows a test on a testing microfluidic chip, colored water (just for easily observing by eyes) is injected into the channel at flow rates in range from 20 to 500 $\mu\text{L}/\text{min}$ using a glass syringe and controlling by a syringe pump (RaZEL[®] R99-FMZ).

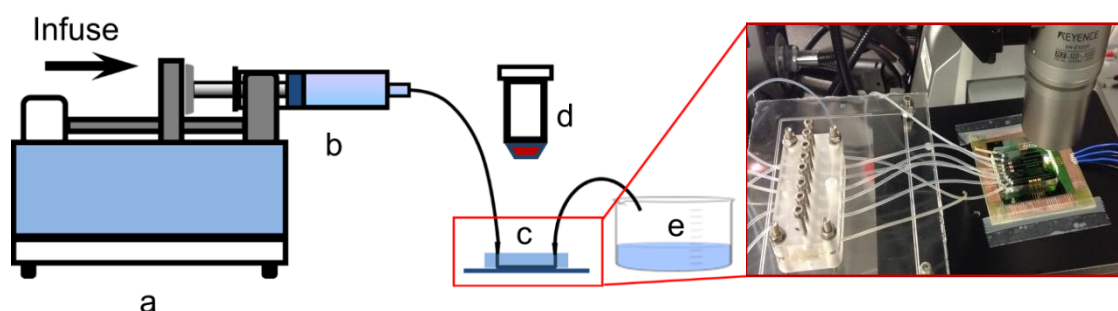


Figure 11. Setup scheme for leakage tests: (a). Flow rate controller syringe pump. (b). Syringe containing the colored water to inject into the channel. (c) Microfluidic chip connecting to valve switch. (d) Digital camera microscope focused on the channel, (e) Liquid reservoir

The flow rate is increased by intervals of 30 – 80 $\mu\text{L}/\text{min}$. For each flow rate, the colored water is kept flowing inside the channel for 10 minutes. The maximum tested flow rate has been fixed at 500 $\mu\text{L}/\text{min}$, which is high compared with working flow in the common microfluidic experiments such as few tens $\mu\text{L}/\text{min}$. Results from this test show that all fabricated microfluidic chips are passed the test at the highest of flow rate, 500 $\mu\text{L}/\text{min}$, without any leakages.

- *Information of supported devices:*

- The entire process of experiment at trapping zone is tracked by digital microscope KEYENCE.
- Micro-pumps for supplying liquids: syringe pump - RaZELTMR99-FMZ, and Micro 4 – Microsyringe Pump Controller (World Precision Instruments).
- Tube for connection: TETFE tubing (Tefzel[®] Tubing Natural, OD 1/16" and ID 0.01").

APPENDIX 4. Chapter 4

Summary of the protocol interpretation in micro test tube and in microfluidic chip

Steps	Protocol in micro test tube ($V_{\Sigma} = 500 \mu\text{L}$)	Protocol inside microfluidic chip
Pre-step	Dispersing 10 μL original beads in 100 μL PBS 1x	Dispersing 10 μL original beads in 500 μL PBS 1x.
1. Washing	<ul style="list-style-type: none"> - Washing beads 3 time with PBS 1x (500 μL each time). - Beads are separated by permanent magnet 	<ul style="list-style-type: none"> - Injecting PBS 1x into channel to wash beads at trapping zone, with flow rate 0.3 $\mu\text{L}/\text{min}$ for 10 minutes. - Beads are trapped by coils/
2. Activation	<ul style="list-style-type: none"> - EDC and Sulfo-NHS are added to clean beads, and incubated in 10 min at 25°C (ambience condition) under shaking. - Washing activated beads after activating 3 time with 500 μL PBS 1x - Beads are separated by permanent magnet 	<ul style="list-style-type: none"> - EDC and Sulfo-NHS are injected in channel with 0.3 $\mu\text{L}/\text{min}$ of each solution for 10 minutes. - Washing activated beads after activating by injecting PBS at 0.59 $\mu\text{L}/\text{min}$ for 20 minutes - Beads are trapped by coils
3. Grafting	<ul style="list-style-type: none"> - Antibodies - IgGs are added to activated beads and incubated in 2 hours at 25°C under shaking - Washing activated beads after activating 3 time with 500 μL PBS 1x - Beads are separated by permanent magnet 	<ul style="list-style-type: none"> - Antibodies - IgGs are injected in channel to graft IgGs on activated beads at trapping zone, with 0.3 $\mu\text{L}/\text{min}$ of flow rate at 36°C for 2 hours - Washing grafted beads after grafting by injecting PBS at 0.59 $\mu\text{L}/\text{min}$ for 20 minutes - Beads are trapped by coils
4. Blocking	<ul style="list-style-type: none"> - BSA (0.5 %) is added to grafted beads and incubated in 30 minutes at 25°C under shaking - Washing activated beads after activating 3 time with 500 μL PBS 1x - Beads are separated by permanent magnet 	<ul style="list-style-type: none"> - BAS (0.5 %) is injected in channel to block the surface of grafted beads at trapping zone, with 0.59 $\mu\text{L}/\text{min}$ of flow rate at 37°C for 20 minutes - Washing beads after blocking by injecting PBS at 0.59 $\mu\text{L}/\text{min}$ for 20 minutes - Beads are trapped by coils
5. Labeling	<ul style="list-style-type: none"> - FITC-conjugation is added to grafted beads and incubated in 2 hours at 25°C under shaking - Washing activated beads after activating 3 time with 500 μL PBS 1x - Beads are separated by permanent magnet - Experiment is kept in dark place. 	<ul style="list-style-type: none"> - FITC-conjugation is injected in channel to label grafted IgGs on beads' surface at trapping zone, with 0.3 $\mu\text{L}/\text{min}$ of flow rate at 37°C for 2 hours, - Washing beads after labeling by injecting PBS at 0.59 $\mu\text{L}/\text{min}$ for 20 minutes - Beads are trapped by coils - Experiment is kept in dark place
6. Detection	- Fluorescence imaging	- Fluorescence imaging